

Structural Analysis of Reconstituted Collagen Type I - Heparin Cofibrils

zur Erlangung des akademischen Grades

Doktoringenieur (Dr.-Ing.)

Von der Fakultät Maschinenwesen
der Technischen Universität Dresden

angenommene Dissertation

von

DIMITAR STAMOV (M.Sc.)

geboren am 02.10.1979. im Varna, Bulgarien

Tag der Einreichung: 24.11.2009.

Tag der Verteidigung: 15.03.2010.

1. Gutachter: Prof.Dr.phil.habil. DANIEL MÜLLER
2. Gutachter: Prof.Dr.rer.nat. CARSTEN WERNER

gez: Prof.Dr.rer.nat.habil. THOMAS BLEY
Vorsitzender der Promotionskommission

“Nature composes some of her loveliest poems for the microscope and the telescope.”

THEODORE ROSZAK (1933 -)

“A scientific truth does not triumph by convincing its opponents and making them see the light, but rather because its opponents eventually die and a new generation grows up that is familiar with it.”

MAX PLANCK (1858 - 1947)

“I am enough of an artist to draw freely upon my imagination. Imagination is more important than knowledge. Knowledge is limited. Imagination encircles the world.”

ALBERT EINSTEIN (1879 - 1955)

Contents

Contents	iv
1. Introduction	1
2. Theoretical background	5
2.1. The extracellular matrix as a biological scaffold	5
2.1.1. Collagens and glycoproteins	6
2.1.2. Glycosaminoglycans and proteoglycans	8
2.1.3. Therapeutic necessity for xenogeneic scaffolds	10
2.2. Collagen type I	11
2.2.1. Structure of tropocollagen	11
2.2.2. Molecular packing of collagen type I in fibrils	13
2.2.3. Structural polymorphism	17
2.3. Factors affecting collagen fibril formation and structure <i>in vitro</i>	19
2.3.1. Temperature	20
2.3.2. <i>pH</i> value	21
2.3.3. Presence/absence of telopeptides	21
2.3.4. Effect of concentration	22
2.3.5. Impact of GAGs and PGs	23
2.3.6. Interplay with other collagens	25
2.4. SFM as 'nanotool' for morphological and mechanical characterization	26
2.4.1. Basic principle and operating modi	26
2.4.2. 'Non-invasive' tool for structural analysis	29
2.4.3. Application in nanomechanical characterization of proteins	31
3. Materials and Methods	35
3.1. Materials	35
3.1.1. Chemicals	35
3.1.2. Materials	38
3.1.3. Devices	39
3.1.4. Software	41

3.1.5. Microscopes	42
3.1.6. Cantilevers	42
3.2. Methods	43
3.2.1. Biochemical methods	43
3.2.2. Chemical modifications	45
3.2.3. Microscopical methods	49
4. Results and Discussion	53
4.1. Morphological characterization of collagen type I - GAG assemblies	53
4.1.1. Impact of GAG type on the morphology of the cofibrils	54
4.1.2. Impact of concentration on the morphology of collagen I - LMWH cofibrils	56
4.1.3. Kinetics of PSC - LMWH cofibrillogenesis	57
4.1.4. Intercalation of heparin within the cofibrils	59
4.1.5. Impact of degree of sulfation, molecular weight and <i>pH</i> value	62
4.1.6. Discussion	64
4.2. Structural polymorphism of collagen type I fibrils	68
4.2.1. Structural levels and banding periodicities	68
4.2.2. Cofibrils with asymmetric D-banding	70
4.2.3. FLS IV nanofibrils with symmetric periodicity	73
4.2.4. Nucleic origin of polymorphic forms	74
4.2.5. Discussion - Transition and coexistence of the different structures	77
4.3. Impact of heparin intercalation on intrafibrillar packing and mechanics of collagen I fibrils	80
4.3.1. Impact of heparin and telopeptides on collagen type I fibrillar ul- trastructure (WAXS)	80
4.3.2. Covalent immobilization of freestanding fibrils	83
4.3.3. Micromechanical bending	84
4.3.4. Bending and shear moduli of collagen fibrils	86
4.3.5. Discussion - Competitive binding site of telopeptides and heparin in collagen fibril assembly	88
5. Conclusion	93
6. Summary	97
Bibliography	99
List of Figures	III

List of Tables	V
Nomenclature	VI
A. Appendices	A-1
A.1. Impact of PSC concentration on the kinetics of fibril formation	A-1
A.2. Impact of <i>pH</i> on the kinetics of PSC fibrillogenesis	A-2
A.3. Impact of HS concentration on the size distribution of PSC - HS fibrils . .	A-2
A.4. Routine for fitting of adherent fibril cross-sections via modified inverse poly- nomial function	A-3
B. Others	B-1
B.1. Statements	B-1
B.2. List of publications	B-4
B.3. Acknowledgments	B-5
B.4. Declaration	B-6

1. Introduction

One of the most challenging tasks of tissue engineering nowadays is to exploit the principles of rational design of scaffolds and to elicit appropriate signals to cells. Such scaffold characteristics are expected to promote biological processes, thus leading to production of new tissues or repair of damaged ones. In this context, the nature's ideal biological scaffold - the extracellular matrix (ECM), comes as a key regulator of cell behavior, providing individual cells with architectural cues of time and space, modulating bioavailability of soluble growth and differentiation factors, and organizing the multicellular tissue development (1). Since the complex 3-dimensional organization of the ECM has not been fully understood and characterized, it is pivotal to find means to explore the interaction between different structural and functional molecules, and thus provide a tool for controlling cell behavior and tissue morphogenesis upon contact with these microenvironments (2).

Although naturally derived ECMs have proved effective in many basic and clinical applications, the need for custom-made matrices for tissue-specific cell biological investigations drives reconstitution of their key characteristics in synthetic or biohybrid materials (3), especially in the light of problems with immunologic responses (4,5). In the absence of nature's superior building mechanisms facilitating such a supramolecular hierarchy as the ECM, it is pivotal to define and furthermore fulfill the requirements for a native matrix on the way of producing a novel bioscaffold which is to be used for tissue engineering later on.

In their most elemental biomechanical function, synthetic ECMs should provide a structural scaffold that in combination with the surrounding interstitial fluid, should be able to resist tensile (via the fibrils) and compressive (via the hydrated network) stresses (3). In this context, the majority of structural proteins (mostly collagens type I and IV) can build mechanically robust structures with typically less than 1% mass proportion to the whole system. At one level, ECM can be considered a network of tensile elements, consisting of fibrillar and amorphous structural proteins, bicontinuous with a network of compressive elements, consisting of amorphous glycosaminoglycans (GAG) and proteoglycans (PG) (6). In addition to mimicking the structural character of the ECM, a very important step is to parallelly comply with the bioadhesive properties, or else called molecular recognition of its elements. In that sense, collagen type I is predestined for tissue engineering for its ability to not only maintain tissue integrity but also interact with nearly 50 different molecules,

including almost all natural PGs, and the majority of ECM proteins (7). Other molecules with recognized adhesive functions include fibronectin, laminin, collagen IV. Because of the tight connection between the cytoskeleton and the ECM through cell surface receptors, cells sense and respond to the mechanical properties of their environment by converting mechanical signals into chemical ones (8,9).

The viscoelastic behavior, biomechanical properties, and ability to support cell attachment through collagen, fibronectin and laminin ligands are insufficient alone to explain the constructive remodeling events that are observed following *in vivo* implantation of ECM scaffolds (2). It is essential that synthetic matrices are designed in such a way that they also serve as reservoir for growth factors and cytokines and thus allowing the flexibility to modulate tissue dynamics (3,10). In nature, these bioinductive properties are ensured by the presence of negatively charged GAGs and PGs which act as mandatory coreceptors for number of growth factors as fibroblast growth factors (FGF), hepatocyte growth factors (HGF), vascular endothelial growth factors (VEGF), etc (11–13). By interacting electrostatically with these molecules the growth factors may become sequestered from their signaling receptors, they may become activated (via proteolytic processing), and they may be presented to the cells in a manner significantly altering their bioactivity (10).

As growth factors are required in only small amounts to elicit a biological response, the main focus in designing synthetic matrices for growth factor presentation is to control their localized delivery. Several strategies to engineer growth factor release from biomaterials have been presented over the past years and some initial success have been reported in animal models for regeneration of bone and skin as well as induction of vascularization, exploiting various polymer matrices and hydrogels (14–16). Nevertheless as many cellular processes involved in morphogenesis require a complex network of several signaling pathways and usually more than a single growth factor type, other reports focused on schemes for sequential delivery of multiple growth factors (17). The use of biological feedback mechanisms in growth factor delivery has also been explored (18). In this case, a growth factor is bound to the matrix and released upon cellular demand through cell-mediated localized proteolytic cleavage from the matrix (19,20); this approach substantially mimics the mechanism by which these factors are released *in vivo* from depots in the natural ECM by invading cells in tissue repair. An intriguing conundrum is to what extent the covalent binding affects the structural recognition, folding and ability of the growth factors to elicit their effect. Therefore, recent years have seen a substantial interest in the growth factor delivery based on the pure electrostatic interaction coming from the high negative charge of GAG chains (21).

The aim of the work is to analyze and structurally characterize a matrix build-up based on two native ECM components, collagen type I and the high negatively charged GAG heparin. Utilizing a structural analysis via a range of microscopy techniques we shed some

light on the kinetic aspects of the characteristic collagen I fibrillogenesis in the presence of heparin (22). Additionally, we studied in detail the ability of the fibrillar collagen I to exhibit varying structural and hierarchical characteristics influenced by a potentially intercalating agent as the polysaccharide (23). At the end, we provide means via which to mechanically characterize such a protein-polysaccharide coassembly and to relay the results to the previously observed kinetic and structural properties of the system. The already performed analysis is of particular interest for understanding and gaining a control over a rather versatile and already heavily exploited advanced cell culture system (24–27).

2. Theoretical background

2.1. The extracellular matrix as a biological scaffold

The development and normal functioning of all cell types in an organism depend upon interactions with molecules in their environments. The major classes of molecules that regulate cellular development and function include growth and differentiation factors, cell adhesion molecules, and components of the ECM. Originally defined morphologically as extracellular material, visible as fibrils and sheets in electron microscopy, extracellular matrix is now understood in a much broader way as to include essentially all secreted molecules that are immobilized outside cells (28) (Fig.2.1).

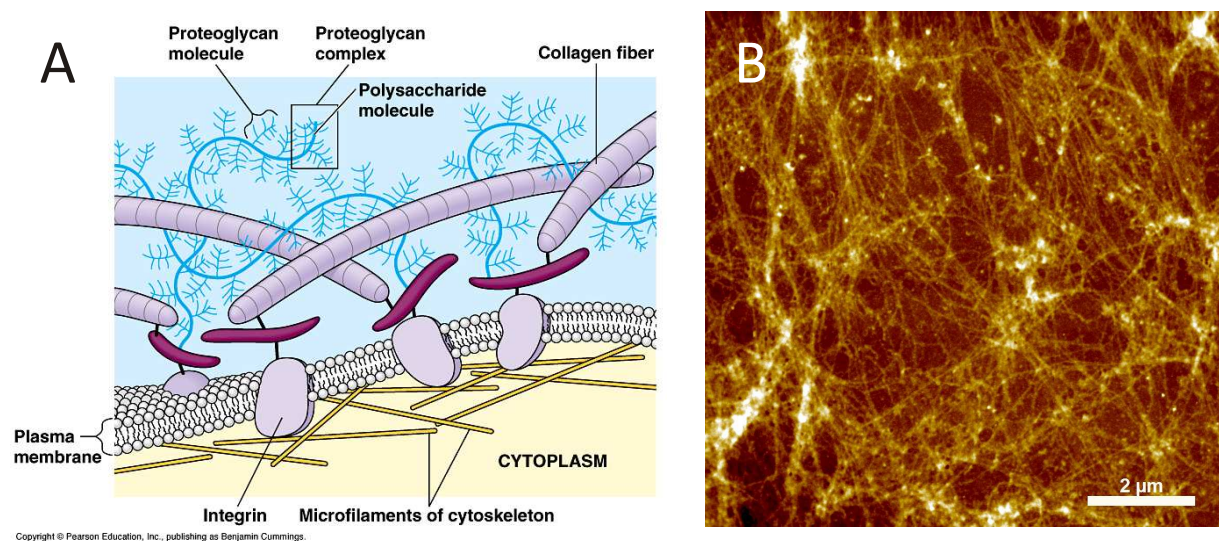


Figure 2.1.: *Schematic structural organization (A) (modified after (29)) vs. native complexity (B) of the ECM. (B) represents native ECM produced by human umbilical vein endothelial cells (HUVECs) seeded at polymeric substrates.*

The composition and ultrastructure of the ECM are determined by factors that influence the cell phenotype including mechanical forces, biochemical milieu, oxygen requirements, pH and inherent gene expression patterns (30). Major constituents include collagens, non-collagenous proteins, PGs and GAGs. In turn, ECM influences the behavior and type of the resident cells. It is in a state of a 'dynamic equilibrium' with the cells, organs and tissues it is a part of, while serving at the same time as an 'information highway' between

cells. Furthermore, cell attachment, migration, proliferation and three dimensional spatial arrangement are strongly affected by matrix composition and structure.

2.1.1. Collagens and glycoproteins

Most ECM components appear to be present in all metazoans and are therefore evolutionary ancient, as can be seen from their amino acid sequence and quaternary structure which are highly conserved across species lines. Collagen is the most abundant protein within the mammalian ECM, accounting for more than 90% of the dry weight of ECM from the most tissues and organs (31). The vertebrate family of collagens contain more than 40 genes encoding various α chains which can form at least 29 different subtypes (32). Each type of collagen is of course a product of specific gene expression patterns as cells differentiate in tissues, and tissues and organs develop and spatially organize (Table 2.1).

Sub-family	Members
Fibrillar collagens	Types I, II, III, V, XI, XXIV and XXVII
FACIT collagens	Types IX, XII, XIV, XVI, XIX, XX, XXI and XXII
Beaded filament forming collagen	Type VI
Basement membrane collagens	Types IV, VII, XV and XVIII
Short chain collagens	Types VIII and X
Transmembrane collagens	Types XIII, XVII, XXIII and XXV
Other collagens	Types XXVI and XXVIII

Table 2.1.: *Classification of collagen types in vertebrates (modified after (33)).*

Collagen type I is the major structural protein present in tissues and is ubiquitous within both animal and plant kingdoms. It is typically abundant in tendinous and ligamentous structures thus providing the necessary strength to accommodate the uniaxial and multi-axial mechanical loading to which these tissues are commonly subjected. Other fibrillar collagen types include type II which has a more specific tissue distribution being limited essentially to cartilage; type III, found in relatively elastic tissues such as embryonic skin, lung and blood vessels, as well as submucosal tissue of selected organs such as the urinary bladder, a location in which tissue flexibility and compliance are required for appropriate function as opposed to the more rigid properties required of a tendon or ligament; type V, found as a quantitatively minor collagen in association with type I, with particularly high amounts in cornea; and type XI, which is normally minor component of cartilage in association with collagen type II (33).

Basement membrane collagens constitute of predominantly collagen type IV which is found within the basal lamina of most vascular structures and at tissue boundaries, underlying epithelial, endothelial, fat, muscle and nerve cells. Other representatives of the same sub-family include collagen type VII which is found in epidermal region and functions as an anchoring fibril to protect the overlying keratinocytes from shear stress. The largest collagen subfamily includes the fibril associated collagens with interrupted triple helices (FACITs). Some of them decorate the surface of the fibrillar collagens and mediate their interaction with other matrix proteins (acting as molecular bridges). However, since there's no direct evidence about the association of all subfamily members to fibrils, they are most likely to have other functions, too. Another interesting subfamily is represented by the collagens with transmembrane domains (34), which participate in the formation of cell-matrix contact sites such as hemidesmosomes and focal adhesions. Furthermore their extracellular parts can be proteolytically shed out from the cell surface and the ectodomains can contribute to the remodeling of the matrix. The beaded filament forming collagen type VI has a relatively small molecular size, serving as a connecting unit between GAGs and larger structural proteins such as type I collagen, thus providing a gel-like consistency to the ECM.

The genetic code of collagens determines both the structural interactions among them and with other glycosylated non-collagenous proteins and PGs, thus contributing to the tissue specific ultrastructure of every ECM. In nature, collagens are intimately associated with glycosylated proteins, growth factors, and other structural proteins to provide unique ECM properties. The glycosylated protein fibronectin is the second most prominent as quantity molecule after collagen type I. It is typically a dimeric molecule of 250 kDa subunits existing in both soluble and tissue-bound isoforms and found typically in the ECM of submucosal structures, basement membranes, and interstitial tissues. The cell-adhesive characteristics of this protein have made it an attractive substrate for *in vitro* cell culture. It possesses ligands for adhesion of many cell types, being particularly rich in Arg-Gly-Asp (RGD) subunits; a tripeptide which is important in cell adhesion via some cell receptors (i.e. $\alpha 5 \beta 1$ integrins). It is usually found at an early stage within ECM of developing embryos and is typical for the normal biologic development, especially the development of vascular structures. Another complex basement membrane adhesion protein is the trimeric laminin who exists in numerous forms dependent on the particular mixture of peptide chains (e.g. $\alpha 1, \beta 1, \gamma 1$). Similarly to fibronectin the protein also plays a prominent role in early embryonic development and particularly in the formation and maintenance of vascular structures. The protein appears to be among the first and most critical ECM factors in the process of cell and tissue differentiation. This molecule carries numerous binding sites for other proteins typically proteins and GAGs (30).

The ECM abounds with number of cell surface receptors and adhesion molecules re-

sponsible for both cell-cell and cell-matrix interactions. The most prominent cell surface receptors are comprised of the integrin and discoidin domain receptor (DDR) families which have evolved particularly in directing the cell adhesion to specific types of both fibrillar and non-fibrillar subfamilies of collagen (35). Furthermore, it was suggested that collagen receptors participate in the organization of some of the collagen monomers into fibrils. Current *in vitro* models suggest that $\alpha 2\beta 1$ and $\alpha 11\beta 1$ integrin promote fibril formation (36), while DDR2 receptors may inhibit it (37).

ECM is a dynamic and constantly developing structure. Proteolytic enzymes including those in the matrix metalloproteinases (MMPs), serine protease and cysteine protease families influence matrix dynamics and contribute to its constant remodeling at multiple levels. Most common ways are by converting structural molecules into signaling molecules via the release of small bioactive peptides and growth factors stored within the ECM or direct degradation of matrix proteins (38).

2.1.2. Glycosaminoglycans and proteoglycans

The ECM contains various mixtures of GAGs depending upon the tissue location of the ECM in the host, the age of the host and the microenvironment (30). These are long linear heteropolysaccharides possessing a characteristic disaccharide repeat sequence composed of hexosamine and an uronic acid (39,40). Both units are variably N- and O-sulfated, which adds to the heterogeneity of these complex macromolecules. Literature abound with classifications of different GAG structures but most commonly they are separated into 4 groups: 1) chondroitin/dermatan sulfate (CS/DS); 2) heparin/heparan sulfate (HS); 3) keratan sulfate (KS); 4) hyaluronic acid (HA), representative structures for which are shown in Fig.2.2.

All GAG structures are strongly negatively charged due to their high content of uronic acids and partly of sulfate groups. With the exceptions of heparin and HA, GAG chains are covalently attached at their reducing end through an O-glycosidic linkage to a serine residue or N-linked to asparagine residue of a protein, thus resulting in macromolecules termed PGs (41). A major function of cell surface PGs is their involvement in cell adhesion and migration, dynamic processes that are mediated through interactions between the GAG chains and other ECM components, such as laminin, collagen, fibronectin. These interactions contribute to the general architecture and permeability properties of the ECM, and thus they also play a structural role. Furthermore, GAGs are known to affect the functionality of other ECM molecules with regards to cell adhesion, coupling, release and presence of cell-specific growth factors and enzymes that are immobilized in the ECM (10,42). In addition to their conventional structural roles, CS and DS have important functions in central nervous system development, wound repair, infec-

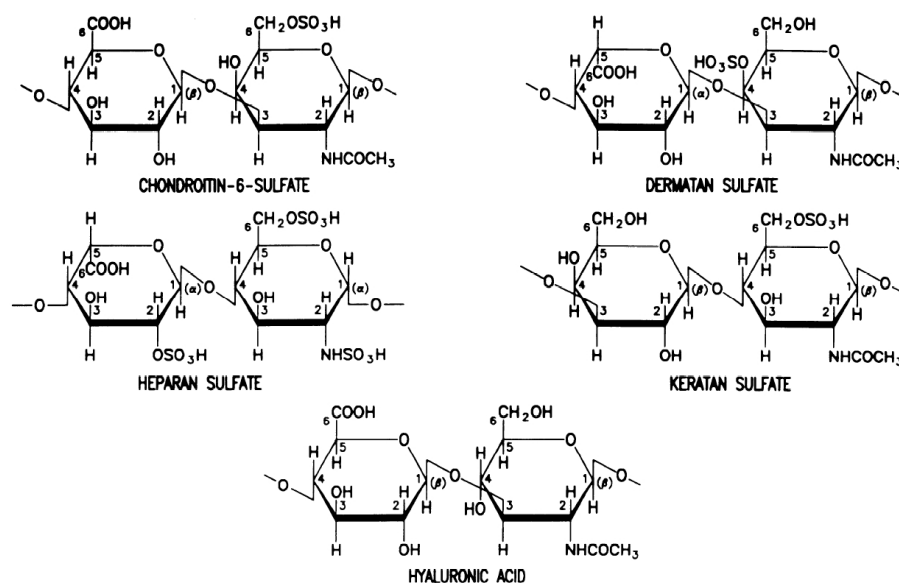


Figure 2.2.: Representative structures of GAGs (from (41)).

tion, growth factor signaling, morphogenesis (43, 44). DS has been particularly shown to participate in inflammatory processes by interacting with various GAG binding proteins like fibroblast growth factor 2 (FGF2), platelet factor 4 (PF4), interleukin 7 (IL7), P- and L-selectins (45). CSPGs are often related to neural development and neural cell migration, brain plasticity, axon regeneration via interactions with growth factors (46). Another important biological function is mediated by the CS chains of the PG aggrecan which together with collagen type II contributes to the structure and mechanical stability of articular cartilage (1).

Among the various physiological processes in which HS is involved, the interaction with extracellular signaling molecules, i.e. growth factors and chemokines, with lipid- and membrane-binding proteins, with adhesion proteins, and with certain proteases and esterases, as well as with HS degrading enzymes, deserves special attention (47–49). HS was shown to protect chemokines from proteolytic degradation and to induce their oligomerization thus promoting local high concentrations in the vicinity of their G-coupled signaling receptors (50). It has been established that HS is required for the activation of the FGF1 and FGF2 while several models have been proposed trying to explain FGF/HS/FGF-receptor complex formation and its stoichiometry which are essential to promote angiogenesis (51,52). Additionally, heparin and HSPGs bind to a number of ECM proteins such as collagens, fibronectin, laminin, thrombospondin, tenascin, vitronectin and others (40, 53). Similarly to HS, heparin also interacts with FGF1 and FGF2, PF4, VEGF, platelet derived growth factor (PDGF), heparin-binding epidermal growth factor (HBEGF), as well as with a number of cytokines like stromal cell-derived factor 1 (SDF1) and PF4 (48).

HA is the only non-sulfated and the largest of all GAGs with a molecular weight of usually several MDa which is widely distributed in most of adult and embryonic tissues.

Due to its intramolecular charge repulsion, hydrophilic and hydrophobic self-interactions and molecular entanglement, HA forms an expanded, stiffened, coiled and intertwined network, that encompasses an enormous volume of immobilized water. Consequences of these properties are its high viscosity and dramatic effects on molecular exclusion, flow resistance, tissue osmosis, lubrication, and hydration (54), all of which are likely to be important for HA-rich matrices such as are found in synovium, umbilical cord, bone marrow, connective, subcutaneous tissues, and so on. Its most prominent function in most tissues is to act as a structural organizer, a function which is normally relayed by interaction with other PG like aggrecan in cartilage and versican in other tissues (55,56). The molecule is especially enriched in the bone marrow where it is produced by both stromal and hematopoietic stem cells, at which surface it is retained by interaction with its hyaladherin receptors like CD44 and receptor for hyaluronan-mediated motility (RHAMM) (57).

2.1.3. Therapeutic necessity for xenogeneic scaffolds

The complex 3-dimensional organization of the structural and functional molecules of which the ECM is composed has not been fully understood and characterized, therefore synthesis of this biomaterial in the laboratory is not possible (2). Various forms of intact allogeneic and xenogeneic ECM has been used to promote the constructive remodeling of tissues and organs, typically harvested from small intestine (58), urinary bladder (59), skin (60). A number of these materials have also been commercialized for a variety of therapeutic applications (2).

Another typical complication from the use of intact xenogeneic ECMs regards the so called 'host-recipient' immune response. Although a number of non-autologous biologic materials have been used in humans for many years without evidence of adverse immunologic outcomes, major concerns still remain for the use of xenogeneic ECMs. For example it was shown that some xenogeneic ECMs contain various amounts of galactosyl-1,3-galactose epitope (α -gal epitope) (61), naturally not expressed in humans who can specifically interact with anti-gal antibodies (1% of circulating immunoglobulins) and thus lead to complement activation or cell mediated rejection following transplantation (62). Other studies emphasize the role of mononuclear macrophages in the host response towards implanted biological scaffolds, suggesting either pro-inflammatory or anti-inflammatory differentiation towards a phenotype associated either with cytotoxic inflammation or constructive remodeling (63). Further complications arise from the incomplete decellularization of intact ECMs upon their transplantation, a problem which seems to be related to the very tight control of matrix turnover in some tissues (e.g heart muscles) by MMPs and tissue inhibitors of matrix metalloproteinases (TIMPs) (64). The incomplete decellularization

leaves a number of donor active MMPs which makes the chances of receding such a matrix slim at the very best case. Another drawback of the incomplete decellularization is the tissue cytokine and humoral response, typically associated with activation of the Th1 pathway producing interleukin 2 (IL2), interferon γ (IFN γ) and tumor necrosis factor β (TNF β) leading to macrophage activation, stimulation of complement fixing antibody isotypes (IgG2a and IgG2b in mice) and differentiation of CD8⁺ cells to a cytotoxic phenotype (65).

Although naturally derived ECMs have proved effective in many basic and clinical applications, the need for custom-made matrices for tissue-specific cell biological investigations drives reconstitution of their key characteristics in synthetic or biohybrid materials (3), especially in the light of problems with immunologic responses. In the absence of nature's superior building mechanisms facilitating such a supramolecular hierarchy as the ECM it is pivotal to define and furthermore fulfill the requirements for a native matrix on the way of producing a novel bioscaffold which is to be used for tissue engineering later on.

2.2. Collagen type I

As previously discussed collagen I is the most abundant protein in mammals, having outstanding mechanical properties, and being present in virtually every extracellular tissue with mechanical function. Its versatility as a building material is mainly due to its complex hierarchical structure. It is therefore pivotal to understand the molecular basics leading to the origin of this structural hierarchy that can be adapted at every level.

2.2.1. Structure of tropocollagen

The hallmark of collagen is a 300 nm long and 1.5 nm thick molecule called tropocollagen that is composed of three polypeptide α chains, each of which contains one or more regions characterized by the repeating amino acid motif (Gly-X-Y), where X and Y can be any amino acid (33). This motif allows the chains to form a right-handed triple-helical structure accepted today, with all glycine residues buried within the core of the protein, and residues X and Y exposed on the surface, having a single interstrand helical bond per triplet and a tenfold helical symmetry with a 28.6-Å axial repeat (10/3 helical pitch) (Fig.2.3 A,B).

Depending on the type of α -chains which comprise the tropocollagen molecules, the triple helices can be either homo- or heterotrimeric. Individual α chains are identified by the following nomenclature: $\alpha n(N)$, where N is the Roman numeral indicating collagen type and n is the number of the α chain (33). Usually collagen type I is found in nature mainly as an $(\alpha 1)_2\alpha 2$ heterotrimer, but the $\alpha 1$ chain is also able to form homotrimers.

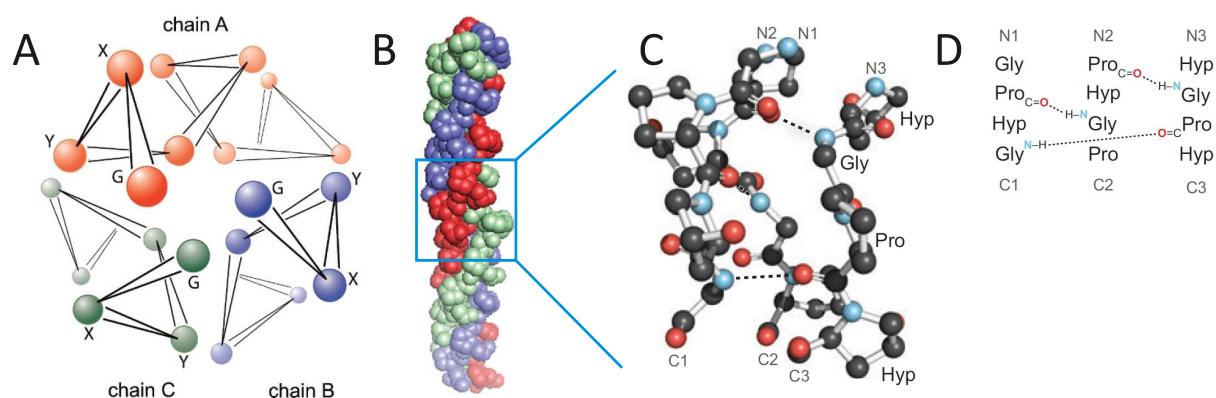


Figure 2.3.: Triple-helical organization of collagen type I. (A) Viewed along the molecular axis (α -carbons only), showing the paths of the individual polypeptide chains and the locations of residues in the Gly-X-Y triplets (G = Gly) (adapted from (66)). (B) Viewed from the side (molecule tilted toward the reader at the top; space-filling representation), showing the right-handed helical twist (from (33)). (C) PyMOL representation of a segment of collagen triple helix (PDB entry 1cag (67)), highlighting the ladder of interstrand hydrogen bonds. (D) Stagger of the three strands in panel (C).

It appears that a homotrimeric *vs.* a heterotrimeric molecular composition has only minor effects on the triple-helix stability, but may have further effects on fibril diameter and mechanical properties (68). Earlier X-ray crystallographic studies on proline-rich sequences of collagen-related peptides (CRPs) have shown that the resulting structures have a $7/2$ helical pitch (20.0-\AA axial repeat), in contrast to the $10/3$ helical pitch assumed for native collagen by fiber diffraction (69). Recent revisiting work in this direction (70) suggested that the correct average helical pitch for native collagen is $7/2$, although the generality of this hypothesis remains unclear, as there are few existing regions in native collagen which are as proline-rich as previously analyzed CRPs. Most likely the helical pitch varies across domains and various collagen types, being $10/3$ in proline-poor and $7/2$ in proline-rich regions. Such a variability in the triple-helical pitch of native collagen could play a role in the interactions of collagenous domains with other biomolecules (71–73).

The stability of the tropocollagen molecules is ensured by interstrand hydrogen bonding forces. The ubiquity of the molecule makes the recurrent $\text{N-H}_{\text{Gly}}\cdots\text{O}=\text{C}_X$ hydrogen bonds that form within the triple helix one of the most abundant amide-amide hydrogen bonds in nature (74) (Fig.2.3 C,D). For the triple helix, the individual polyproline II-like helices are stabilized by a high content of Pro and Hyp. The trimerization of chains is favored by close packing and hydrogen bonding between three chains. There is no intrinsic dipole moment in the triple-helix, so electrostatic interactions relate only to side chains. It is striking to find that the side chains of residues in X and Y positions have only relatively minor effects on triple helical stability, but are highly exposed to the solvent and available for intermolecular interactions (66, 75, 76).

The importance of collagen in nature predetermines its number of essential characteris-

tics, such as thermal stability, mechanical strength, and the ability to engage in specific interactions with other molecules (74). It is important to understand how these properties relate to the fundamental structural unit of collagen - the triple helix - as well as the mechanisms underlying its triple helical structure and stability. The Gly residue in Gly-X-Y repeat is essential in native collagen, while triple-helical substitutions in any form result in severe genetic mutations, as osteogenesis imperfecta (77). The abundance of Pro and Hyp (e.g. 22% in human collagen) preorganizes the individual strands in a polyproline II-like conformation, thereby decreasing the entropic cost for collagen folding (78). Surprisingly, Pro derivatives can also have rather deleterious consequences for triple helical bonding due to the presence of a secondary amino group which forms tertiary amides with other peptides or proteins. Tertiary amides represent a mixed population of *cis* and *trans* isomers, while all peptide bonds in collagen are *trans*. Thus, before a (Pro-Hyp-Gly)_n strand can fold into a triple helix, all *cis* peptide bonds must be converted into *trans* (74). The hydroxylation of Pro residues in Yaa position changes dramatically the thermal stability of the triple helices (79,80). It is resultant from the proposal that the 4R configuration of the prolyl hydroxy group is privileged in alone enabling the formation of water-mediated hydrogen bonds that stitch together the folded triple helix (81). This is additionally enhanced by internal inductive effects favoring the requisite *trans* conformation of the Hyp peptide bond (82,83).

The common characteristic of the classical fibrillar collagens, and type I in particular, is the long central triple-helical region in each α chain, consisting of abovementioned continuous (Gly-X-Y)_n repeat, where n is 337–343 (depending on collagen type and source). This region is flanked by short non-helical regions called telopeptides, typically about 20 residues in length, at both N- and C-termini. Additionally, all fibrillar collagens are synthesized in the form of soluble precursor molecules, called procollagens, with large N- and C-terminal propeptides domains. The C-propeptides are removed during the later stages of collagen biosynthesis, usually by specific metalloproteinases, leaving the short C-telopeptides. The N-terminal processing is usually complete and leaves the short N-telopeptides which are involved in the later fibril formation (33,84) (Fig.2.4).

2.2.2. Molecular packing of collagen type I in fibrils

Collagen type I triple helices self-assemble into D-periodic cross-striated fibrils (where D = 67 nm, the characteristic axial periodicity of collagen) as seen by electron microscopy (Fig. 2.5). The assembly of collagen molecules into fibrils is an entropy-driven process, similar to that occurring in other protein self-assembly systems (85). These processes are driven by the loss of solvent molecules from the surface of protein molecules and result in assemblies of long fibrillar structures with tapered ends and circular cross-section, which

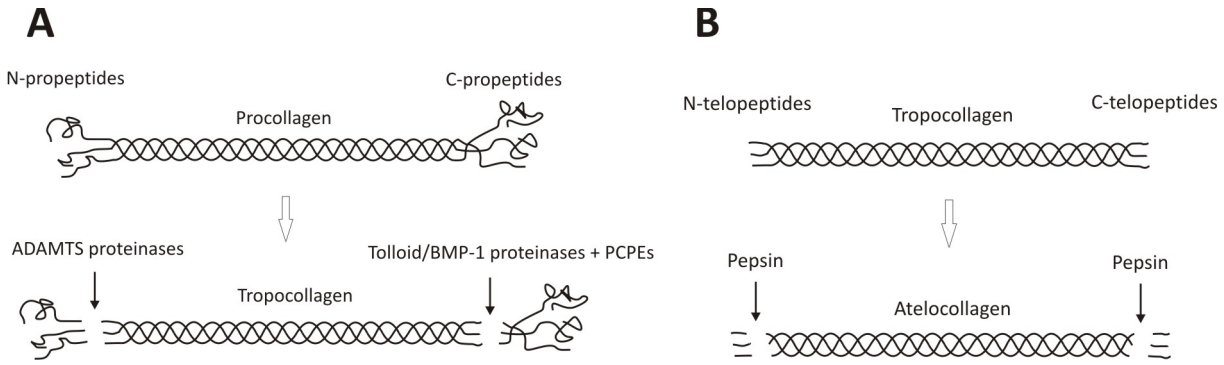


Figure 2.4.: *N- and C-terminal in vivo processing of procollagen type I to tropocollagen (A). For in vitro application tropocollagen is sometimes further processed by a non-specific pepsin hydrolysis of the telopeptides resulting in atelocollagen (B).*

minimizes the surface area to volume ratio of the final assembly. The least contentious aspect of collagen molecular packing is the axial structure within a fibril. The frequently observed 67 nm density step function repeat of fibrils is explained by the molecular stagger between molecules, or an integer multiple of this. Since the tropocollagen molecular length of 300 nm corresponds to 4.4 D, the molecular stagger leads in projection to regions of high and low electron density, these being the overlap and gap regions (86) (Fig.2.5 A-C).

The association between tropocollagens is driven by electrostatic and hydrophobic interactions, where a 234-amino acid pseudoperiodicity observed within the collagen sequence of all fibril-forming types is the key to optimal electrostatic pairings between adjacent triple helices and maximizes the contact between hydrophobic regions (88, 89). Further small adjustments in the alignment of collagen molecules in the D stagger may be required for the optimization of interactions between triple helices (90). These interactions are further stabilized by the development of molecular cross-links between the collagen molecules. They occur between sites in the short non-helical N- and C-terminal telopeptides of the collagen molecules and the main chain of the helix (91).

The minor bands in the collagen pattern originate from the grouping of charges along the collagen fibrils which in native fibrils is typically asymmetric. Reading from the N- (left) towards the C-terminus (right) the fibril pattern is characterized by the appearance of 12 minor bands which asymmetric arrangement, while often being used as a molecular fingerprinting tool for the alignment of tropocollagen helices within the fibrils (92, 93) (Fig.2.5 D).

There is strong evidence that certain fibril types contain subdomains of structure that lie between molecular and fibrillar levels. Such nanoassemblies are of great interest, since they may reveal important information that relates to the overall mechanical properties of the fibrils by preventing crack propagation and also to the nucleation and growth of fibril formation. The presence of pentameric microfibrillar structural units (94) is often viewed as a convenient link between the axial and lateral structures. Direct evidence is

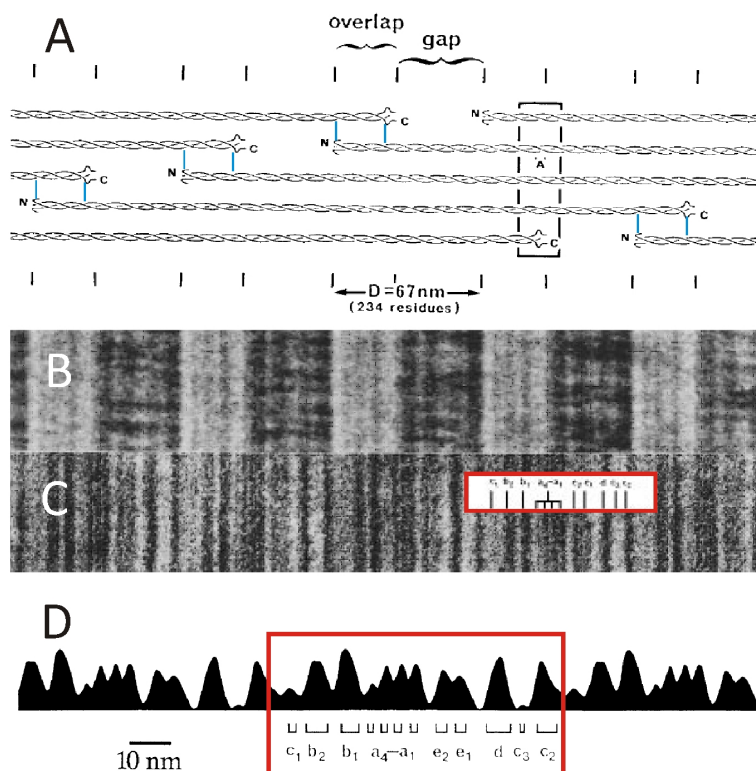


Figure 2.5.: Axial structure of *D*-periodic collagen fibrils (adapted from (84, 87)). (A) Schematic representation of the axial packing arrangement of triple-helical molecules in a fibril, as derived from analysis of positively (B) and negatively stained (C) specimens. Detailed banding density along a single *D*-period resulting from the grouping of charged amino acid residues is given in (D).

scarce, however, many measurements have indicated the presence of a 4 nm lateral periodicity or growth phenomenon that points to evidence of a subfibrillar structure. Evidence for a microfibrillar structure has also been obtained using a number of other physical characterization techniques. For example, electron tomographic reconstructions in dry cornea fibrils revealed 4 nm microfibrillar type structures (95). X-ray diffraction data was used to modulate the rather simplistic pentameric model of collagen association into one arranged as compressed microfibrils on a triclinic unit cell lattice (96,97), distortion of a regular pentagon to a compressed structure that allows quasi-hexagonal lateral packing (98). These units have been revealed in more detail recently by the determination of the structure of a single collagen unit cell from electron density map derived from X-ray diffraction (99,100) and high-resolution scanning force microscopy (SFM) studies (101). A consensus of opinion from these studies points to a one-dimensional staggered microfibrillar structure with interfibrillar cross-links. Such interfibrillar links are important in the hierarchical connectivity at the supramicrofibrillar level and also provide the basis as to why individual microfibrils have proven so difficult to isolate. The molecular topology of compressed microfibrillar structure is shown in Fig.2.6:

Contemporary X-ray diffraction studies show that the diagrams coming from analyzed

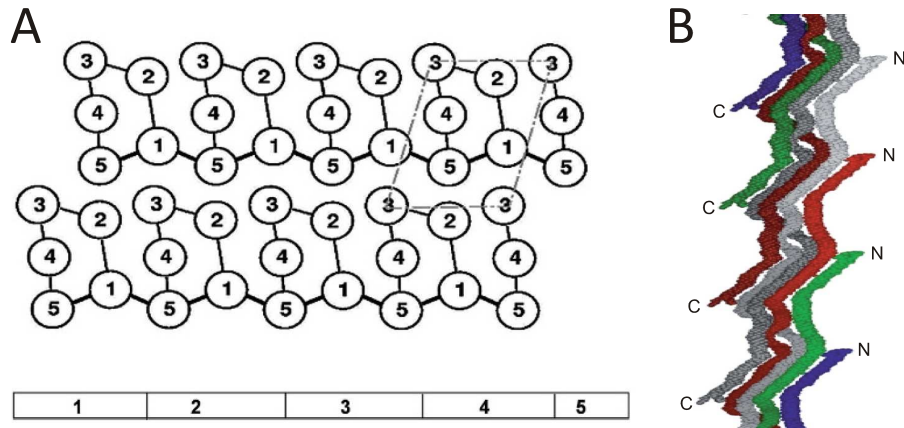


Figure 2.6.: *Microfibrillar structure of collagen type I (adapted from (86)). (A) Top - Topology of interactions of collagen molecular segments within a crystalline region of a fibril. Bottom - A collagen molecule can be represented by five pseudoperiodic 'd' segments where the final C-terminal segment is approximately half the length of other segments. In cross-section through a fibril, the molecular packing allows the in-plane interactions of segments to be revealed. Here the segments of collagen molecules adopt a cyclic microfibril structure where the connectivity in the plane reflects the slow helical climb of contiguous segments within the fibril. The proposed positioning of the cross-linkage (shown as a thicker line) between microfibril structures further stabilizes the collagen molecules. The compatibility between the base of a triclinic unit cell (axes shown in grey) and microfibril topology is shown. (B) Previously suggested microfibrillar structure of collagen, showing the path of 5 tropocollagen molecules as they pass around each other in successive D-periods.*

collagen samples contain a high level of diffuse scatter, thus indicating that they contain a large amount of static or even dynamic disorder. Fibrils that contain crystalline regions are also thought to contain significant levels of liquid-like disorder (102, 103). Therefore the molecular packing of collagen is sometimes compared to that of a liquid, or a liquid crystal, where only local molecular interactions are of significance (104). In some fibril structures, this type of scatter is the only feature observed by X-ray diffraction, and the overall molecular packing is described as liquid-like. These observations point to a variety of levels of lateral molecular organizations in collagen fibrils, ranging from liquid-like to crystalline. The relationship between crystallinity, disorder and supramolecular topology of crystalline packing within a fibril requires explanation and is related to fibril formation, overall morphology, and mechanical properties (105).

Hand in hand with the contrasting evidence of crystallinity and liquid-like disorder of collagen in a fibril is the evidence for partitioning of structures within the fibril. Earlier SFM studies (106, 107) revealed subfibrillar structures and led to the concept that the collagen fibril is an inhomogeneous 'tube-like' structure composed of a relatively hard shell and a softer, less dense core. Long range, organized lateral packing within a fibril also results in partition of substructures within a fibril; this can be understood simply enough in the observation that the fibril cross-section is a disc, which is incompatible

with a crystalline lattice. Previously suggested model (108,109) based on concentric rings of microfibrillar structures was found to have the best agreement with x-ray diffraction data. The structure contained sectors of crystalline order interfaced by disordered grain boundaries which allowed the crystallites to be accommodated systematically within a fibril with a circular cross-section. The model also provided a structural basis for growth with the incremental deposition of molecules or microfibrils at the fibrillar surface, as suggested by the 8 nm quantal variation in fibril diameter observed by PARRY and CRAIG (110). The cross-section of the proposed fibrillar structure is given in Fig.2.7.

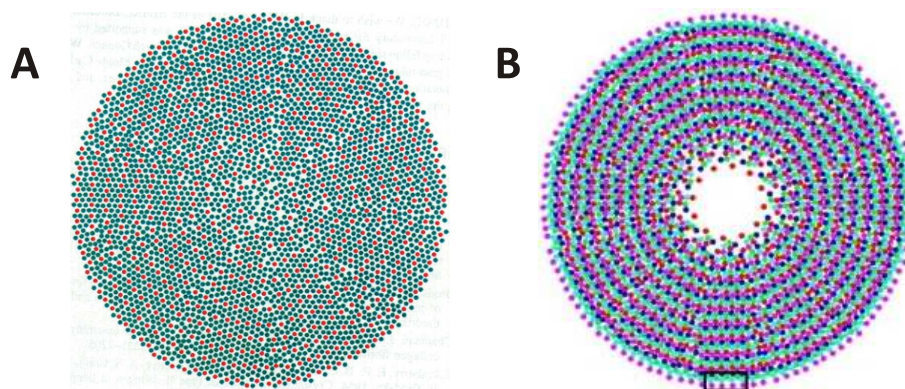


Figure 2.7.: Cylindrical packing models of collagen type I based on previous work by (A) HULMES (108) and (B) ORGEL (99,111). The model demonstrates the location of crystalline regions of collagen lateral packing within a structure, which is circular in cross-section. It is produced as an explanation of order and disorder in collagen fibrils. The center of the fibril (50 nm in diameter) is also relatively disordered which may explain some of the observations of hollow fibrils from SFM imaging.

2.2.3. Structural polymorphism

The property of the collagen systems to exhibit varying structural and hierarchical characteristics, else known as collagen polymorphism, has been observed both *in vitro* (112,113) and *in vivo* (114,115). It was shown that the collagen polymorphism is significantly influenced by factors like presence of GAGs (116,117), other forms of collagen (118,119), presence/absence of telopeptide regions (120,121), methods of purification (122), temperature (123), *pH* and salinity of the solutions (124,125). The numerous reports account for the identification of novel banding patterns, growth mechanisms, and morphological properties of these systems deviating to a different extent from the classical collagen type I. Due to the very heterogeneous nature of the collagen type I polymorphic forms obtained from either the alignment of the tropocollagen (parallel or non-parallel) or the lateral staggering, a uniform classification does not exist. However, there is a good overall agreement about the molecular structure of these axially projected tropocollagen arrangements. The most studied classical forms, apart from the native asymmetric collagen type

I D-banding of 67 nm, include various types of fibrous long spacing (FLS) collagen (utilizing symmetric arrangement of tropocollagen) (126, 127) and segment long spacing (SLS) fibrils (128, 129) (with asymmetric pattern), both sharing non-D periodic bandings. Other examples include D-periodic fibrils generally being D-periodic symmetric (DPS) (112, 115) and oblique-striated asymmetric tactoids (112, 130). The most commonly observed polymorphic forms of collagen obtained over the last 5 decades mainly via transmission electron microscopy (TEM) but also SFM techniques are given in Table 2.2.

Name	Description	Banding periodicity	References
Native	Fibrils with periodic, asymmetric banding pattern	67 nm (D)	(131–133)
DPS I - IV	Same as native but with D-periodic centrosymmetric banding pattern	67 nm	(112, 115, 132, 134, 135)
D/3 periodic	Fibrils with asymmetric periodicity	22 nm (D/3)	(136, 137)
D/6 periodic	Tactoids with asymmetric banding	11 nm (D/6)	(138)
Oblique striated	Tactoids of D-periodic polar subfibrils staggered with respect to nearest neighbors by about 9 nm (D/7)	67 nm	(112, 130, 134, 139, 140)
SLS	Segments equal to the molecular length of tropocollagen with asymmetric banding pattern	280 – 300 nm	(141–144)
SLS symmetric	Equivalent to SLS but with symmetric banding periodicity	280 – 300 nm	(117, 145)
SLS fibrils	Fibrils with periodic asymmetric banding pattern	270 nm	(116, 146, 147)
FLS I - IV	A class of non-D-periodic symmetric fibrils	90 – 260 nm	(113, 114, 117, 127, 148–150)

Table 2.2.: *Observed polymorphic forms of collagen type I (modified after (138)).*

Apart from experimental conditions mentioned above, collagen polymorphism also originates from both the amino acid sequence of the tropocollagen molecules as well as the predominant type of interactions driving the fibrillar assembly. It was already demonstrated that for the case of native-type aggregation, the $n \times 67$ nm stagger between neighboring molecules has its origins in the pseudo-periodic distribution of hydrophobic and charged side chains (88). On the other side, D-periodic symmetric collagen is mainly

produced either at low pH (4.3–5.5) or after enzymatic treatment. Such a low pH is usually associated with a very low extent of dissociated aspartic and glutamic acid chains, thus creating conditions which are inhibiting the electrostatic interactions between collagen molecules, leaving the hydrophobic interactions as the only possible driving forces for assembly of DPS structures (138). The origin of FLS forms usually lies in the distribution of unpaired positively charged side chains in the amino acid sequence. Adjacent molecules are typically held together by a bridging interaction between these charges using a variety of polyanions. The electrostatic interactions of the remaining positive charges must be effectively neutralized as a consequence of each one being paired with a negatively charged side chain within the sequence. The formation of polar SLS is either associated with a direct hydrophobic interaction between large, uncharged side chains, or an indirect bridging interaction between charged side chains via some non-collagenous molecule. Earlier studies that small high negatively charged molecules as ATP (141) or synthetic polysulfonates (129) successfully participate in the formation of SLS fibrils by bridging adjacent side chains having a net positive charge. It appears, that the principles governing the arrangement of collagen molecules in SLS and FLS are similar, since in both cases the interaction between tropocollagens are mediated by another type of molecule. There's the general notion that in the case of SLS that is usually a high negatively charged and small molecule, while the FLS formation is favored by the presence of less electronegative type of GAG or glycoproteins (138).

2.3. Factors affecting collagen fibril formation and structure *in vitro*

As already mentioned, collagen type I fibrillogenesis is a very well studied and described entropy-driven self-assembly process. It has been shown that the *in vitro* fibril formation is multistep process, conventionally separated in 2 phases – a lag (nucleation) phase with almost none or minuscule increase in turbidity of the solution, and a growth (exponential) phase which is distinguished by a sigmoidal increase of the solution optical density (151, 152). Previous studies on the kinetics of this process have shown that the nucleation phase, in which the soluble collagen particles accrete to preform nuclei (activation centers), predominates over growth and that the size of the fibrils is determined during this lag period (153). The nucleation phase accounts for the formation of linear dimers and trimers in which the neighboring molecules are 4D-staggered. Later on lateral accretion of these discretely sized intermediates leads to formation of narrow fibrils which strongly interact until bigger molecules are formed, resulting in a sharp increase in solution turbidity and sigmoidal slope of the turbidimetry curve (152) (Fig.2.8).

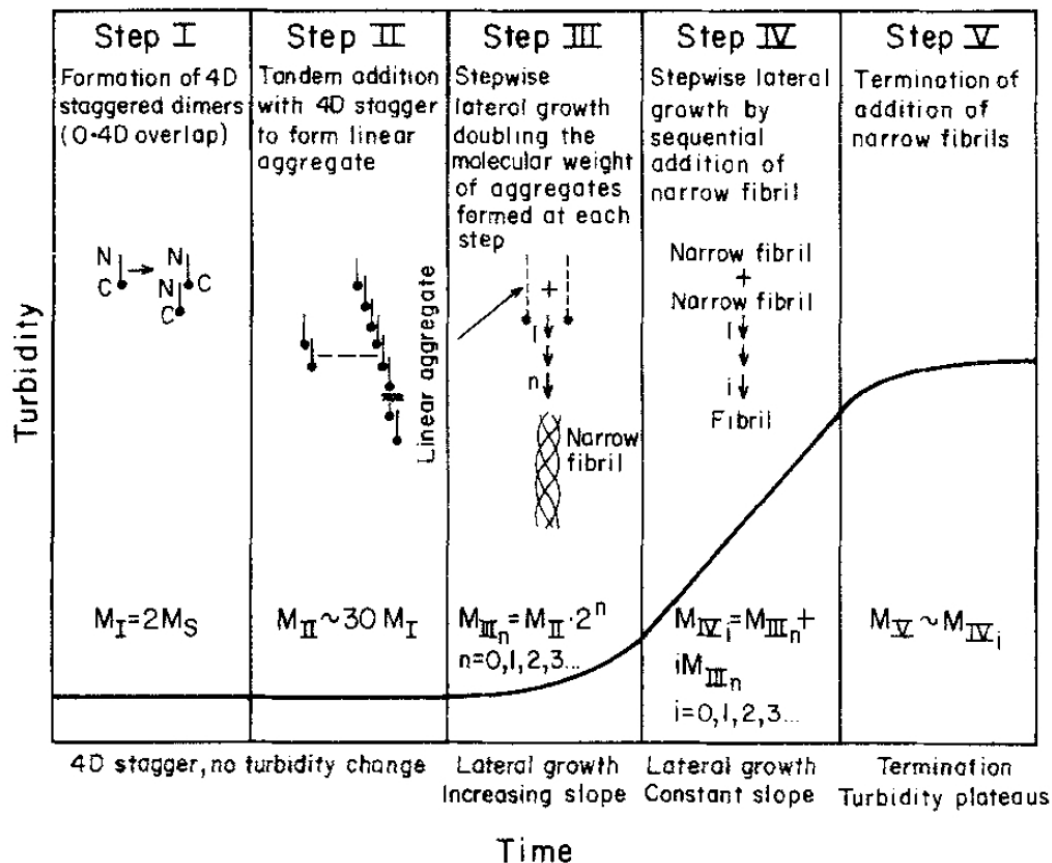


Figure 2.8.: Schematic linear and lateral growth models for type I collagen fibrillogenesis (adapted from (152)). Single molecules are represented by the symbol $N \text{---}\bullet \text{---} C$ where N and C are the amino and carboxylic ends of the molecule and M_S is the molecular weight. Steps I and II involve the formation of 4D staggered dimers (0.4D overlap, $D = 67 \text{ nm}$) and 4D linear growth of these initial aggregates. Step III involves lateral aggregation of linear aggregates in a stepwise fashion, such that the rate of change of molecular weight increases in each successive step. Narrow fibrils are formed at the end of the step III wrap around each other in step IV increasing fibrillar diameter. Growth terminates when no additional narrow fibrils are available.

A number of factors have been shown to influence both the kinetics of the process and the resulting structure of the collagen fibrils.

2.3.1. Temperature

Usually an increase of temperature decreases the lag time, and therefore accelerates either initiation or linear growth (151, 154, 155). There is a so-called memory effect, observed if a sample is cycled between temperatures of 20–37 °C and 4 °C during the nucleation phase. It suggests that initiation of formation of an active linear species is the rate limiting step (154, 155). The temperature independence of the lag time after short periods at high temperature (155) is an evidence that once formed active initial linear species are stable even at 4 °C. Other studies with increasing the temperature of the reaction in the range 29–35 °C showed a similar decrease in the turbidity lag and increased rate of

propagation as assayed by turbidimetry (123). However, the effects of temperature on the rate of assembly above 37 °C were opposite to the effects, seen at temperatures below 37 °C. In the range of 37–41 °C, the turbidity propagation rate decreased markedly with temperature. Also the turbidity lag increased. It has to be pointed out that only lag is affected by temperature while growth phase is particularly independent (154). A similar study by the same group also showed a pronounced differences in the morphology of the fibrils. Fibrils formed at 37 °C had highly tapered and symmetrical pointed tips, and the pattern of cross-striations in the pointed tips indicated that all the molecules were oriented so that the N-termini were directed towards the tip. At the same time, fibrils grown at 29–32 °C were thicker, while one of the ends formed at 29 °C was blunt and the other one was pointed (156). Similar dependence on fibril diameter was observed for temperatures of 37, 30 and 25 °C (124).

2.3.2. *pH* value

Usually the lag or exponential half-time decreases with increasing *pH* between 6 and 8 (135,151) even though the net charge on type I collagen does not change significantly within this *pH* range (157). A separate study of the effect of *pH* value (5.5–8.5) on fibril size showed that in general, fibrils formed at acidic *pH* tended to have larger fibril diameters than those formed at the neutral and basic *pH* values, a trend which was also observed as a combined effect with temperatures in the range 25–37 °C (124). Below *pH* 4.6 and above 10.3 at 23 °C lateral aggregation occurs less rapidly than at *pH* 7.9 indicating that the lateral aggregation occurs most rapidly at a *pH* where the net charge is minimized (152). Additionally the solution *pH* has been shown to affect the collagen type I morphology. *pH* 5–6 leads to the formation of large D-banded spindle-like bundle of fibrils with multiple lateral misalignments of the D-banding across the bundles. Increasing the *pH* to 7–9 results in the characteristic parallel-sided typical 'mature' D-banded collagen type I fibrils (125).

2.3.3. Presence/absence of telopeptides

Intactness of the N- and C-telopeptides has a marked effect on fibril formation. It is generally accepted that the extrahelical terminal peptides play a crucial part in fibril nucleation and growth (158,159). Commercially available fibrillar collagens are of two types, either acid soluble or pepsin-solubilized (33). In acid soluble collagen (ASC), the telopeptides are usually intact, and these help both to initiate fibril formation and to produce long cylindrical fibril. Pepsin-solubilized collagen (PSC) is produced by preparing tissue extracts with pepsin, which digests most protein structures except for the main

collagen triple-helical region depending on the degree of treatment. As a consequence, the non-helical telopeptides are mostly removed by this procedure making self-assembly more difficult. Additionally, selective removal of the N-telopeptides is known to result in the formation of D-periodic symmetric fibrils, in which molecules assemble in an antiparallel manner throughout the fibril length, while partial loss of the C-telopeptides results in relatively short cigar-shaped D-periodic tactoids (84). The importance of telopeptide interactions has been further demonstrated by PROCKOP and FERTALA (160) who showed that exogenous peptides corresponding to N- or C-telopeptides could inhibit fibril formation. Other studies also emphasized the importance of telopeptide to collagen type I kinetics by showing that tropocollagens with more intact telopeptides form fibrils more rapidly than those with degraded telopeptides (158). It also has to be noted that the degree of telopeptide removal seems to play a significant role in defining the fibril morphology/symmetry as endorsed in earlier studies (120, 121, 161). Nevertheless, there are also cases where the asymmetry of the fibrils is preserved (130, 154), once again suggesting that the extent of telopeptide removal can govern either symmetric or asymmetric alignment.

2.3.4. Effect of concentration

Both linear and lateral growth have been shown to be accelerated with incremental increase of concentration in the range of 0.1–10 mg/ml (147, 151). It is proposed that the rate and extent of fibrillogenesis *in vitro* is controlled by the concentration of the linear aggregates and that the effects of concentration on fibrillogenesis is affected by the concentration of these aggregates. Concentration dependence of the lag time is probably also associated with initiation via its effect on the single molecule-linear dimer equilibrium and on the rate of conversion of dimers to linear trimers (162) (Fig.2.8). It is also interesting to note, that the reversibility of lateral growth between narrow and wide fibrils seems to be both temperature and concentration dependent (152). On other side, it is also rather interesting to know what is happening in the high concentration range which is close to that of living tissues (40–300 mg/ml). One of the most remarkable properties of collagen solutions is that they form lyotropic liquid-crystal phases above critical concentration of 80–85 mg/ml. While increase of concentration above 100 mg/ml in both acidic and neutral *pH* resulted in increase of collagen kinetics, it is interesting to note that the increase of concentration in that range had a non-linear effect on fibril morphology. In the 40–80 mg/ml range fibrils were small and thin (with a length/diameter aspect ratio of approximately 10–20), with little size polydispersity and no preferred orientation. Their width increases with concentration, from 40 to 80 nm at 40 mg/ml collagen to 80–120 nm at 80 mg/ml. At 100 mg/ml, there is a significant change in the fibril morphology with a

much lower aspect ratio of 4–5 and diameters exceeding 1.2 μm . Further increase of 200–300 mg/ml led to formation of shorter (1 μm) and thinner (< 100 nm) homogeneously distributed fibrils (163).

2.3.5. Impact of GAGs and PGs

The relatively complex nature of collagen and GAG interaction involves both electrostatic and short range non-electrostatic forces. The first one is determined by the high negative charge of the GAG sulfate groups and the positive amino acid residues along the collagen chains. The latter one leads to the protein core attached to some GAGs in nature interacting with the non-cationic regions of the collagen helix (164, 165). It has already been shown that the preincubation of tropocollagen and GAGs led to an overall change of the fibrillogenesis curves resulting in either retardation or acceleration of the fibril formation (166, 167). It has been proposed that both size of the PG/GAG and its sulfation degree can influence together the final fibril size. Due to the different nature of these 2 component systems in comparison to pure collagen, it has been also suggested that not only the nucleation but also the exponential phase plays a significant role in the overall fibril formation, size and shape (166, 168). It was also suggested that glycoproteins from bovine tendon and bovine nasal cartilage and PGs from nasal cartilage have no effect on the lag time of self-assembly implying that any effect of these macromolecules on fibrillogenesis involves lateral growth (169). A large body of evidence shows that interactions with the so-called small leucine-rich proteoglycans (SLRPs) have marked effects on collagen assembly (170, 171). At present, 15 different types of SLRPs are known, each consisting of a single polypeptide chain (or protein core) with an N-terminal cysteine rich cap, followed by several leucine-rich repeat motifs and in most cases a C-terminal disulphide bonded cap. In PG form, a small number of GAG chains, either CS/DS or KS, are covalently attached to the protein core. SLRPs known to affect collagen assembly include decorin, fibromodulin, lumican, biglycan, keratocan and osteoglycin/mimecan. Early *in vitro* studies showed that decorin and fibromodulin can markedly interfere with collagen fibril formation, resulting in delayed assembly and usually reduced fibrils diameters. Removal of the GAG chains has little effect, showing that this is largely a property of the protein core. Lumican has similar effects *in vitro*, while biglycan appears to bind to collagen without affecting fibril assembly (33).

The interaction of decorin and collagen I has been studied in some detail (172). Unlike fibrils formed *in vitro*, fibrils isolated from tissues show diameter limitation for most of their length, as evidenced by a constant axial mass distribution. This is thought to be, at least in part, due to interactions with decorin that coats the fibrils preventing further accretion. Interestingly, the amount of decorin appears to be less at the fibril tips. This

is to be expected if the stoichiometry of binding of decorin to collagen is constant, since the number of molecules exposed on the surface, as a proportion of the total number of molecules in a fibril cross-section, increases as the tip diameter becomes smaller. Thus, tips are coated with a relatively small amount of decorin that will therefore no longer prevent fibril growth, until a limiting diameter is reached. This provides a mechanism for fibril to grow in length whilst maintaining a constant diameter. It also permits early fibrils to fuse end to end, with the molecules pointing in the same direction, or in an antiparallel manner by C-C fusion, which creates bipolar fibrils with two N-terminal tips. The contemporary model for localization of the DS-containing decorin utilizes a specific interaction between the non-covalently attached 'horseshoe-shaped' leucine-rich-repeat (Fig.2.9 B) to its binding site along the collagen fibril (173). The anionic GAG chain linked to the N-terminal part of the protein core stretches out to a neighboring collagen fibril, duplexing head-to-tail (antiparallel) with a DS chain from a decorin attached to the second fibril, thereby producing an interfibrillar bridge (Fig.2.9 A).

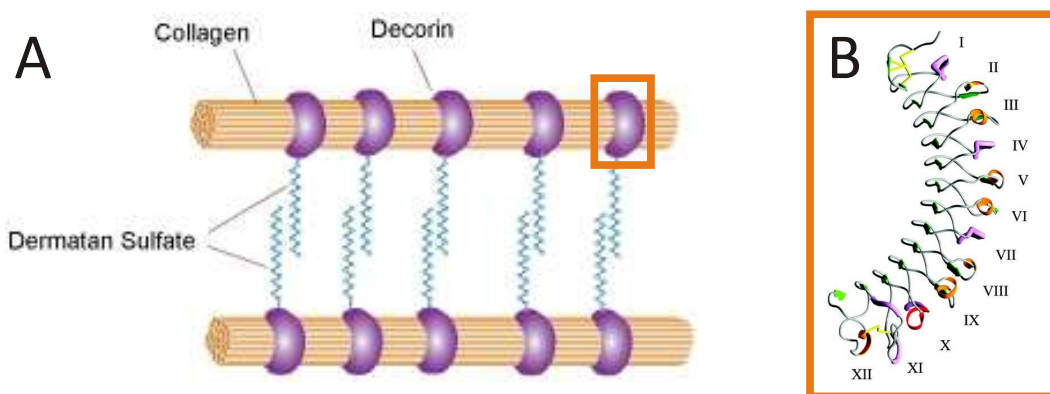


Figure 2.9.: 'Horseshoe' model for interfibrillar localization of decorin (modified after (173, 174)) (A). (B) Ribbon-diagrammatic representation of the structure of the 12-LRR domain of bovine decorin (adapted from (175)) interacting with the collagen surface.

While SLRPs have usually been found to diminish the rate of fibril formation, this is not always the case. Recombinant lumican, for example, has been found to accelerate fibril formation *in vitro* (176), as have other ECM molecules, such as dermatopontin (177), tenascin-X (178), perlecan (179), hevin (180) and cartilage oligomeric matrix protein (181). It is likely that such interactions stabilize the initial nuclei that form during the lag phase prior to subsequent fibril growth.

The presence of high negatively charged molecules as GAGs was also shown to affect fibril morphology. Previous studies show that various GAGs in the presence of both ASC (24), as well as PSC (129, 182, 183) could lead to the formation of fibrils with spindle-like morphology.

2.3.6. Interplay with other collagens

Fibril size and interface properties of collagen fibrils vary widely across various tissues, which is often related to the heterotypic composition of these microenvironments. The current model considers the interplay of heterotypic collagens, fibril-associated collagens, and cofibrillar macromolecules that alter the accretion properties of available procollagen molecules as a requirement to form a typical collagen fibril with its characteristic cylindrical central shaft section and differential tip shapes. Such heterotypic fibrils are quite usual for most connective tissues, particular examples being collagens I, III and V in skin, as well as types I and V in cornea. Due to the rather slow N-terminal processing of procollagen III, the amount of bound pN-collagen III exerts negative steric control on the fibril diameter *in vitro* (119). Similar reasoning applies also to collagen I/V fibrils in cornea, where the N-terminal processing is at best only partial, leaving largely located N-terminal extensions which impede fibril growth, with the rest of the molecules being buried within the fibril interior (Fig.2.10).

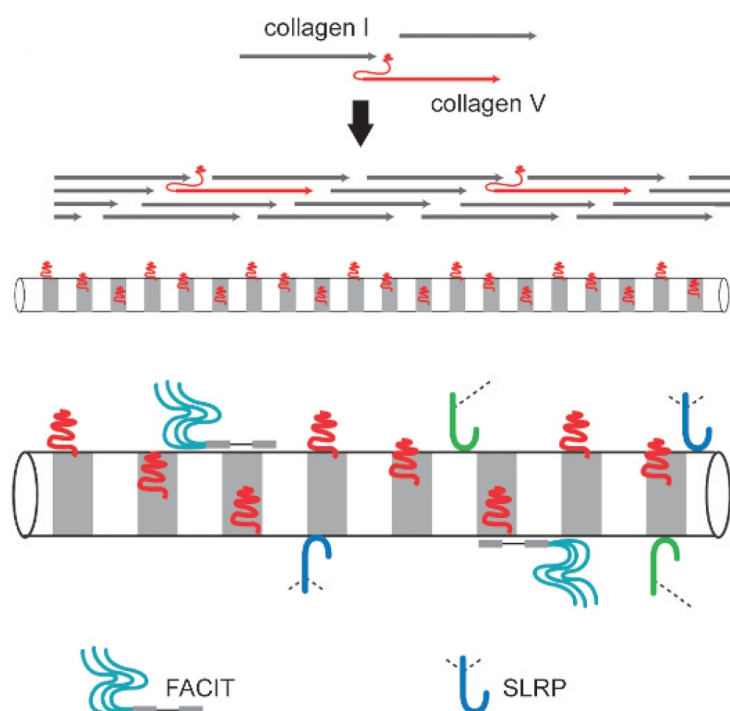


Figure 2.10.: Heterotypic assembly of collagen type I and V (modified after (184)). The complex landscape of the corneal collagen fibril surface, showing N-terminal extensions of collagen V, surface bound FACITs and SLRPs.

Steric blocking by N-terminal extensions is not the only mechanism by which the minor fibrillar collagens might limit heterotypic fibril diameter. Another mechanism is by altering the rate of fibril nucleation. This has been shown most dramatically in the case of collagen V, where complete deficiency of pro- $\alpha 1(V)$ chain leads to the absence of procollagen V molecules and an almost total lack of collagen fibrils in the dermis, despite

the normal levels of collagen type I (185). The minor fibrillar collagens therefore seem to act as initiators of fibril formation, during the early nucleation stage. Large amounts of collagen V would therefore lead to a greater number of heterotypic fibrils. For a given amount of collagen, the presence of a greater number of fibrils would result in the average fibril diameter being smaller (33).

2.4. SFM as 'nanotool' for morphological and mechanical characterization

2.4.1. Basic principle and operating modi

In the last 2 decades, SFM has emerged as a powerful tool in life sciences and medicine research giving ultrahigh resolution in real time under near physiological conditions. Being essentially a local probe technique, SFM extends our sense of touching into the micro- and nanoworld and thus provides us with new complementary insights and details which are not observable with other instruments (186). Introduced as a technique, by BINNIG, together with QUATE and GERBER in 1986, it utilizes local probes as small objects (the very end of a sharp nanostylus/tip) which interactions with the sample surface can be sensed at selected positions (187). With no electron transport involved the device was superior to other optical microscopy techniques that all kinds of molecules, including insulators, could be studied down to atomic resolution. The essential part of an SFM, is the tip that determines by its structure, the type of interaction with a surface; and by its geometry, the area of interaction. The original idea for the SFM was to measure the van der Waals interaction of an atom at the very end of the tip with atoms at a surface of a solid substrate. To bring a single atom at a tip close to within an Angstrom distance toward a surface is only possible if the surface is atomically flat, such as for example, the crystalline surface of mica (Fig.2.11 C). If the surface is rough on a nanometer scale (Fig.2.11 B), groups of atoms can interact and determine the possible resolution, according to their size. With a roughness at the micrometer scale (Fig.2.11 A) the macroscopic level is reached where instruments like the surface profiler are able to measure surface roughness.

The tip, which is mounted at the end of a small cantilever, is brought in closest contact with the sample and gives rise to the image through its force interactions with the surface (188). The contemporary tip-cantilever assemblies are typically fabricated from silicon or silicon nitride, using a technology similar to that applied to integrated circuit fabrication, thus allowing a good uniformity of characteristics and reproducibility of results (189, 190). The choice of cantilevers is essentially made according to their force (or spring) constant and resonance frequency, which in terms depends on the substrate

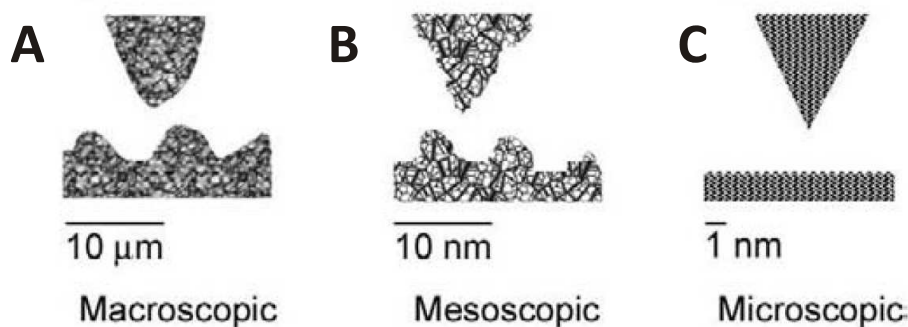


Figure 2.11.: *Scanning probe tip structures shown at different scales (adapted from (186)).*

stiffness and imaging environment (dry or in liquid). Images are formed by recording the effects of the interaction forces between tip and surface as the cantilever is scanned over the sample. The movement of the tip closer to the surface and scanning with precision fitting to the highest resolution is ensured by a piezo-electric tube scanner which allows for easy movement in all three directions due to its ability to respond with change in size proportionally to and applied electric field (188). A laser beam is reflected from the backside of the cantilever (often coated by a thin metal layer to make a mirror) onto a position-sensitive photodetector consisting of two side-by-side photodiodes. The difference between the two photodiode signals indicates the position of the laser spot on the detector and thus the angular deflection of the cantilever. The scanner and the electronic feedback circuit, together with the sample, cantilever, and optical lever form a feedback loop, ensure not only the possibility to measure forces acting on the sample but also control by allowing acquisition of images at very low tip-to-sample forces. The scanner is an extremely accurate positioning stage used to move the tip over the sample (or the sample under the tip) to form an image, and generally in modern instruments is made from a piezoelectric tube. As the probe is scanned over the surface, a topographic image is obtained by storing the vertical control signals sent by the feedback circuit to the scanner at moving the tip up and down to follow the surface morphology while keeping the interaction forces constant. A schematic diagram of the basic SFM operating principle is shown in Fig.2.12 A:

Depending on the presence or absence of an additional control mechanism that forces the cantilever to oscillate in proximity to its resonant frequency there are a 2 general 'families' of SFM modes of operation: static and dynamic. The static (DC) modes, record the constant (static) deflection of the cantilever, whereas in dynamic (AC) modes the feedback loop will try to keep at a set value not the deflection but the amplitude of the oscillation of the cantilever while scanning the surface. From a physical point of view, one can make a distinction between the two modes depending on the sign of the forces involved in the interaction between tip and sample, that is, by whether the forces there are attractive or repulsive (188, 192). Idealized plot of the forces between tip and sample

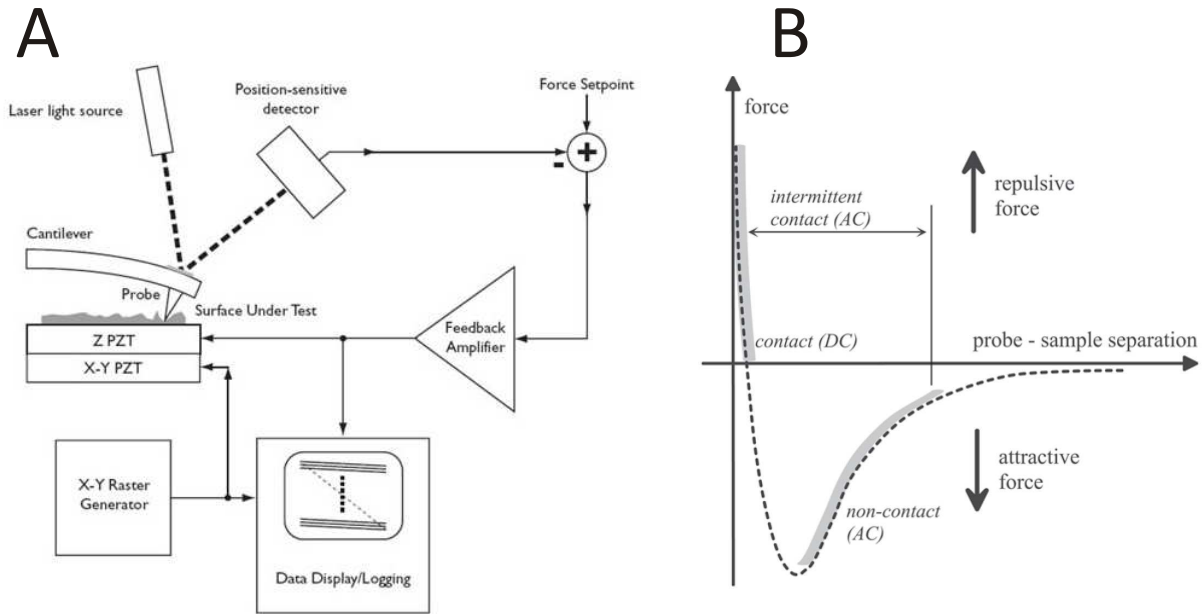


Figure 2.12.: *Principle and setup of SFM. (A) Elements of a basic sample-scanned SFM (from (191)). (B) 'Anatomy of an idealized plot' of the forces between tip and sample, highlighting regions where typical operating modes take place (from (188)).*

is shown in Fig.2.12 B, highlighting the regions where typical imaging modes occur.

A list of the most commonly used DC and AC modes with their description, pros and cons is given in table 2.3:

The most common and heavily used DC operation mode is the contact mode in which the tip is raster-scanned across the surface and adjusted to maintain a constant deflection, and therefore constant height above the surface. Image contrast depends on the applied force, which again depends on the cantilever spring constant. Because the SFM relies on the forces acting between the tip and sample, knowing these forces is important for proper imaging. The force is not measured directly, but calculated by measuring the deflection of the lever, and knowing the stiffness (force constant) of the cantilever. The force is calculated from HOOK's law, where F is force [N], k is the spring constant of the cantilever [N/m], and v is the cantilever deflection [m]:

$$F = -kv \quad (2.1)$$

In intermittent contact (AC) mode the cantilever is driven to oscillate up and down near its resonant frequency (w). The amplitude of this oscillation is usually greater than 10 nm, typically 100–200 nm. During scanning a number of adhesive/repulsive forces are acting between the tip and the sample which leads to either decrease/increase of the amplitude of the cantilever (dampening effect). Similar to contact mode, an electronic servo uses the piezoelectric actuator to adjust the height between the tip and the surface in order to maintain a preset cantilever oscillation amplitude. As implied in the name of

SFM mode	Applied forces, N	Pros vs. cons
Contact	$10^{-9} - 10^{-6}$	<ul style="list-style-type: none"> + High scan speed/throughput + Able to achieve high (atomic) resolution + Better tracking of samples with extreme changes in vertical topography - High lateral/shear forces leading to distortion of image features - High capillary forces in ambient atmosphere - Combination of high lateral and normal forces can result in reduced spatial resolution and damaging of soft biological samples (scraping)
Intermittent contact	10^{-9}	<ul style="list-style-type: none"> + High lateral resolution on most samples (1–5 nm) + Lower forces and less damage to soft samples imaged in air + Lateral forces are virtually eliminated (no scraping) - Slower scan speed in comparison to contact mode
Non-contact	$< 10^{-12}$	<ul style="list-style-type: none"> + Extremely low forces exerted on the sample surface - Lower lateral resolution due to tip-sample separation - Slower scan speed than intermittent contact and contact modes (to avoid contact with adsorbed fluid layer) - Usually applicable only to extremely hydrophobic dry surfaces, where adsorbed fluid layer is at minimum

Table 2.3.: Comparison of the most basic SFM modi (adapted from (193)).

the non-contact mode, the oscillating probe is brought into proximity (but not touching) the sample while it senses attractive VAN DER WAALS forces that induce a frequency shift in the amplitude of the cantilever (usually less than 10 nm). Images are taken by keeping a constant frequency shift during scanning, and usually this is performed by monitoring the amplitude of the cantilever oscillation at a fixed frequency and feeding the corresponding value to the feedback loop exactly as for the DC modes (188).

Depending on the application additional SFM modi include lateral force microscopy, phase contrast microscopy, etc.

2.4.2. 'Non-invasive' tool for structural analysis

With respect to life sciences, first and foremost, historically SFM was heavily used for studying and characterization of numerous single molecules, protein complexes and structural characterization of supramolecular architectures. Soon after its discovery there was a particular increase in reports studying biologically relevant molecules as bulk crystals of

amino acids (194) and polymers (195). Followed by the first molecular resolution images of individual actin filaments in solution (196), DNA (197), purple membrane fragments (198), gap junction membranes (199), etc., SFM gave enough evidence for its applicability for imaging of biological molecules in their native environment.

Although it is able to analyze molecules in their almost native physiological conditions, SFM has been called 'unnatural' since it looks at biomaterials on surfaces instead of 'test tubes'. However, living systems are filled with surfaces, especially membranes, hence surfaces are arguably more relevant biologically than test tubes. In this context, a valuable direction for biological SFM is the development of flat biologically relevant surfaces, a good example of which are lipid membranes (200). It is exactly the lipid membranes, which allowed some of the most impressive work in the area of imaging single protein complexes embedded in lipid membranes. Excellent examples include the first real high resolution images of membrane protein porin OmpF (201), bacteriorhodopsin (202, 203) in which authors were able to show individual beta-turns and loops and even manipulate them on the nanoscale. Cells are much more difficult to image due to their softness and susceptibility to tip-induced membrane damage (204). Nevertheless, high-resolution images have been acquired for fungal (205), bacterial and mammalian cells (206).

Being superior to any other imaging technique in terms of resolution, current novel SFM technologies such as 'high speed bio-SFM' aim towards understanding and unraveling processes occurring in the millisecond regime at the molecular level (207–209). Conventional SFMs take at least 30–60 seconds to capture an image, while dynamic biomolecular processes occur on a millisecond timescale or less. Most conventional modifications utilizing the use of high resonant frequency cantilevers operating at more than 1–2 MHz which allows for ultra high rate scanning both of dry and liquid samples with more than 1000 frame per second (fps). The approach have been successfully presented for both high resolution imaging of single molecules and organelles as collagen, chromosomes, and for tracking of structural changes of biological molecules while they are at work, such as sliding of filaments on molecular motors, etc (210).

The potential of SFM to measure ultra-low forces at high lateral resolution has paved the way for measuring of inter- and intramolecular forces of biomolecules on the single molecule level. Current molecular recognition force microscopy studies open the possibility to detect specific ligand-receptor interaction forces and to observe molecular recognition of a single ligand-receptor pair. The general strategy usually involves binding of ligands to SFM tips and receptors to probe surfaces (or vice versa) (211). Such experiments require that one or few ligand molecules are permanently tethered to the apex of the SFM tip, usually by covalent bonding via a flexible linker molecule. Cross-linkers with 6–8 nm length (corresponding to 18 ethylene glycol units plus termini) are a good compromise between high mobility of the ligand and narrow lateral resolution of the target site. A

typical polyethyleneglycol (PEG) linker has one amino-reactive end for attachment to the tip and one reactive end for linking of ligands (212) (Fig.2.13 A). The interaction forces are measured in a 'force-distance' cycle, an example of which is shown in Fig.2.13 B.

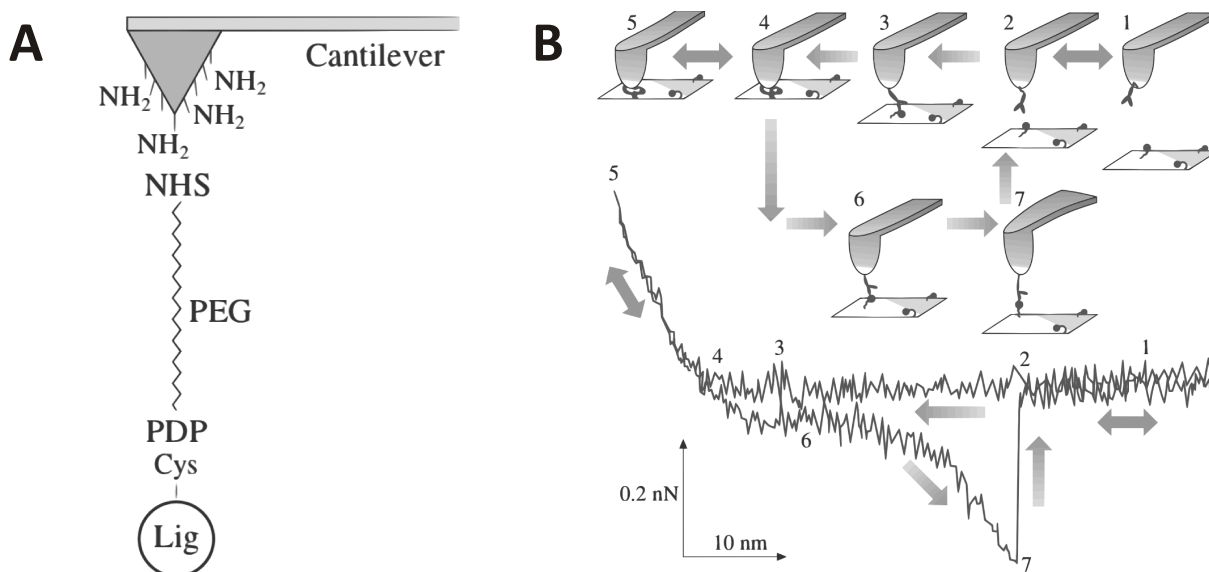


Figure 2.13.: *Tip modification (A) and subsequent single molecule recognition event (B) detected by SFM (adapted from (211, 213)). Binding of the antibody on the tip to the antigen on the surface during approach (trace points 1 to 5) physically connects the tip to the sample. This causes a distinct force signal of distinct shape (points 6 and 7) during tip retraction, reflecting extension of the distensible cross-linker-antibody-antigen connection. The force increases until unbinding occurs at an unbinding force of 268 pN (points 7 to 2). If the ligand on the tip doesn't form a specific bond with one of the receptors on the sample surface, the recognition event is missing and the retrace curve looks like trace.*

2.4.3. Application in nanomechanical characterization of proteins

As mentioned above mechanical forces exerted by cells onto various substrates and vice versa are important for their function and differentiation behavior. At the most basic level stiffness can regulate cell growth and viability, as well as resistance to apoptosis. It can also affect lineage commitment and differentiation of precursor cells (214, 215). Therefore, experiments measuring the mechanical properties of proteins and bioscaffolds on the nanoscale are key to understanding their role in processes and phenomena they're a part of. In this context, SFM comes as a very powerful tool to mechanically characterize such molecules by making use of earlier previously defined biophysical and mechanical formulations. This is typically done while working in static mode in order to obtain force-distance curves (see above, Fig.2.12). Ideally, this provides the force applied to the tip and the tip sample distance, which furthermore are corrected by subtracting the sample (Z-piezo) and the deflection of the cantilever. Essentially, by implementing this force-distance behavior in various setups and regimes one can calculate various parameters as

stiffness (216, 217), tensile stress (218, 219), bending and shear moduli (220, 221), and so on.

Being the main structural elements in the ECM, collagens and collagen-containing xenogeneic scaffolds attract a lot of interest with respect to their mechanical characterization. Depending on the type of interaction between the cells and ECMs, they can exert different forces ranging from crawling through the matrix and bending its elements, as well as reorganizing the fibrils by pulling and stretching on them (tensile stress). Nevertheless due to the morphological properties of the fibrillar collagens, last decade has seen a keen interest in the analysis of their bending modulus (E_B).

The expected beam deflection of a freestanding nanobridge upon the application of a concentrated point load (F) at a certain position (x) can be modeled by using the EULER-BERNOULLI beam equation with the basic assumption of linear elastic deformations of an isotropic beam.

$$\frac{d^2}{dx^2} \left(EI \frac{d^2 v}{dx^2} \right) \quad (2.2)$$

If a cylindrical beam (i.e. collagen fibril) with a radius (r) is considered homogeneous and isotropic, the bending stiffness (flexural rigidity) would correspond to YOUNG's modulus (E) and could be written as EI , with I being the second moment of the cylindrical cross-section (area) ($I = \pi r^4/4$) (222). Depending on the different boundary conditions there are a few typical models which implement the mobility of the beam's end. Variations include clamped (completely fixed), pinned (fixed at a single point), simple supported (freely sliding) ends. At moderate force regimes (up to 20 nN and deformation below 5%) the adhesion forces in dried state between substrate and the beam are considered sufficient to ensure a complete immobilization. Nevertheless at physiological conditions, the collagen filaments are prone to sliding. Therefore, the following most common 4 models should be considered (Fig.2.14).

To examine the E_B of the fibrils we examine the linear behavior (slopes) (dF/dv) of deflections during force spectroscopy. In the case of the 4 models discussed above the slopes of the force-deformation curves are expressed as follows (for $0 \leq a \leq L$) (223):

$$\frac{dF}{dv}(a) = 3E_B I \frac{L^3}{(L-a)^3 a^3} \quad (2.3)$$

$$\frac{dF}{dv}(a) = 3E_B I \frac{L^2}{(L-a)^2 a^2} \quad (2.4)$$

$$\frac{dF}{dv}(a) = 12E_B I \frac{L^3}{a^3 (L-a)^2 (4L-a)} \quad (2.5)$$

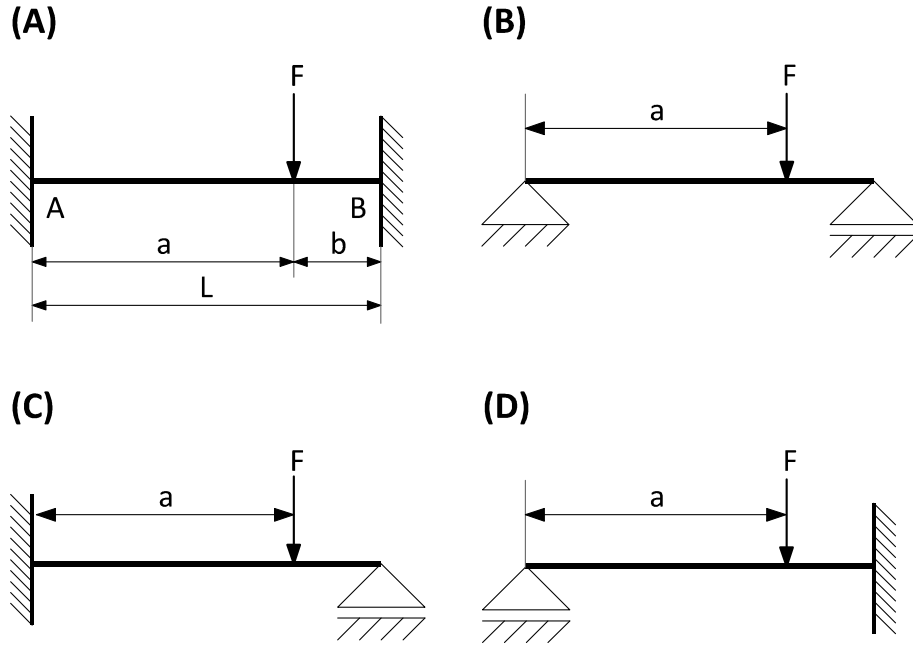


Figure 2.14.: Models for the deflection of a concentric beam upon application of concentrated load. (A) Clamped - Clamped (double-clamped) (Eq.2.3) vs. (B) Pinned - Simple supported (Eq.2.4) vs. (C) Clamped - Simple supported (Eq.2.5) vs. (D) Simple supported - Clamped (Eq.2.6).

$$\frac{dF}{dv}(a) = 12E_B I \frac{L^3}{a^2(L-a)^3(a+3L)} \quad (2.6)$$

The most commonly applied model with collagen fibrils in dried state is the double-clamped since the fixed-end conditions are usually met. Nevertheless, in liquid environment a further modification of the substrate should be considered in order to ensure the chemical binding of the ends of the suspended fibrils to the substrates. If a double-clamped model is assumed, the elastic deformation of the suspended part of the fibril resulting from a concentrated load can be regarded as the sum of deflections contributed by bending (v_B) and shearing (v_S) (224). In this case, neglecting the end effects of the substrate yields the following equation:

$$v = v_B + v_S = \frac{FL^3}{192EI} + f_S \frac{FL}{4GA} = \frac{FL^3}{192E_B I} \quad (2.7)$$

where v is the deflection, G is the shear modulus, A is the cross-sectional area of the fibril, f_S is a geometric factor of shear (equal to 10/9 for a cylindrical beam). If the shear contribution is neglected (when $\frac{L}{R} \geq \sqrt{\frac{E}{G}}$ condition is met), then E_B corresponds to E . When G cannot be ignored, the expression of E_B for a cylindrical rod follows from Eq.2.7 in the form (221):

$$\frac{1}{E_B} = \frac{1}{E} + \frac{120}{9G} \times \left(\frac{r^2}{L^2} \right) \quad (2.8)$$

Furthermore, G can be determined from the slope of the linear relation between $1/E_B$ and r^2/L^2 .

3. Materials and Methods

3.1. Materials

3.1.1. Chemicals

Product	Supplier
β-mercaptoethanol (2-mercaptoethanol)	Fluka, Sigma-Aldrich Chemie GmbH, Steinheim, Germany
2-Morpholinoethanesulfonic acid monohydrate (MES)	Fluka, Sigma-Aldrich Chemie GmbH, Steinheim, Germany
(3-Aminopropyl)triethoxysilane, ≥ 98%	Sigma-Aldrich Chemie GmbH, Steinheim, Germany
4'-n-octyl-4-cyanobiphenyl (8CB)	Sigma-Aldrich Chemie GmbH, Steinheim, Germany
Acetone 99.5+ %, for analysis	Acros Organics, Geel, Belgium
Agarose type IX-A, ultra-low gelling temperature	Sigma-Aldrich Chemie GmbH, Steinheim, Germany
Ammonium hydroxide, for analysis, 28–30 wt% solution of NH ₃ in water	Acros Organics, Geel, Belgium
Blyscan sulfated glycosaminoglycan assay kit	Biocolor Ltd., Newtownabbey, Northern Ireland
Chloroform, for analysis	Merck Chemicals KGaA, Darmstadt, Germany
Collagen type I from bovine skin (acid soluble), 7 mg/ml	USB Europe GmbH, Staufien, Germany
Collagen type I from bovine skin (pepsin-solubilized), 2.9–3.2 mg/ml (PureCol)	Nutacon, Leimuiden, Netherlands

Product	Supplier
Cysteine	Sigma-Aldrich Chemie GmbH, Steinheim, Germany
Ethylenediaminetetraacetic acid (EDTA) disodium salt	Amersham Pharmacia Biotech, Uppsala, Sweden
Ethanol 100% absolute, for analysis	VWR International GmbH, Darmstadt, Germany
Glutaraldehyde (25% in water)	SERVA Electrophoresis GmbH, Heidelberg, Germany
Heparan sulfate sodium salt from bovine kidney	Sigma-Aldrich Chemie GmbH, Steinheim, Germany
Heparin sodium salt from porcine intestinal mucosa (4–6 kDa), 170 USP U/mg	BioChemika, Fluka, Sigma-Aldrich Chemie GmbH, Steinheim, Germany
Heparin sodium salt from porcine intestinal mucosa, Grade I-A (17–19 kDa), ≥ 140 USP U/mg	Sigma-Aldrich Chemie GmbH, Steinheim, Germany
Heparin sodium salt from porcine intestinal mucosa, ≥ 140 USP U/mg	Sigma-Aldrich Chemie GmbH, Steinheim, Germany
Heparin, fluorescein conjugate	Invitrogen, Molecular Probes, Leiden, Netherlands
(Heptadecafluoro-1,1,2,2- tetrahydrodecyl)dimethylchlorosilane	ABCR GmbH & Co. KG, Karlsruhe, Germany
Hyaluronic acid potassium salt from human umbilical cord	Sigma-Aldrich Chemie GmbH, Steinheim, Germany
Hydrochloric acid solution	Fluka, Sigma-Aldrich Chemie GmbH, Steinheim, Germany
Hydrogen peroxide 35%	Merck Chemicals KGaA, Darmstadt, Germany
Hydroxylamine hydrochloride	Fluka, Sigma-Aldrich Chemie GmbH, Steinheim, Germany
Isopropanol 99.5%, for analysis	Acros Organics, Geel, Belgium

Product	Supplier
Methanol for HPLC	Acros Organics, Geel, Belgium
Modified SPURR embedding kit	SERVA Electrophoresis GmbH, Heidelberg, Germany
Mowiol® 4-88 antifade medium	Polysciences Inc., Warrington, PA, US
N-(3-dimethylaminopropyl)-N'-ethylcarbodiimide hydrochloride (EDC)	Fluka, Sigma-Aldrich Chemie GmbH, Steinheim, Germany
n-Heptane, GR for analysis	Merck Chemicals KGaA, Darmstadt, Germany
N-Hydroxysuccinimide (NHS)	Fluka, Sigma-Aldrich Chemie GmbH, Steinheim, Germany
o-Phthaldialdehyde	Sigma Aldrich-Chemie GmbH, Steinheim, Germany
Osmium tetroxide solution 4% (for electron microscopy)	Carl-Roth GmbH & Co, Karlsruhe, Germany
Papain (from <i>Carica papaya</i>)	Fluka, Sigma-Aldrich Chemie GmbH, Steinheim, Germany
Phenol	Sigma Aldrich-Chemie GmbH, Steinheim, Germany
Phosphate buffered saline (PBS)	Sigma Aldrich-Chemie GmbH, Steinheim, Germany
Phosphotungstic acid hydrate (PTA)	Fluka, Sigma-Aldrich Chemie GmbH, Steinheim, Germany
Poly(ethylene- <i>alt</i> -maleic anhydride) (PEMA), 400 kDa	Polysciences Inc., Warrington, PA, US
Poly(octadecene- <i>alt</i> -maleic anhydride) (POMA), 30 – 50 kDa	Polysciences Inc., Warrington, PA, US
Sodium acetate anhydrous	Fluka, Sigma-Aldrich Chemie GmbH, Steinheim, Germany
Sodium borohydride	Fluka, Sigma-Aldrich Chemie GmbH, Steinheim, Germany

Product	Supplier
Sodium chloride	Fluka, Sigma-Aldrich Chemie GmbH, Steinheim, Germany
Sodium cyanoborohydride	Fluka, Sigma-Aldrich Chemie GmbH, Steinheim, Germany
Sodium hydroxyde, for analysis	Fluka, Sigma-Aldrich Chemie GmbH, Steinheim, Germany
Sylgard 184 Silicon elastomer kit	Dow Corning, Arrow Direct, Leipzig, Germany
Tetrahydrofuran 99.6%, for analysis ACS, stabilized with BHT (THF)	Acros Organics, Geel, Belgium
Uranyl acetate	Plano GmbH, Wetzlar, Germany
Volusol cleaning agent (pepsin/hydrochloric acid)	VWR International GmbH, Darmstadt, Germany

3.1.2. Materials

Material	Supplier
3.05 mm Au-grids (400-mesh)	Plano GmbH, Wetzlar, Germany
3.05 mm Cu-grids (400- and 1500-mesh)	Plano GmbH, Wetzlar, Germany
3.05 mm Cu-grids (400-mesh) with Holey carbon films	Quantifoil Micro Tools GmbH, Jena, Germany
3.05 mm Cu-grids (400-mesh) with Formvar films	Plano GmbH, Wetzlar, Germany
3.05 mm Cu-grids (400-mesh) with Pioloform films	Plano GmbH, Wetzlar, Germany
3.05 mm Ni-grids (2000-mesh)	Plano GmbH, Wetzlar, Germany
6/12/96 well tissue culture plates	TPP, St. Louis, MO, US
Accu-Jet® pipette controller	BrandTech Scientific, Essex, UK
Borosilicate glass coverslips (24x24 cm ² , circular with ø 15–18 mm)	Carl-Roth GmbH & Co, Karlsruhe, Germany

Material	Supplier
Eppendorf Flex-Tubes® microcentrifuge tubes (0.5–2.0 ml)	Eppendorf AG, Hamburg, Germany
Filter paper discs	Whatman GmbH, Dassel, Germany
Millipore filters VivaSpin 20	Sartorius AG, Göttingen, Germany
Muscovite mica	Plano GmbH, Wetzlar, Germany
Polypropylene pestles (length 8.5 cm)	Bel-Art Products, Pequannock, NJ, US
Polystyrene tubes (15 and 50 ml)	Greiner Bio-One GmbH, Frickenhausen, Germany
Polytetrafluoroethylene (PTFE) filters (pore size 0.2 µm)	Carl-Roth GmbH & Co, Karlsruhe, Germany
Quarz capillaries (ø 1.5 mm)	Glasstechnik Fa. Wolfgang Müller, Schonwalde bei Berlin, Germany
Silicon wafers (microstructured)	GeSiM, Großerkmannsdorf, Germany
Zorbax SB-C18 columns (4.6 x 150 mm, 3.5 µm)	Agilent Technologies, Böblingen, Germany

3.1.3. Devices

Device	Supplier
Agilent 1100 LC-system with fluorescence detection	Agilent Technologies, Böblingen, Germany
Analytical scales CP 2245 (accuracy ± 1 µg)	Sartorius AG, Göttingen, Germany
Bandelin Sonorex Super 10P ultrasonic bath	SCHALLTEC GmbH, Mörfelden-Walldorf, Germany
BDK clean bench	Luft und Raumtechnik GmbH, Germany
Microtome RM2255	Leica Microsystems GmbH, Heerbrugg, Switzerland

Device	Supplier
Milli-Q water filtration system Q-Gard® 2	Millipore, Eschborn, Germany
Minishaker MS2	IKA® Werke GmbH & Co. KG, Staufen, Germany
Pellet pestle cordless motor	Kontes, Würzburg, Germany
<i>pH</i> meter pH538	WTW GmbH, Weilheim, Germany
Plasma cleaner Harrick	Laseranalytik Starna GmbH, Pfungstadt, Germany
RC5 spin coater CT62 C101	SUSS MicroTek AG, Garching, Germany
Rocking stage	IKA® Labortechnik GmbH & Co. KG, Staufen, Germany
SnowJet cleaning device	Applied Surface Technologies, New Providence, NJ, US
Specord S 10 spectrophotometer	Carl Zeiss GmbH, Jena, Germany
Sputter coater SCD 050	BAL-TEC GmbH, Schalksmühle, Germany
STAT-FAN YI B01-ODR	Ion-Care AB, Malmö, Sweden
Swivelling table KS 250 basic	IKA® Labortechnik GmbH & Co. KG, Staufen, Germany
Tabletop centrifuge 5403 (fixed rotor)	Eppendorf AG, Hamburg, Germany
Tabletop centrifuge <i>pico</i> (swing bucket rotor)	Heraeus Instruments, Gera, Germany
Temperature controller ETS-D4 fuzzy	IKA® Werke GmbH & Co. KG, Staufen, Germany
Thermoheater RCT basic	IKA® Labortechnik GmbH & Co. KG, Staufen, Germany
Thermomixer comfort	Eppendorf AG, Hamburg, Germany
Thermostat with Kelvitron t°C control	Heraeus Instruments, Gera, Germany

Device	Supplier
Ultra-Turrax T8 homogenizer	IKA® Werke GmbH & Co. KG, Staufen, Germany
Vacuum exicator DURAN	DURAN Group GmbH, Mainz, Germany
Vacuum oven	Heraeus Instruments, Gera, Germany
UV-VIS spectrophotometer GENios	Tecan Group Ltd., Männedorf, Switzerland

3.1.4. Software

Software	Developer
Chemstation software Rev. 08.01	Agilent Technologies, Böblingen, Germany
Chemwindow 5.1	Bio-Rad Laboratories GmbH, München, Germany
CorelDRAW Graphics Suite 13, X4	Corel Corporation, Ottawa, Ontario, Canada
Igor Pro 6.040	WaveMetrics Inc., Lake Oswego, OR, US
ImageJ 1.41f	National Institute of Health, US
LAS 1.8.2 build 1465	Leica Microsystems CMS GmbH, Wetzlar, Germany
MFP-3D software	Asylum Research, Santa Barbara, CA, US
NanoScope 5.12 R3 and 6.13 R1	Digital Instruments/Veeco, Santa Barbara, CA, US
Origin Pro 6.5, 7.5, 8.0	OriginLab Corporation, Northampton, MA, US
PicoScan 5.x	Agilent, US
PyMOL™ 0.99 rc 6	Delano Scientific LLC, Palo Alto, CA, US
SPIP 4.402 - 5.001	Image Metrology A/S, Hørsholm, Denmark
WSxM 4.0 Develop 8.6	Nanotec Electronica SL, Madrid, Spain

3.1.5. Microscopes

Microscope	Type	Supplier
MultiMode AFM (NanoScope IV controller)	SFM	Veeco, Santa Barbara, CA, US
BioScope AFM (NanoScope IIIa)	SFM	Veeco, Santa Barbara, CA, US
PicoSPM (SPM 1000)	SFM	Molecular Imaging, UK
MFP-3D™ Stand Alone AFM (ARC2 SPM)	SFM	Asylum Research, Santa Barbara, US
Omega EM 912 (at 120 kV)	TEM	Carl Zeiss, Germany
Tecnai 12 BioTWIN (at 100 kV)	TEM	FEI, Netherlands
XL 30 ESEM FEG (SE detector at 30 kV)	SEM	FEI-Phillips, Netherlands
Leica TCS SP1	cLSM	Leica Microsystems CMS GmbH, Wetzlar, Germany
Leica TCS SP5	cLSM	Leica Microsystems CMS GmbH, Wetzlar, Germany
Bruker AXS Nanostar (CuK α radiation, $\lambda = 1.54 \text{ \AA}$, generator power 4.05 kW)	WAXS	Bruker AXS, Karlsruhe, Germany

3.1.6. Cantilevers

Cantilever	Material	ω , kHz	ROC, nm	k_f , N/m	Supplier
Tap300	Si	300	< 10	40	BudgetSensors, Sofia, Bulgaria
Multi75	Si	75	< 10	3	BudgetSensors, Sofia, Bulgaria
SSS-NCL	Si	190	< 2	48	Nanosensors, Neuchatel, Switzerland
MLCT-AU (pos. C)	Si ₃ N ₄	7	< 50	0.01	ThermoMicroscopes, Sunnyvale, US

Cantilever	Material	ω , kHz	ROC, nm	k_f , N/m	Supplier
MLCT-AU (pos. D)	Si ₃ N ₄	15	< 50	0.03	ThermoMicroscopes, Sunnyvale, US
MLCT-AU (pos. E)	Si ₃ N ₄	38	< 50	0.10	ThermoMicroscopes, Sunnyvale, US
MLCT-AU (pos. F)	Si ₃ N ₄	120–	< 50	0.50	ThermoMicroscopes, Sunnyvale, US
DNP (pos. D)	Si ₃ N ₄	18	< 60	0.06	Veeco, Santa Barbara, US

3.2. Methods

3.2.1. Biochemical methods

3.2.1.1. Collagen type I - heparin cofibrillogenesis

Collagen-GAG cofibrils were reconstituted from a sterile solution of either pepsin-solubilized bovine dermal collagen (PSC) in 0.012 N HCl at *pH* 2.0 (PureCol™) or acid soluble calf skin collagen (ASC) in 0.075 M acetic acid (including thimerosal) at *pH* 3.7, with low molecular weight heparin (LMWH) ($M_W \approx 4-6$ kDa), high molecular weight heparin (HMWH) ($M_W \approx 17-19$ kDa), heparan sulfate (HS), or hyaluronic acid (HA). The acidic PSC stock solution was diluted with 0.1 M NaOH and 10–15x phosphate buffered saline (PBS) (depending on the stock collagen concentration) to a concentration of 2.4 mg/ml. The ASC stock solution was also diluted with 0.1 M NaOH and 2.9x PBS (0.2 M Na₂HPO₄, 1.3 M NaCl, *pH* 7.4) to a final concentration of 2.4 mg/ml. All components were kept on ice both prior and after mixing. Furthermore, the collagen solution (*pH* corrected to 7.4) was mixed with a chilled solution of the corresponding GAG in 1x PBS which resulted in solutions with collagen concentration of 1.2 mg/ml and descending concentration of the polysaccharide from 10 to 0 mg/ml (Table 3.1)

The collagen-GAG binding was initiated for 30 min at 0 °C. When a different *pH* was required, it was corrected prior to the 30 min binding initiation. The cofibrillogenesis was initiated by transfer of the solutions to a thermostat and a temperature shift to 37 °C, and typically lasted not longer than 24 h (depending on the goal of the experiment).

Sample	1	2	3	4	5	6	7	8	9	10	11	12
Collagen conc., mg/ml	1.20	1.20	1.20	1.20	1.20	1.20	1.20	1.20	1.20	1.20	1.20	1.20
GAG conc., mg/ml	10.00	4.00	2.00	1.00	0.40	0.20	0.10	0.07	0.05	0.02	0.01	-
Collagen (1.2) volume, μ l	750	750	750	750	750	750	750	750	750	750	750	750
GAG dilution factor	1	2.5	5	10	1	2	4	5.71	8	20	40	-
GAG (20) volume, μ l	750	300	150	75	-	-	-	-	-	-	-	-
GAG (0.8) volume, μ l	-	-	-	-	750	375	187.5	131.25	93.75	37.5	18.75	-
PBS (1x), μ l	-	450	600	675	-	375	562.5	618.75	656.25	712.5	731.25	750

Table 3.1.: Protocol for preparing collagen-GAG gels.

3.2.1.2. Turbidimetric analysis–

The kinetics of the collagen-GAG cofibrillogenesis was followed by turbidimetric analysis using a GENios spectrophotometer. Six aliquots of 200 μ l from each sample, after the binding initiation on ice, were placed in a randomized order in an RNase-/DNase-free 96-well plates. In order to avoid condensation on top of the well plate lid, all samples were preheated for 2–3 min at 37 °C. The optical density (turbidity) was measured at 405 nm, 37 °C for 4 h (240 cycles of 1 min each).

3.2.1.3. Quantitation of collagen (HPLC)

After 24 h, the resulting collagen gels were centrifuged at $5\,000 \times g$ for 30 min and the supernatant was removed while determining its volume. For the quantitation of residual collagen, 2 x 30 μ l were removed from the supernatant and kept at -18 °C before protein quantitation. Collagen content in solutions and supernatants of centrifuged collagen-heparin pellets was quantified using acidic protein hydrolysis with subsequent amino acid based high pressure liquid chromatography (HPLC). Collagen containing aliquots were subjected to vapor hydrolysis in vacuum using 6 M HCl at 110 °C for 24 h and subsequently neutralized. The resulting hydrolysates were dissolved and further diluted in defined volumes of 50 mM sodium acetate buffer at $pH \approx 6.8$. The released amino acids were chromatographically separated after pre-column derivatization with ortho-phthalaldehyde on a Zorbax SB-C18 column (4.6 x 150 mm, 3.5 μ m) using an Agilent 1100 LC-system with

fluorescence detection. Amino acids were quantified using an external standard and the analysis was controlled by the Chemstation software Rev. 08.01. For detailed description refer to (225).

3.2.1.4. Quantitation of heparin (Blyscan™ GAG assay)

LMWH was separately quantified in the supernatant and in the collagen pellet formed after centrifugation using the Blyscan™ sulfated GAG assay. The pellets were resuspended in 1 ml freshly prepared 50 mM PBS, *pH* 6.8 containing 20 µg/ml papain, 1 M NaCl, 5 mM cysteine and 1 mM EDTA and agitated in a thermostated shaker at 60 °C and 600 rpm for 24 h. Depending on the primary GAG concentration, aliquots of different volumes were taken from the resulting suspension and subjected to the assay procedure. In some cases the aliquots had to be further diluted in PBS before performing the assay. The assay kit was used according to the supplier's protocol – to 100 µl of GAG containing solution 1 ml of the dye reagent was added and subsequently placed into a shaker. After 30 min the samples were centrifuged and the supernatant was separated from the precipitated GAG-dye-complex. The precipitate was diluted again by the addition of 1 ml dissociation reagent. After complete resuspension of the GAG-dye complex, blue-colored solutions were formed whose absorption was measured at 655 nm using a spectrophotometer Specord S 10. The corresponding GAG amounts were calculated using a standard curve prepared with 1, 2, 3, and 5 µg GAG.

3.2.2. Chemical modifications

3.2.2.1. Polymer coating of coverslips

For the preparation of stable thin polymer films of poly-(octadecene *alt* maleic anhydride) (POMA) or poly-(ethylene *alt* maleic anhydride) (PEMA), a 0.1–0.2% (w/w) copolymer solution in tetrahydrofuran (THF) was spin-coated onto cleaned and aminosilanized SiO₂-surfaces (silicon wafers or borosilicate glass coverslips (24x24 mm²)). The coverslips were initially precleaned via ultrasonication for 30 min in double distilled water (Milli-Q), followed by a 2–3× rinsing, subsequent 30 min ultrasonication in ethanol, and 2–3× washing with Milli-Q. In order to chemically sweep and prehydrophylize the surfaces, the coverslips were further subjected to RCA cleaning in a mixture of medical extra pure 35% H₂O₂, 29% aqueous solution of NH₃ and Milli-Q in volumetric ratio of 1:1:5. A teflon rack containing the coverslips was kept in the solution at 70 °C for 10 min, followed by 2–3× rinsing with Milli-Q and drying with N₂. The functionalization with 20 mM 3-aminopropyltriethoxysilane (APTES) in ethanol/Milli-Q (9:1) solution took place for 2 h at room temperature (RT) in a sealed glass beaker. Upon completion of the aminosi-

lanization, each substrate was thoroughly rinsed with ethanol and immediately dried with N_2 . In order to further stabilizing the APTES coating, the samples were dried for 1 h at 120 °C. Within 20 min after drying, filtered copolymer solutions (polytetrafluoroethylene (PTFE) syringe filters with pore size of 0.2 μm) of 0.16% POMA (in THF) and 0.15% PEMA (in acetone:THF = 1:2) were spin-coated onto the surfaces for 30 s, at 4 000 rpm, and acceleration of 1 500 rpm/s. The thin polymer films were furthermore annealed for 2 h at 120 °C, and stored for not longer than 3 months.

3.2.2.2. Curing of polydimethylsiloxane (PDMS)

The microstructuring of polydimethylsiloxane (PDMS) was carried out via a reactive ion etched (RIE) silicon masters with channel-like topology. The wafers were initially fluorosilanized (in a protocol similar to the aminosilanization above) with (heptadecafluoro - 1,1,2,2 - tetrahydrodecyl) dimethylchlorosilane). Furthermore, the hydrophobic silicon structures were subjected to SnowJet cleaning with CO_2 on a preheated (200 °C) thermoplate in order to remove any unbound submicron fluorosilane chains. The PDMS was further cured from a viscous elastomer kit Sylgard 184, consisting of components A (base) and B (curing agent) by mixing them in ratio 10:1. After stirring with a glass rod, the prepolymer solution was degassed in a vacuum desiccator for 5–10 min, followed by a deposition of the prepolymer on a precleaned with isopropanol silicon master. In order to remove air bubble formation, the silicon structures were fixed to the bottom of a glass Petri dish via a silicon glue. The curing took place in an oven over 4 h at 65 °C, after which the PDMS casts were peeled off the silicon masters and cut via a whole puncher to circular discs with diameters of 15–18 mm. In order to discard unbound PDMS chains, the casts were rinsed in heptane for 24 h on a swiveling table, and furthermore dried in a vacuum oven at 90 °C overnight (ON). At the end, the back of the PDMS structures was glued on prehydrophobized glass coverslips with similar diameters.

3.2.2.3. Glutaraldehyde functionalization of silicon surfaces

The PDMS or silicon gratings were initially rinsed in isopropanol, subsequently dried and subjected to SnowJet cleaning. Furthermore, in order to remove any residual chemistries and hydrophilize the surface, they were subjected to oxygen plasma treatment for 120 s at RF coil power of 29.6 W. Following 2 h functionalization of the surfaces with 2% APTES solution in Ethanol/Milli-Q (9:1), the structures were thoroughly rinsed in ethanol, immediately dried by nitrogen flow and furthermore stabilized in a designated oven for 1 h at 120 °C. After introduction of NH_2 -groups on the surfaces, the structures were further functionalized with 2.5% aqueous solution of glutaraldehyde for 2 h at 37 °C, followed by 2x 15 min removal of the unreacted glutaraldehyde by rinsing with ethanol. After nitrogen

stream drying of the substrates, the rinsed cofibril supernatants were deposited over the aldehyde-derivatized surfaces and allowed to bind for at least 8 h at 4 °C. If necessary the resulting labile SCHIFF's base (imine group) was further stabilized by reductive amination either with 50 mM NaBH₄ or NaBH₃CN to an amide chemistry (Fig.3.1).

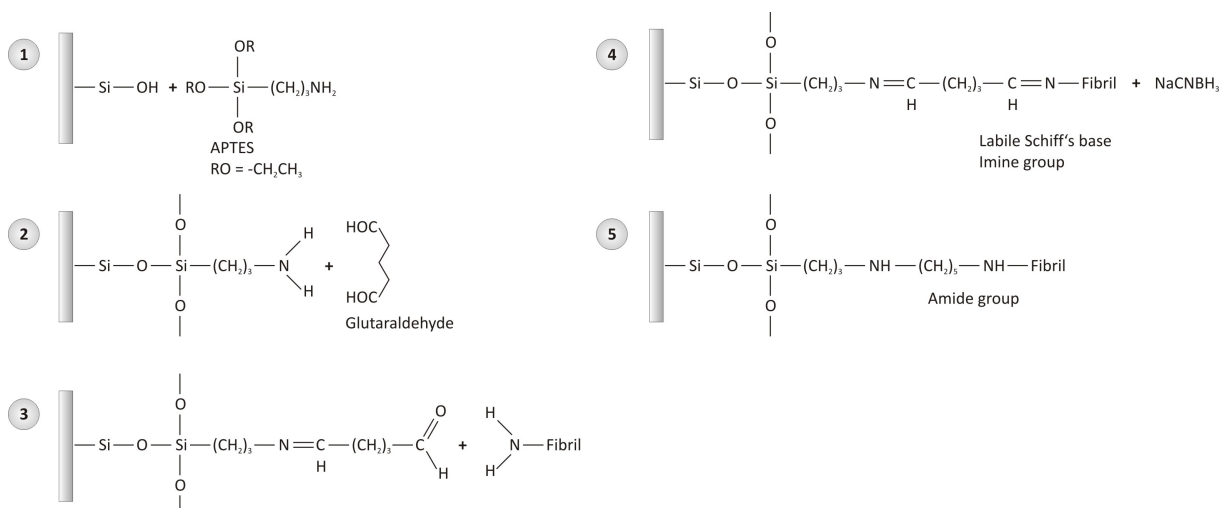


Figure 3.1.: Aldehyde-derivatization strategy applied for covalent immobilization of collagen fibrils.

3.2.2.4. Carbodiimide functionalization of PDMS

The EDC/NHS functionalization of the silicon surfaces included a PEMA copolymer coating step described above. Furthermore, the maleic anhydride functionalities were hydrolyzed (in order to expose the COOH-groups on the surface of the gratings) either by autoclaving them at 120 °C under water or by simple hydrolysis in PBS (1x) at RT for a few hours. Afterwards, the surfaces were rinsed with an activation (conjugation) 0.1 M 2-[morpholino]ethanesulfonic acid (MES) buffer (*pH* 6) for 5 min. Further functionalization with 10 mM carbodiimide (EDC) (N-[3-dimethylaminopropyl]-N'-ethylcarbodiimide hydrochloride) solution in MES buffer. The unstable reactive o-acylisourea esters were further activated by further addition of 25 mM N-hydroxysuccinimide (NHS) solution and allowed to react for 15 min at RT. The unreacted EDC was optionally quenched by addition of a few drops of β -mercaptoethanol (BME) for 2–3 min, which does not interfere with the semi-stable amine-reactive – NHS-esters which lifetime around *pH* 7 is 4–5 hours. The surfaces were furthermore desalted by 2–3 \times rinsing with PBS (1x) and reacted with the primary amines from the cofibrils for 2 h at RT until stable amide bond formation occurs (Fig.3.2).

3.2.2.5. Embedding of the protein samples in epoxy resin

Suspensions of cofibrils were primarily fixed with 2.5% of glutaraldehyde in ratio 1:1 (or 1:2) for 30 min at 4 °C. The crosslinked proteins were encapsulated in 1 ml 2% solution

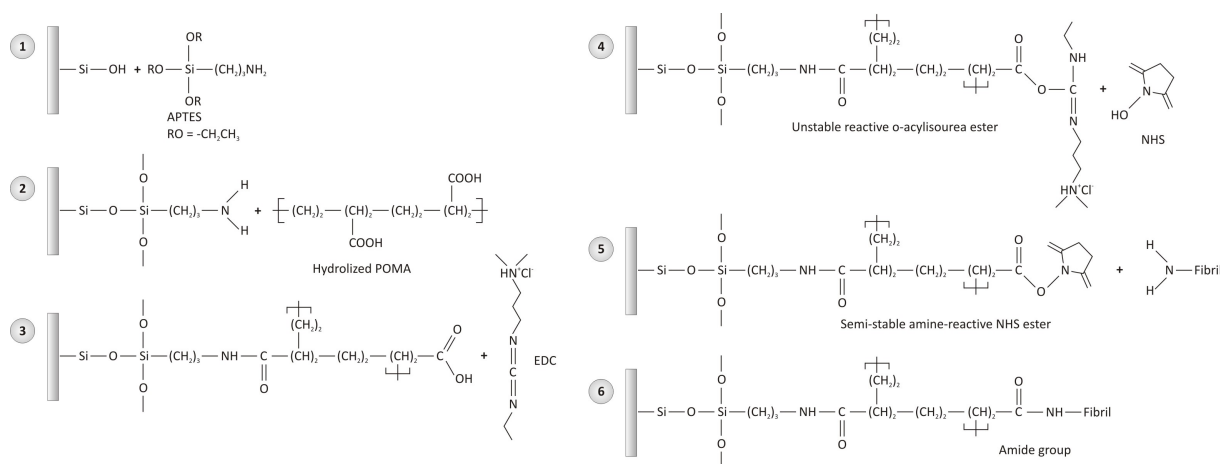


Figure 3.2.: NHS-derivatization strategy applied for covalent immobilization of collagen fibrils.

of high quality agarose for 15–20 min at 4 °C, followed by a secondary fixation with 2.5% glutaraldehyde solution for 6–8 hours at 4 °C. Furthermore, samples were secondarily fixed with 2% OsO₄ solution, ON, at RT. Following 2–3× rinsing with Milli-Q, the fully crosslinked samples were dehydrated and concomitantly stained with 1% uranyl acetate (UA) in ascending acetone series as it follows:

- 1x 25% acetone (30 min)
- 1x 50% acetone + 1% UA (2 h)
- 1x 70% acetone (15 min)
- 1x 90% acetone (15 min)
- 3x 100% acetone (20 min each)

Each sample was infiltrated with a resin kit containing components which were used in a ratio providing the highest crosslinking, hence stiffness of the resin:

V _{RESIN} , ml	40	30	20	10	V _{RESIN} , %	V _{ACETONE} , %	T _{INFILTRATION} , h
NSA, g	26	19.5	13	6.5	25	75	4
ERL-4221 D, g	10	7.5	5	2.5	50	50	12
D.E.R. 736, g	6	4.5	3	1.5	75	25	4
DMAE (S-1), g	0.4	0.3	0.2	0.1	100	-	20

Table 3.2.: Modified SPURR kit components and resin infiltration protocol.

Furthermore the samples were slowly infiltrated with the prepared resin as described in Table 3.2. At the end of the infiltration step, samples were once again embedded into freshly prepared resin and subsequently polymerized in a temperature programmed oven for 72 h at 50–60 °C according to the following protocol (Table 3.3):

Cycle	Length	Temperature	Cycle	Length	Temperature
1	10 min	0 \Rightarrow 50 °C	5	10 h	55 \Rightarrow 60 °C
2	12 h	50 °C	6	40 h	60 °C
3	10 min	50 \Rightarrow 55 °C	7	10 h	60 \Rightarrow 25 °C
4	12 h	55 °C	8	STOP	25 °C

Table 3.3.: Programme for polymerization of epoxy resin embedded with biological samples.

3.2.3. Microscopical methods

3.2.3.1. Scanning force microscopy (SFM)

At the required end of the 24 h cofibrillogenesis, the gels were homogenized for 30 seconds using a pellet pestle cordless motor. The homogenized solution was diluted 40-fold in 1x PBS and 200 μ l were deposited either on circular glass cover slips ($d = 12$ mm) or freshly cleaved atomically flat muscovite mica layers and allowed to adhere for 10 min at RT. Prior to the sample deposition, the cover slips were treated with a carbon dioxide SnowJet cleaner in order to remove submicron particles and hydrocarbon-based contamination. After aspiration of the fluid from the cover slips they were carefully washed in Milli-Q. The samples were dried ON at RT and were subsequently analyzed via intermittent contact scanning force microscopy with a MultiMode, BioScope AFM or PicoSPM using silicon cantilevers (Tap300 or Multi75) with a radius of the tip curvature (ROC) < 10 nm, or for higher resolution - SuperSharp silicon probes (SSS-NCL) with $ROC \approx 2$ nm. For contact mode imaging in dried state and in liquid, samples were analyzed with non-sharpened silicon nitride cantilevers (MLCT-AUHW – reflective gold coating, type C-F; or DNP, type E), in which case the measurements were carried out with a MFP-3D instrument.

3.2.3.2. Micromechanical bending

Bending experiments were carried out using non-sharpened silicon nitride cantilevers (MLCT-AUHW – reflective gold coating, type C-F; or DNP, type E). All measurements were carried out with a MFP-3D instrument. Images were recorded predominantly in intermittent contact mode, while force curves were collected in contact mode. Micromechanical bending tests were performed by bending the elastic fibrils at single point in the middle of suspended filaments, or via a multiple point bending test along the length of the fibrils. The collected deflection vs. piezo displacement curves, obtained directly from the micromechanical bending tests and converted to force-separation curves. Cantilevers were calibrated via the thermal method using an algorithm directly implemented in the MFP-3D software. The samples were kept hydrated at all times. With respect to the

ROC of the cantilever and the diameters from the fibrils, the indentation of the material, as well as the calculated PDMS deformation ($< 3\%$), are considered negligible. Principle of the experimental setup is given in Fig.3.3.

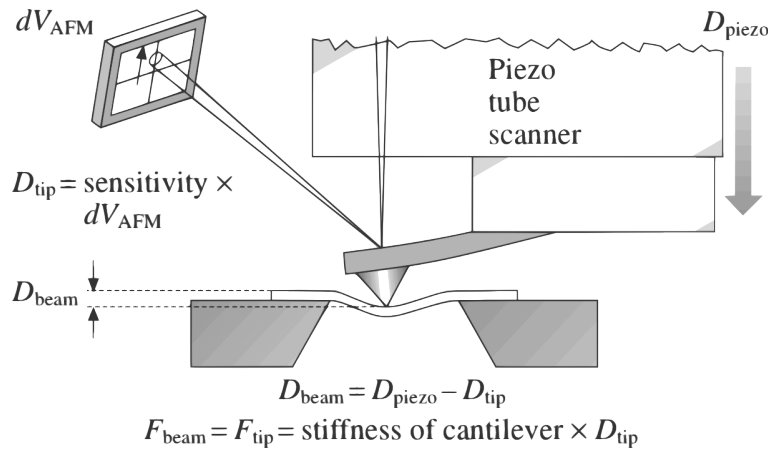


Figure 3.3.: *Experimental setup of the micromechanical bending (adapted from (226)).*

3.2.3.3. Scanning electron microscopy (SEM)

After homogenization and dilution of the gels, as described above (3.2.3.1), 500 μl of the diluted homogenates were transferred onto square cover slips (24 x 24 mm), followed by a subsequent adsorption for 5 min at RT, aspiration of the residual fluid and rinsing in Milli-Q water. The samples were dried ON and prepared for structural analysis by gold deposition in a sputter coater at 60 mV for 50 seconds. The heavy metal deposition on the surface allowed for sample analysis under high vacuum in a Phillips SEM equipped with an SE detector, and operating at 7.5–10 kV, Spot Size 3.

3.2.3.4. Transmission electron microscopy (TEM)

Preparation of negatively stained specimens was carried out in 2 ways: either via direct deposition of cofibril suspension on 300- to 2000-mesh Cu-grids or by embedding of the samples into epoxy resin and subsequent thin sectioning. In the case of direct deposition on the Cu-grids, the samples were initially allowed to adhere for 10 min at RT (cofibril gels) or at 4 °C (nuclei solution). By applying a drop application technique the grids were rinsed 3-fold with deionized water and stained in 1% (w/v) phosphotungstic acid (in 50% (v/v) ethanol) (pH 3.5) 2-fold for 5 min. Furthermore, samples were counterstained in 5% filtered solution of tannic acid for 10 min and negatively stained with 2% aqueous solution of UA (pH 4.2) for 20 min at RT. Some of the samples were stained only with UA (as detailed in section 4.2.2). The second preparation technique for thin sectioning is a modified version of the original SPURR protocol (227). The samples were first fixed in 2.5% glutaraldehyde solution, followed by encapsulation in 2% high quality low melting

temperature agarose and cut into small 2 x 2 mm² blocks. These were subjected to a secondary fixation step in 2.5% glutaraldehyde followed by an ON osmification with 4% aqueous solution of OsO₄. The fixed specimens were dehydrated into ascending acetone series (UA staining included at 50% acetone step) and subsequently infiltrated into epoxy resin by stepwise exchange of the acetone. After 72 h polymerization of the resin at 60 °C the samples were cut with a microtome diamond knife into sections with varying thickness between 50 – 300 nm, and mounted on pioloform film coated 300-mesh Cu-grids. Images were acquired under high vacuum with two different TEM systems namely an Omega EM 912 operating at 120 kV, and a Tecnai 12 BioTWIN operating at 100 kV.

3.2.3.5. Confocal laser scanning microscopy (cLSM)

Complexes of heparin and fibrillar collagen were visualized using FITC-labeled heparin. Surface-bound collagen layers were prepared as described in SALCHERT et al (228). Briefly, fibrillogenesis of PSC-heparin cofibrils was performed in the presence of POMA-coated cover slips at 37°C for 24 h as described above for gel preparation using heparin-FITC diluted with heparin at a 1:10 ratio. After immobilization, the surfaces with bound cofibrils were rinsed at least 6 times before mounting them on a microscope slide. The surfaces were imaged using a confocal laser scanning microscope TCS SP1 with a 40x oil immersion objective. The lateral resolution of the cLSM working under standard conditions (pinhole size = 1 Airy disc) is defined as the full width at half maximum ($FWHM_{LATERAL}$) of an intensity image of a point object by $FWHM_{LATERAL} = 0.51 \times \lambda_{EM}/NA$, with λ_{EM} being the emission wavelength of the image object and NA – the numerical aperture of the microscope objective. For our setup (fluorescein label, $NA = 1.25$) this results in a lateral resolution of 210 nm.

3.2.3.6. Wide angle x-ray scattering

At the end of the cofibrillogenesis, the fibrillar suspensions were rinsed via VivaSpin 20 Millipore filters with molecular weight cut-off of 1 MDa in order to remove residual heparin. Subsequently, all samples were centrifuged for 30 min at 20 000 × g in order to precipitate the fibrous material and then loaded into quartz capillaries with a diameter of 1.5 mm. Experiments were performed using an in-house Bruker AXS Nanostar with a rotating anode X-ray source (CuK α radiation, $\lambda = 1.54 \text{ \AA}$, generator power 4.05 kW) and a virtually noise-free, real-time 2D Hi-Star detector with photon counting ability. The smectic A layer spacing of the liquid crystal 4'-octyl-4-cyanobiphenyl was used as calibration. The resulting 2D images of the diffraction patterns were integrated radially over all azimuthal angles ($\chi = 0$ to 360 °) and covered a q range of 0.1 to 7.5 nm⁻¹. Plots of intensity vs. q reveal scattering peaks which can be translated to a d spacing, in the

case of lateral fibril packing found here, by the relationship $d = 2\pi/q$. Peak positions and widths were measured using Lorentzian fits obtained with the data analysis program Origin.

4. Results and Discussion

The rationale to use two native ECM components as collagen type I and heparin, with respect to their further involvement in designing novel xenogeneic scaffolds requires a broader characterization of their intimate structural interaction. Thereby a wide range of microscopy techniques was implemented to analyze the kinetic aspects of the characteristic collagen I fibrillogenesis in the presence of heparin (section 4.1). Additionally, the ability of the fibrillar collagen I to exhibit varying structural and hierarchical characteristics influenced by a potentially intercalating agent as the polysaccharide, was studied in detail (section 4.2). At the end, we provide means via which to mechanically characterize such a protein-polysaccharide coassembly and to relay the results to the previously observed kinetic and structural properties of the system (section 4.3). The already performed analysis is of particular interest for understanding and gaining a control over a rather versatile and already heavily exploited advanced cell culture system.

4.1. Morphological characterization of collagen type I - GAG assemblies

As previously discussed (section 2.3.5) various GAGs are known to influence differently the kinetics of the acid soluble collagen I (ASC) fibrillogenesis, as well as the morphology of both *in vivo* and *in vitro* reconstituted fibrils. Nevertheless, studies on pepsin-solubilized collagen type I (PSC) remain scarce and inconclusive. The motivation for using PSC is based on its perspective application in advanced cell culture systems and is due to the absence of telopeptides (characteristic for collagen extraction with pepsin) leading to overall decreased immunogenicity. The effect of three different GAGs, namely LMWH, HA and HS, on the morphological characteristics of gels reconstituted in the presence of PSC was studied via SFM and SEM. PSC concentration was kept constant in all studies (1.2 mg/ml), while the GAG concentration was varied in the range 0–10 mg/ml.

4.1.1. Impact of GAG type on the morphology of the cofibrils

4.1.1.1. Pure PSC fibrils

SFM analysis of pure PSC fibrils showed that they exhibit the typical twisted 'rope-like' long helical morphology with the presence of the typical D-banding of 67 nm. The homogeneity in size with a diameter distribution of the PSC fibrils of 220–230 nm was usually disrupted only by the occasional aggregation of the thinner fibrils into macro-assemblies (Fig.4.1).

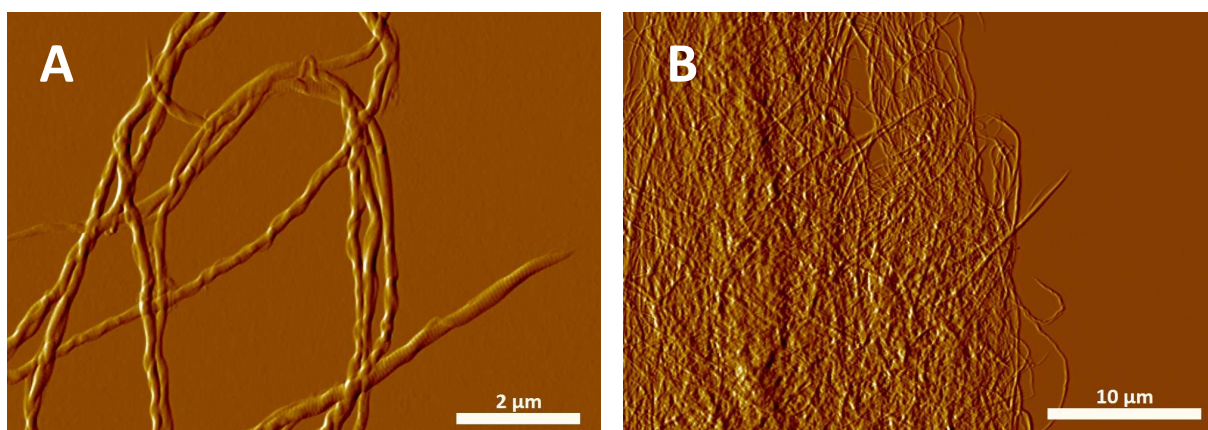


Figure 4.1.: Morphological analysis of pure PSC fibrils (1.2 mg/ml) showing SFM amplitude images.

The occasional kinks along the fibril length are reminiscent of inhomogeneous 'tube-like' structure composed of a relatively hard shell and softer less dense core. The nature of such crimps is characteristic for the liquid-crystalline model supporting the structural organization of collagen type I as hollow tubes (106,107). The appearance of aggregates is typically an aftermath of the very high concentration of PSC, as lower concentrations and shorter fibrillogenesis times showed the tendency of forming individual filaments (data not shown).

4.1.1.2. PSC fibrils reconstituted in the presence of HA

Reconstitution of PSC fibrils in the presence of HA took place in the concentration range up to 5 mg/ml. The overall structure and linearity of the supposedly formed cofibrils resembled the ones of the pure PSC fibrils with the appearance of the characteristic kinks discussed above, as well as the preserved 67 nm D-banding. There was a gradual increase in diameters of the formed macrofibrils (assemblies) as portrayed in Fig.4.2. Concentrations up to 1 mg/ml retained the range of diameters typical for pure PSC fibrils (180–250 nm), while increase to 5 mg/ml HA resulted in substantial agglomeration to diameters in the range of 350–700 nm.

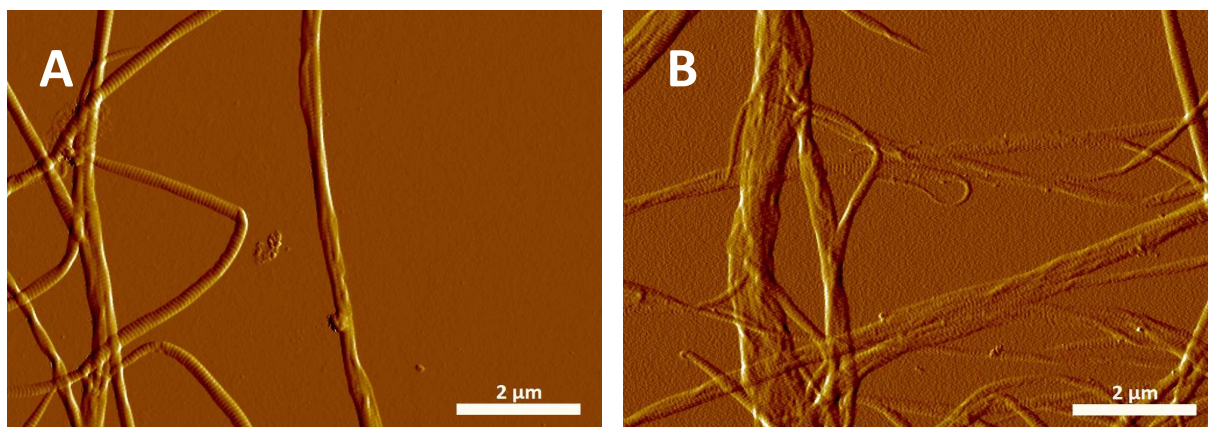


Figure 4.2.: Reconstitution of PSC fibrils in the presence of hyaluronic acid. SFM amplitude images show PSC fibrils (1.2 mg/ml) assembled in the presence of (A) 1 mg/ml HA and (B) 5 mg/ml HA.

4.1.1.3. Impact of HS on the formation of PSC fibrils

The effect of HS on morphology of PSC fibrils was investigated in the range 0.01–4 mg/ml. Fibrillogenesis took place with concentrations of the GAG up to 1 mg/ml, while any further increase resulted in partial or complete retardation of the assembly. Low concentrations of HS (0.01–0.10 mg/ml) resulted in formation of fibrils with similar diameters (220–230 nm) and morphology to the pure PSC fibrils (Fig.4.3 A).

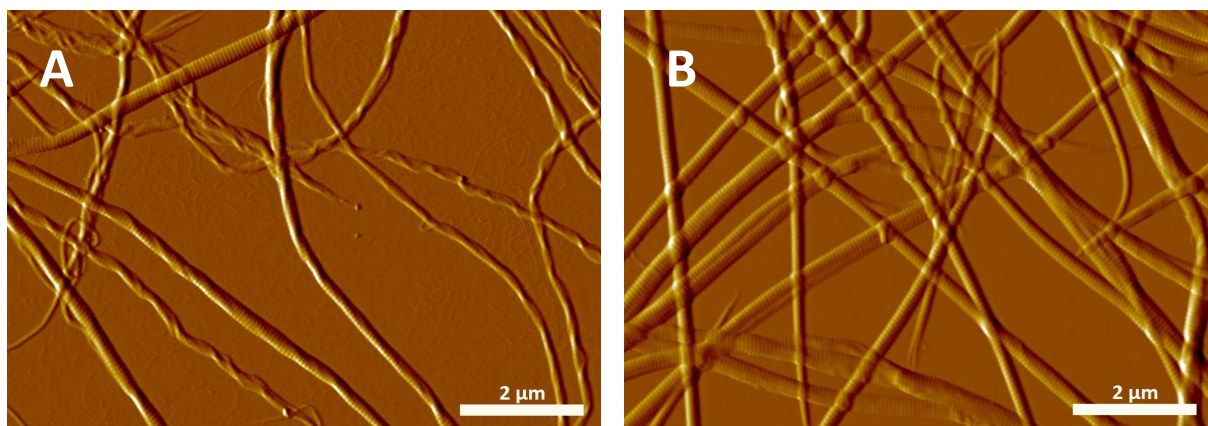


Figure 4.3.: Impact of HS on the morphology of PSC fibrils (1.2 mg/ml) reconstituted in the presence of (A) 0.1 mg/ml and (B) 1 mg/ml GAG, respectively, shown by SFM amplitude images.

Increase of HS concentration above 0.5 mg/ml led to increase in linearity of the filaments, also accompanied by a partial increase in diameters reaching up to 290–320 nm. Nevertheless, the nature of the agglomeration in comparison to the case with HA appears to be different, since the typical twisted morphology of the pure PSC fibrils was not observed in this case (Fig.4.3 B).

4.1.1.4. Effect of LMWH on reconstitution of PSC fibrils

Morphological analysis of the PSC-LMWH gels by SFM revealed straight and thick tactoidal cofibrils, which were rather heterogeneous in size (often exceeding $1\ \mu\text{m}$) (Fig.4.4). Typical for all LMWH containing samples was the presence of a halo of small 'nanofibrils' lying in the vicinity to the bigger ones, something which was not observed in any of the previously two investigated systems with HA and HS. While the 'giant' cofibrils retained the characteristic D-pattern, the 'nanofibrils' appeared to be delineating significantly from them. Another surprising feature of the PSC-LMWH gels was that even the lowest concentrations of GAG (studied in the range $0.01 - 10\ \text{mg/ml}$) led to the formation of this spindle-like morphology which was completely different than the case with pure PSC fibrils.

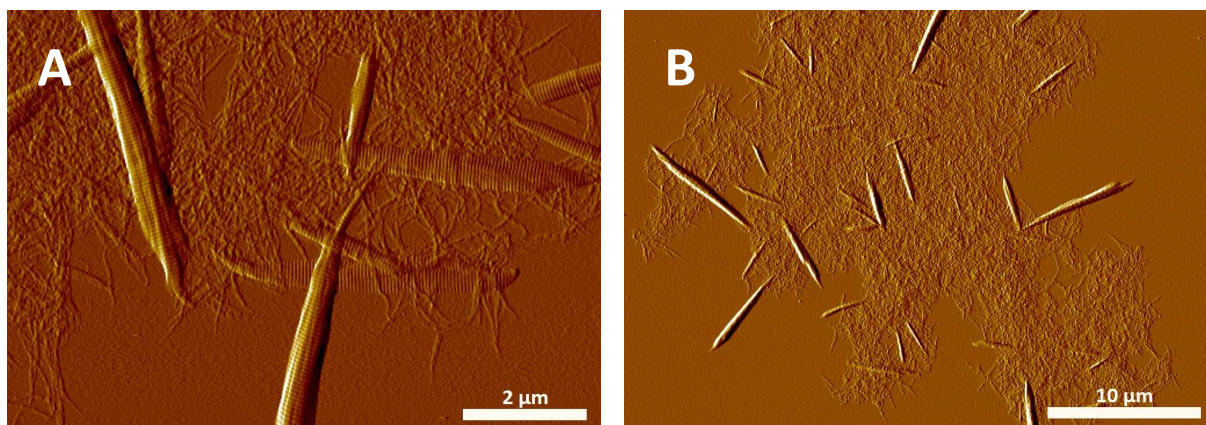


Figure 4.4.: *Morphogenic effect of LMWH on PSC fibrils reconstituted at 0.4 mg/ml GAG.*

4.1.2. Impact of concentration on the morphology of collagen I - LMWH cofibrils

As LMWH had the most significant morphogenic impact on collagen fibrillogenesis, we studied the effect of concentration on the morphology of the PSC fibrils. The presence of LMWH at all concentrations resulted in the formation of spindle-like cofibrils in comparison to the more twisted fibrils of pure PSC. At high ($2 - 4\ \text{mg/ml}$) and low ($0.01 - 0.1\ \text{mg/ml}$) GAG concentrations, less heterogeneous thinner cofibrils with predominantly tapered ends were observed. Intermediate concentrations ($0.1 - 1\ \text{mg/ml}$) led to the formation of very thick fibrils with spindle-like shape and blunt ends. Statistical analysis of the SFM and SEM images showed a significant difference ($n = 200$, $p < 0.05$, 1-way ANOVA, BONFERRONI Multiple Variance Test) in the size distribution of the cofibrils reconstituted at various GAG concentrations. The intermediate concentrations were characterized by broader size distributions representing the heterogeneous mixture of cofibrils formed at these conditions, while the low and high concentrations resulted in the formation of more

homogeneous cofibrils (Fig.4.5 A,B). The highest mean diameters (388 nm) were measured at a heparin concentration of 0.4 mg/ml, while the two extremes (0.01 and 4 mg/ml) resulted in the formation of thinner cofibrils with average diameters of 227 nm and 271 nm, respectively. A similar non-linear dependence on increasing heparin concentration was observed for the width-to-length ratio of the cofibrils ($n = 50$, $p < 0.01$) (Fig.4.5 C). The thickest and shortest fibrils with the highest ratio were determined again at a heparin concentration of 0.4 mg/ml.

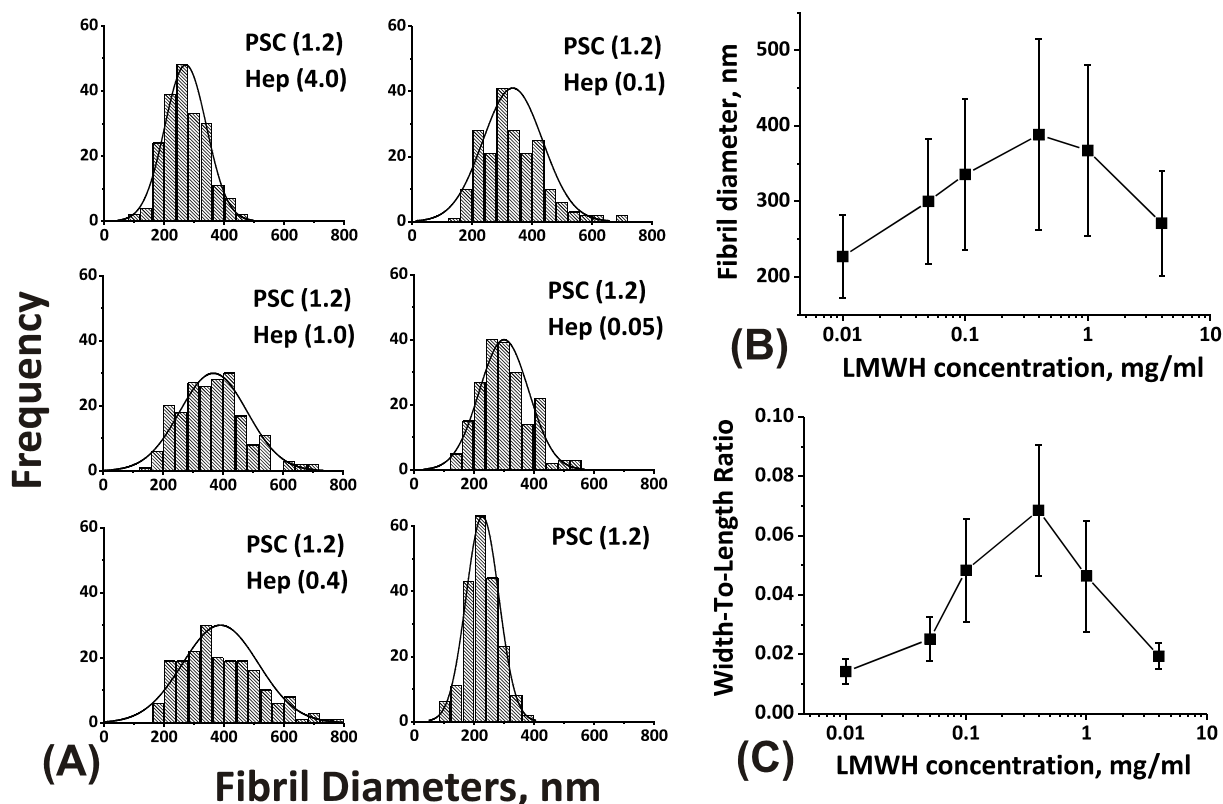


Figure 4.5.: Size distributions of the PSC-LMWH cofibrils (A) at various GAG concentrations with a graphical representation of diameter (B) and width-to-length ratio (C) vs. concentration (error bars representing standard deviation).

4.1.3. Kinetics of PSC - LMWH cofibrillogenesis

The variations in size distribution and cofibril morphologies over the wide range of LMWH concentrations used posed the question whether there were any significant differences in the growth kinetics at the different conditions. The kinetics of the process of fibril formation was followed by turbidimetric analysis after 30 min preincubation time, while in all cases, the presence of heparin led to the formation of sigmoidal curves with a distinct lag and exponential phase (Fig.4.6 A).

As kinetic parameters of fibril growth, the onset of the exponential phase (t_{EXP}) and the slope at the half-time of exponential growth were derived from the turbidimetric curves.

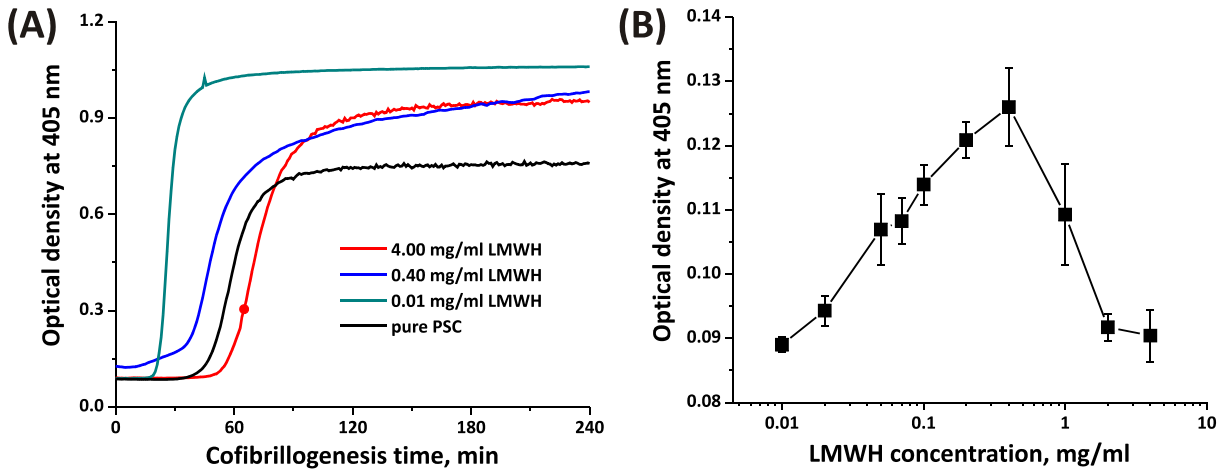


Figure 4.6.: Turbidimetric analysis (405 nm) of the PSC-LMWH cofibrillogenesis at 37 °C after 30 min preincubation at 0 °C (A) and the optical density measured directly at the end of the preincubation period (B) (error bars representing standard deviation).

Briefly, the maximum of the 1st derivative of the sigmoidal curves corresponds to the slope of the turbidity curve at the half-time of exponential growth ($\frac{dOD}{dt}(t_{1/2})$). The linear extrapolation of the tangent at this time-point to the baseline value of the nucleation phase defines the time-point of t_{EXP} in the turbidity curve. Fig.4.7 A,B indicated a drastic shortening of the nucleation phase combined by an increase in growth rate – characterized by $slope_{1/2}$ – for very small LMWH concentrations in comparison to pure PSC. With increasing GAG concentrations t_{EXP} increased in a non-linear fashion in conjunction with a decrease of the growth rate. This was different for the case of pure PSC fibrils which was characterized by a gradual shortening of t_{EXP} with respect to the increasing initial concentrations of atelocollagen (see Appendix, Fig.A.1). At a very high LMWH concentration of 4 mg/ml the values were almost equal to the values of pure collagen samples. Besides the different kinetics, a significantly different turbidity of the solutions was observed after the 30 min preincubation period at 0 °C ($n = 30$, $p < 0.001$) (Fig.4.6 B). For further information on concentration-based kinetics of the pure PSC fibrillogenesis see appendices (A.1).

According to WOOD (151,153) there is a relation between the turbidity of the collagen gels and the corresponding extent of precipitation. This means that the higher turbidity at intermediate GAG concentrations could be interpreted as larger size or amount of the nuclei fibrillar material. The highest mean nuclei optical density (OD) (0.1208) was found for a concentration of 0.4 mg/ml LMWH, which corresponds to the highest mean cofibril diameter and width-to-length ratio from the morphological analysis. A structural comparison of the nuclei at 0.01 and 0.4 mg/ml LMWH by SFM showed no significant differences in size but nonetheless a rather high density, when placed on the glass substrate for SFM imaging, at 0.4 mg/ml in comparison to 0.01 mg/ml (data not shown). Hence, the increase in OD was attributed to the amount of nucleic fibrillar collagen-LMWH

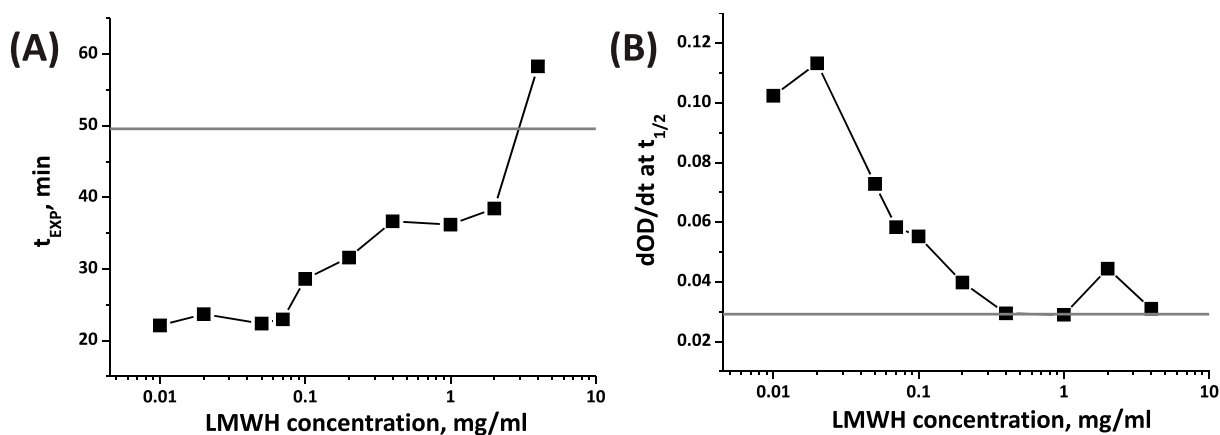


Figure 4.7.: Time of exponential onset t_{EXP} (A) and slope at exponential half-time $\frac{dOD}{dt}$ ($t_{1/2}$) (B) are plotted vs. deployed heparin concentration. Data for pure PSC samples are given as horizontal lines for comparison. (A, B are data from one typical experiment out of 3 independent experiments).

assemblies.

4.1.4. Intercalation of heparin within the cofibrils

In order to elucidate the role of LMWH in the formation of cofibrils with different and heterogeneous morphologies and its potential binding inside the cofibrils, the amount of GAGs associated with them was quantified. The quantitation assay exploits the fact that heparin forms colored complexes with the cationic dye 1,9-dimethylmethylene blue. Test studies suggested that the whole heparin amount is only accessible for the dye complexation after enzymatic digestion with the cysteine protease papain. Interestingly, the test experiments showed that the difference in the amount of heparin measured with and without enzymatic digestion was exactly as high as the amount of heparin revealed by the heparin quantitation after 24 h of rinsing in PBS (see below). This finding provided the first hint that this fraction of heparin might be found inside the cofibrils, because it could not be easily washed away and was only accessible after enzymatic digestion. In order to evaluate the binding of heparin inside/to PSC fibrils, the PSC-LMWH pellets were rinsed for 24 h or 7 days in PBS and the measured heparin amount was compared to the heparin content directly after the end of the cofibrillogenesis (Fig.4.8 A).

Directly at the end of cofibrillogenesis the LMWH quantified in the pellets strongly increased with the deployed ascending GAG solution concentration. Subsequent rinsing of the pellets for 24 h and 7 days (data not shown) in PBS led to a substantial decrease in heparin content with a maximum value measured for 0.4 mg/ml LMWH. Furthermore, acidic protein hydrolysis with subsequent amino acid based HPLC analysis was used to quantify the amount of collagen remaining in the supernatant after the end of the cofibrillogenesis. By subtracting the measured collagen amount from the deployed atelocollagen

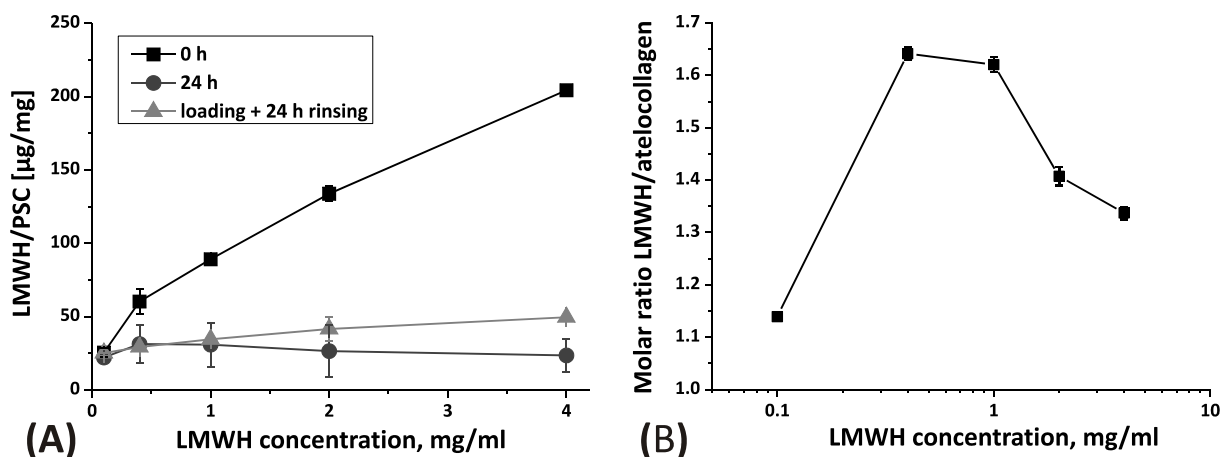


Figure 4.8.: *Stability of PSC-LMWH assemblies and molar (A) quantitation of LMWH in the pellets after 24 h cofibrillogenesis and after subsequent 24 h rinsing in PBS ($n = 8$) (22). For comparison the GAG amounts in experiments with loading LMWH to preformed PSC gels (after subsequent 24 h rinsing in PBS) are also shown. Error bars represent standard deviation. (B) Molar ratio of LMWH and PSC in the pellets after 24 h fibrillogenesis (Values were calculated on the basis of the measured atelocollagen and LMWH amounts using an average M_W for the GAG of 5 kDa and for atelocollagen of 280 kDa).*

in the starting solution, the amount of collagen in the pellet was found to slightly correlate with the deployed LMWH concentration. The lowest collagen content was measured in the pellet for the pure PSC samples (0.976 mg) while the highest amount was found in the sample with 0.1 mg/ml LMWH (1.086 mg). The further increase of the GAG concentration (to 4 mg/ml) resulted in decrease of the pellet-bound collagen to 0.984 mg. From these data a molar ratio of LMWH to collagen in the cofibrillar assemblies was estimated, by taking into consideration an average molecular weight for LMWH of 5 kDa and 280 kDa for the atelocollagen (Fig.4.8 B). A ratio of nearly 1:1 (heparin:collagen) was found for fibrils formed in the presence of 0.1 mg/ml GAG and over 1.6:1 was calculated for LMWH concentrations in the range (0.4–1.2 mg/ml), followed by a steady decrease in the ratio for higher concentrations. The high molar ratio and the highest amount of LMWH associated with the cofibrils at 0.4 mg/ml point towards an intercalation of LMWH inside the collagen fibrils. This was even more obvious after comparison with the morphological data. As the cofibrils at intermediate LMWH concentrations exhibit the greatest diameter and width-to-length ratio, they possess the smallest surface-to-volume ratio, while exhibiting the highest heparin content at the same time. Hence, the LMWH binding can only be explained by an intercalation of the GAG.

In an additional experiment, preformed pure PSC assemblies were incubated with LMWH in order to compare its binding on the surface of the fibrils. Although significant amounts of heparin were bound to collagen after 24 h rinsing in PBS, there was only a linear relation between the amount of bound heparin and the heparin solution concentration, which is in strong contrast to the LMWH-PSC cofibrils (Fig.4.8 A). Thus the significant

binding of heparin to preformed collagen gels could mainly be attributed to the larger surface area of the collagen fibrils in comparison to the cofibrils due to their much smaller diameter and greater length.

The intercalation of heparin inside the cofibrils was supported by conducting an analysis with cLSM and FITC-labeled heparin (0.4 mg/ml). Collagen fibrils were imaged with maximum resolution resulting from the typical tactoidal shapes of imaged filaments. As in implemented setup the lateral optical resolution is approximately 210 nm (see section 3.2.3.5), imaging of cofibrils with diameters in the range of 200 to 800 nm is feasible (Fig. 4.9).

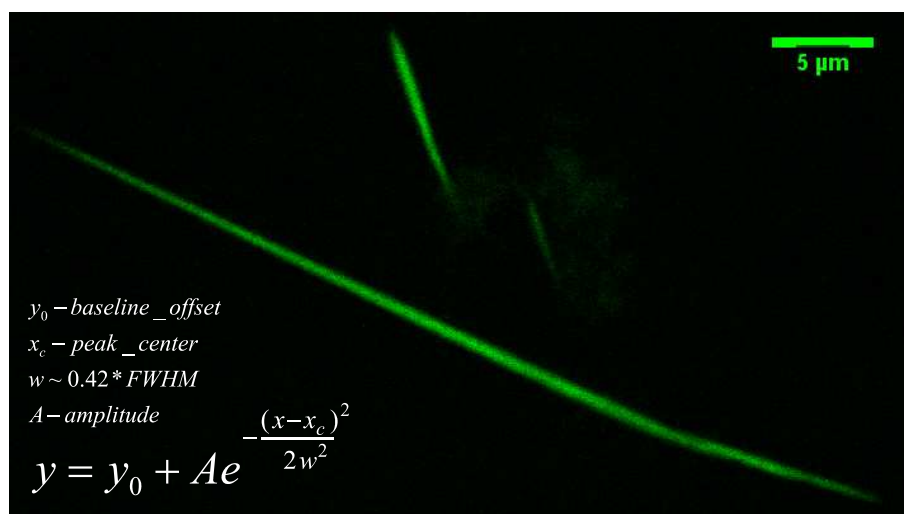


Figure 4.9.: *cLSM image of a single PSC-FITC-labeled heparin cofibril of varying diameter. Inset in bottom left shows the approximation of Gaussian function used to fit the cross-section(s) analyzed later on.*

The full width at half maximum (FWHM) and the maximum fluorescence intensity of multiple cross-sections of imaged PSC-heparin cofibrils, acquired from the non-linear Gaussian fits, were analyzed for both multiple independent cofibrils ($n = 243$) and single cofibrils ($n = 100$) (Fig.4.10 and Fig.4.11). Both parameters were assumed to resemble means of the diameter of the fibrils and the amount of heparin present at this diameter throughout the fibril.

By plotting the maximum intensity against FWHM or the square of FWHM and extrapolating the linear fits to zero fluorescence intensity, the hypothesis whether the amount of bound heparin goes with the circumference or with the area of the cross-section of the cofibrils can be verified. As the linear fit of the square of FWHM for the single cofibrils (Fig.4.10 A) almost crosses the origin of the graph, an intercalation of heparin inside the fibrils can be expected. Even with the strong scatter in the plot of the multiple cofibril analysis (Fig.4.10 B) – possibly coming from different focusing and degree of horizontal alignment of the cofibrils – a linear relation can be anticipated between LMWH amount (maximum fluorescence intensity) and fibril cross-section area (FWHM^2).

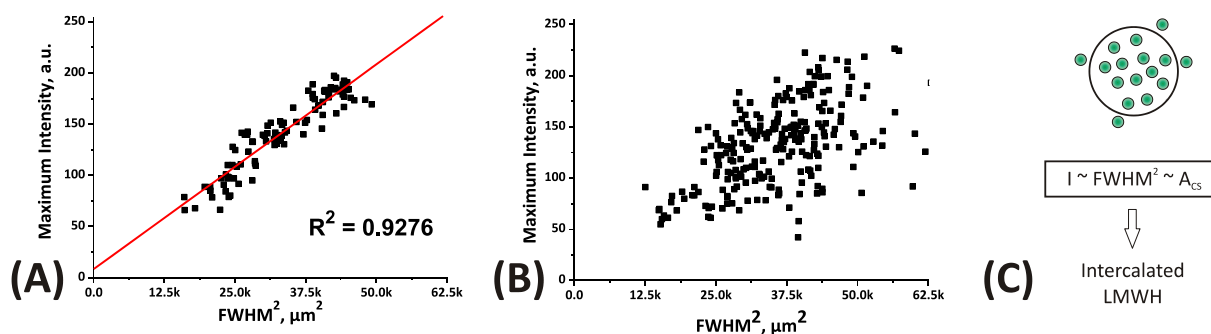


Figure 4.10.: Linear regression of the maximum fluorescence intensity of cofibril cross-section vs. the square of its FWHM for multiple cofibrils (A) and across a single cofibril (B). The sketch in (C) represents the idea behind the relation between the maximum intensity (I) and the FWHM² (or the area of the cross-section (A_{CS})) in the case when the FITC-labeled LMWH is intercalated within the fibril.

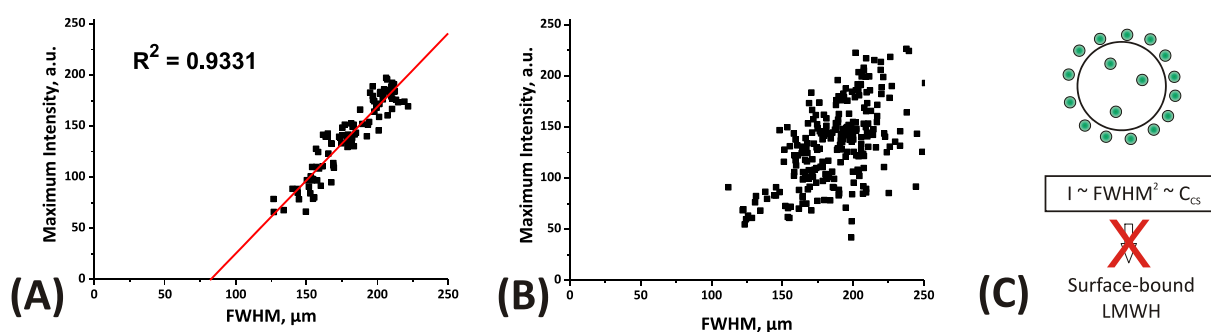


Figure 4.11.: Absence of linear extrapolation of maximum fluorescence intensity vs. FWHM for single (A) and multiple (B) cofibrils. The sketch in (C) represents the idea behind the relation between the maximum intensity (I) and the FWHM (or the circumference of the cross-section (C_{CS})) in the case when the FITC-labeled LMWH is bound only on the surface of the PSC fibril.

4.1.5. Impact of degree of sulfation, molecular weight and pH value

In order to understand the origin of heparin binding inside the cofibrils and to prove the predominant effect of electrostatic interactions in the PSC-LMWH cofibril formation as suggested by MCPHERSON et al. (182), a determination of the structural differences amongst PSC-GAG cofibrils as a function of molecular weight of heparin, as well as charge, the latter by substituting heparin with HS, and varying the pH value during cofibrillogenesis, was carried out. The analysis involved heparin with a higher molecular weight (HMWH) in the range of 17–19 kDa in comparison to the heparin of the preceding experiments with molecular weight of 4–6 kDa (LMWH). Substituting heparin with HS leaves the molecular weight in a similar range (13–15 kDa), however, the negative net charge of the molecule is drastically decreased due to the 3-fold smaller degree of sulfation (41). The morphological and kinetic turbidimetric analysis of the PSC-HMWH gels exhibited the same behavior as observed for LMWH. The size distribution, optical density in the

nucleation phase, growth kinetics (t_{EXP} , $\frac{dOD}{dt}(t_{1/2})$), and width-to-length ratio showed no significant differences ($p < 0.025$) in comparison to LMWH (Fig.4.12).

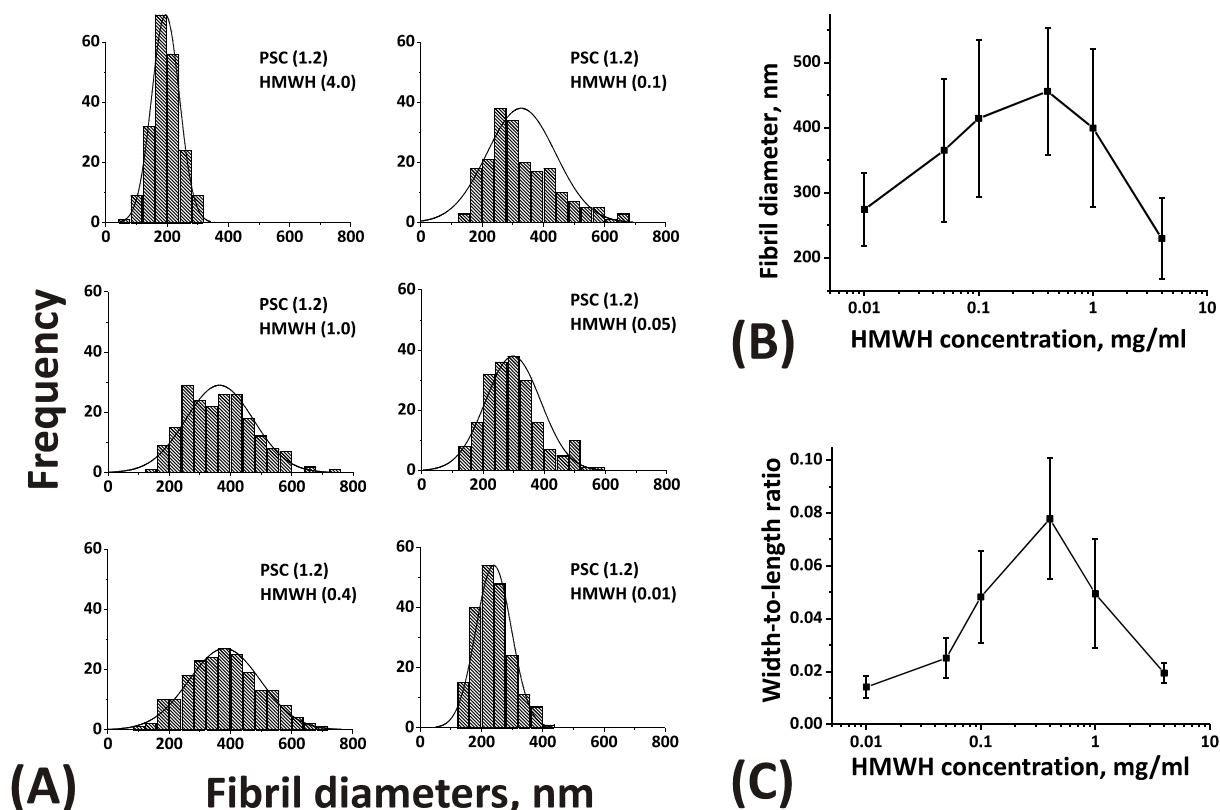


Figure 4.12.: Size distribution of the PSC-HMWH cofibrils (A) at various deployed GAG concentrations with a graphical representation of diameter (B) and width-to-length ratio (C) vs. concentration (error bars representing standard deviation).

In contrast, cofibrillogenesis in the presence of HS resulted in the formation of cofibrils with a much smaller dependence on HS concentration in comparison to the collagen-heparin cofibrils (Fig.4.3). A small, but significant increase in the cofibril size ($n = 100$, $p < 0.001$, 1-way ANOVA, BONFERRONI Test) was only observed for the 1.0 mg/ml and 0.4 mg/ml HS resulting in mean thicknesses of 300 nm and 252 nm respectively, in comparison to 230 – 240 nm for pure collagen (see Appendices, section A.3). Characteristic for the high HS concentrations (particularly 1 mg/ml) was the formation of fibrils with more pronounced straight morphology and tapered ends. Other concentrations of HS influenced neither the size distribution ($p > 0.05$) nor the cofibril structure. A further increase of the HS concentration (4 mg/ml) resulted in a complete inhibition of the cofibril formation over the time range of 24 h.

Variation of pH had a much more pronounced impact on the PSC-LMWH cofibrils (Fig.4.13). An acidic environment led to an inhibition of cofibril formation and resulted in twisted thinner fibrils – similar to pure PSC – with diameters decreasing with descending pH . The effect of the more basic environment was a decrease of cofibril diameter and width-to-length ratio with ascending pH value. The statistical analysis showed that the

increase of pH to 7.9 and 8.4 led cofibril mean diameters to decrease to respectively 282 and 204 nm ($n = 50$). Apparently at the highest pH value the diameters were even smaller than those for the pure PSC fibrils reconstituted at pH 7.4 (230–240 nm). The cofibrils at neutral pH retained the most pronounced spindle-like shape with the greatest thickness and width-to-length ratio. The effect of pH changes on reconstituted PSC-HS cofibrils (Fig.4.13) had a much lower impact on their morphology with no significant variations in diameter. The only difference was that the fibrils at lower pH had a slightly more pronounced linearity (pH 6.9) in comparison to those reconstituted at pH 7.9.

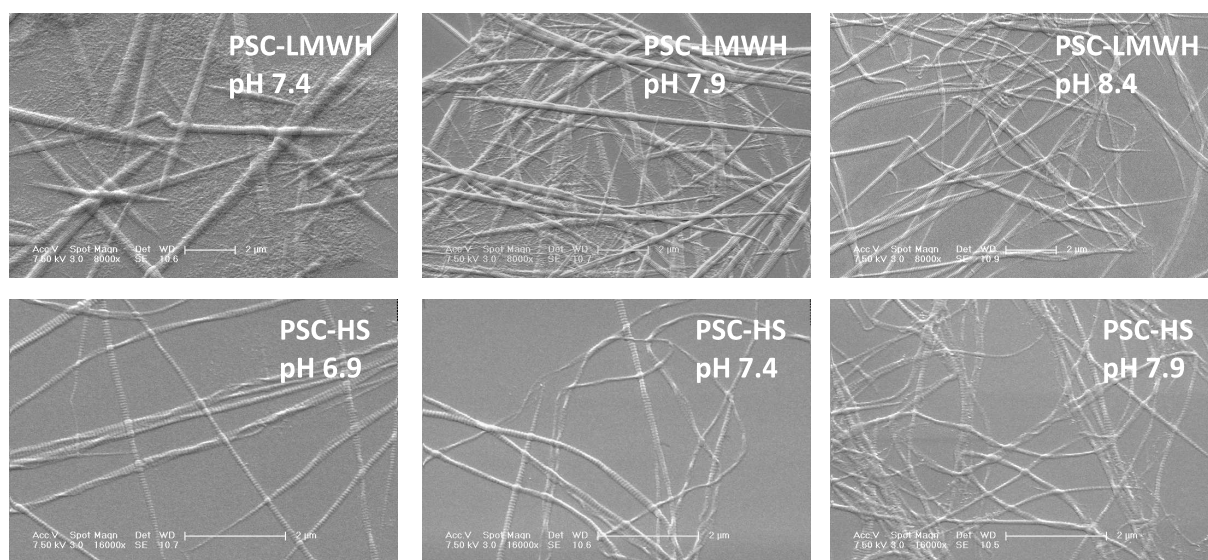


Figure 4.13.: SEM images of PSC-GAG cofibrils summarizing the different effect of pH value on their morphology, PSC-LMWH (0.4 mg/ml LMWH), PSC-HS (0.4 mg/ml HS) (Scale bar: 2 μ m).

4.1.6. Discussion

In vitro collagen fibrillogenesis in the presence of GAGs has already been studied for quite a long time (166–168, 182, 229, 230). These studies revealed a lot of issues concerning the impact of GAG composition, concentration, pH value, and ionic strength on the kind and kinetics of growing fibrils. Beside other results, it was pointed out that the electrostatic interaction between GAG and collagen molecules is a key element in the assembly process (166, 168, 182). Nevertheless, the reconstitution of pepsin-digested collagen in the presence of negative GAGs is poorly understood and remains an intriguing conundrum.

The morphological analysis presented in 4.1, showed that there are substantial morphological and kinetic differences observed while PSC was reconstituted in the presence of non-sulfated (HA), less sulfated (HS) and highly sulfated GAGs (LMWH, HMWH). Increase in HA concentration led to an increase in fibril diameters but no obvious morphological differences. Also with respect to the negligible differences in PSC-HA kinetics at various

GAG concentrations (data not shown), the effect of HA on the size of the reconstituted cofibrils could most likely be attributed to potential accretion of atelocollagen molecules due to steric exclusion by the hyaluronic acid molecules. Essentially, the HA concentrates a lot of atelocollagen molecules in a small volume and sterically forces and accelerates the fibrillogenesis. Additionally, HA at all concentrations did not affect neither the structure nor the linearity of the fibrils, which can tell us that most probably the huge molecule dimensions and small negative charge prevented its incorporation within the fibrils. It would seem that this is a key issue in collagen-GAG systems where the high molecular weight polysaccharide is heavily exploited. On the other side, the presence of sulfate groups had a much more pronounced effect on the linearity and thickness of the cofibrils. Already for HS with a low degree of sulfation there was pronounced and concentration-dependent effect on fibril formation, which was very much enhanced in the case of highly sulfated heparin.

Seen in this context, heparin comes up as an important GAG, because of its high charge density, its occurrence in several living tissues, and its role in binding of growth factors, and cell-surface ligands (231–233). Heparin is known to bear the highest density of negatively charged groups among all other GAG (41) which can trigger the electrostatic interaction with other macroionic molecules (48). Previous studies showed that the monomeric tropocollagen carries specific binding sites between positions 755 and 933 at the carboxy terminal region (234) and/or one near the N-terminus (235), which is also active in its fibrillar arrangement. In the latter work it was proposed, that the binding site near the N-terminus should be the primary one and could act together with other low affinity sites for cross-linking tropocollagen molecules. Former models (182) also suggested the *in vitro* association of the GAG with collagen and the formation of unspecific electrostatic heparin bridges between the tropocollagen monomers and microfibrils. Unspecific electrostatic interaction could take place since it is known that the collagen molecule carries approximately 270 positively charged groups per helix (amino acid sequence: Swiss-Prot/TrEMBL: P02453 (CO1A1_bovine), P02465 (CO1A2_bovine) (236), which are very often just a few angstroms apart (237). Although the concentration range and ratio of collagen and heparin varied considerably in different studies, it was commonly found, that low concentrations of heparin promoted fibril formation, while high concentrations inhibited fibril assembly (167, 182, 229, 230). Based on those findings some principles of association of heparin (or other GAG) in the process of fibril formation were proposed, however, due to the various range of used concentrations and different investigation techniques a consistent picture of the process and the important parameters are not fully established. The binding and fate of heparin molecules during fibril assembly remains hardly addressed, although it is a quite important question in this context. Heparin is proposed as a cross-linking molecule for tropocollagen or microfibril building

blocks during *in vitro* cofibrillogenesis (182, 235), yet no *in vivo* (165, 238–240) nor *in vitro* (24, 129, 183, 241) reports could provide evidences for the intercalation of any GAG or PG in fibrillar structures. All these studies generally address the localization of the GAG as interfibrillar.

The data presented in this section demonstrates the build-up of very thick collagen fibrils with the greatest width at a heparin/atelocollagen solution ratio of 1/3. The cofibrils exhibited a straight spindle-like shape which was not previously reported for similar studies with heparin (182, 230, 241) but was observed in recent studies for other GAGs (24, 183). The current study extends the previous knowledge in this field by implementing analysis on a broad range of deployed heparin concentrations and a more detailed structural investigation of the grown cofibrils by furthermore combining it with kinetic data of the cofibrillogenesis. A strong correlation of the cofibril diameter at the end of 24 h precipitation could be drawn to the OD of collagen-heparin fibrillar material in the nucleation phase. The maximum OD after the nucleation phase was found for intermediate heparin concentrations, which directly translates into the maximum of fibril diameter at the end of the cofibrillogenesis. These findings correlate with previous studies stating the importance of the nucleation phase (166, 242) and earlier research on the kinetics of pure collagen fibrillogenesis showing that the nucleation phase, in which the soluble tropocollagen triple helices accrete to preformed nuclei (activation centers), predominates over growth and that the size of the finally formed fibrils is determined during this lag period (152, 153). Hence, the strong heparin binding to atelocollagen influences the whole assembly process. The current observations support earlier findings, that it is indeed the electrostatic interactions which dominate in heparin-collagen binding (168). This clear hint comes from the variation of the solution pH value during cofibril assembly, varying the molecular weight of heparin, and the variation of the degree of sulfation of the used GAG, i.e. replacing heparin by HS or HA (229, 233). In that way the decrease of fibril formation at very high heparin concentrations or its inhibition at lower pH can be interpreted as an effect of overcharging and resulting repulsion between tropocollagen molecules as suggested in (182), too. After the nucleation phase, the lateral accretion of nuclei is proposed as the dominant growth mode, which should be promoted by the electrostatic interaction of heparin bound to the collagen. The halo of smaller fibrils lying in vicinity to the big cofibrils in the SFM investigations correlates very well with the high amount of preformed nuclei nevertheless no direct structural relation between them and the cofibrils was found, an issue which will be elaborated in section 4.2. The kinetic data of the turbidimetric analysis support this finding as low concentrations of heparin tend to accelerate fibril formation, which comes as a result of an electrostatic binding between the numerous nucleic material charged with heparin. The increase of the heparin amount in solution leads to slowing down the cofibril growth, probably due to issues of local transport and positional arrangement of

the nucleic material. As a result of this growth process, the difference in width-to-length ratio in dependence on heparin concentration can be interpreted as the outcome of two concurring growth mechanisms: a more longitudinal growth which is common for the early growth stages of the pure collagen I system (152) and a mode of lateral accretion by parallel interaction of nuclei which is promoted by the heparin-collagen interaction.

The conducted experiments determine the specific binding of heparin inside the cofibrils as one of the very important findings of this work. In the process of lateral accretion heparin is intercalated inside the growing fibrils acting as promoter and stabilizer of the assembly of microfibrils into thick straight cofibrils. This interesting feature can be revealed from the heparin quantification data and cLSM analysis. The correlation of heparin content with cross-section area of the cofibrils and the necessity of their enzymatic digestion for complete detection of all bound heparin clearly shows that heparin is located inside the fibrils. The equality of the difference in detected heparin amounts with and without enzymatic digestion to the amount of heparin after 24 h rinsing confirms the binding of the part of quantified heparin intercalated inside the PSC fibrils. The conclusion is supported by the fact that the highest amount of bound heparin was measured in the case of the thickest cofibrils (smallest surface area per collagen amount). Additionally, the molar ratio of heparin to atelocollagen of approximately 1 (even for the highest heparin solution concentration) calls for a specific binding of heparin to PSC at one primary binding site on tropocollagen and eventually inside the cofibrils, as previously reported (235). This is in agreement with the suggestion of heparin acting as cross-linker of atelocollagen molecules in the process of fibrillar assembly (182), but adds the clear message that it is stably intercalated inside the cofibrils with a specific binding, a feature not reported up to now for neither *in vivo* nor *in vitro* systems containing other GAGs (24, 183, 238–240, 243).

In summary, Fig.4.14 provides a scheme of the important steps of collagen fibril formation in the presence of heparin elucidating the dominant parameters in this process. The nucleation phase has the dominant function (Fig.4.14 A) in which heparin binds to the atelocollagen monomers via strong electrostatic interaction leading to the formation of an increasing number of nuclei (Fig.4.14 B) with increasing amounts of available heparin. The very high heparin concentration has a visible oversaturating effect probably caused by electrostatic repulsion –due to an excess of negative charges- and/or steric hindrance by the heparin molecules. The nucleation phase determines the destiny of the subsequent cofibril assembly in which a lateral accretion of nucleic material leads to the build-up of large cofibrils. The kinetics of this process is influenced by the transport properties of the available building blocks and the increased lateral accretion for higher loadings of collagen molecules with heparin. At these conditions acceleration is observed due to the electrostatic interaction of heparin with PSC for lower amounts of heparin, while at the same time a retarding effect acts on the system due to the larger amount of nucleic material

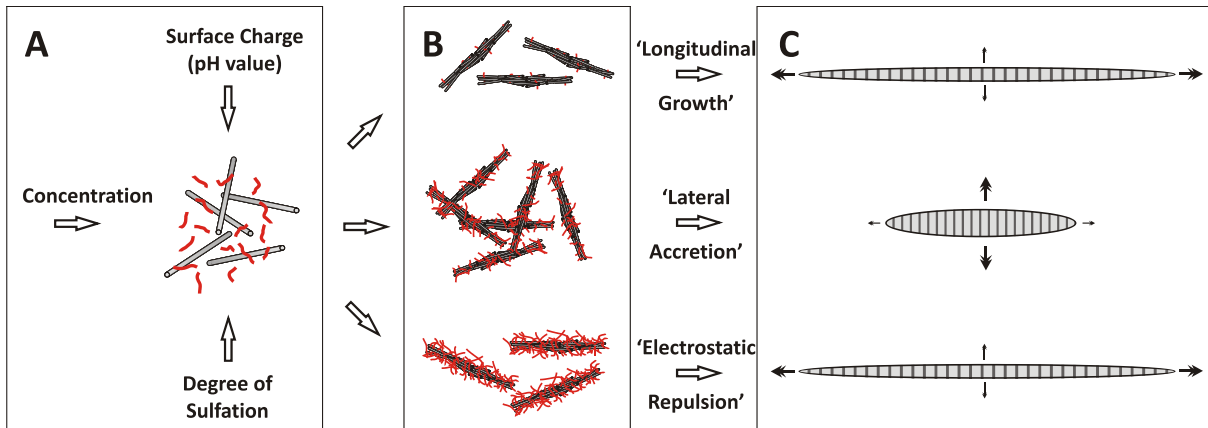


Figure 4.14.: Proposed scheme of the important steps of PSC – heparin cofibrillogenesis portraying the dominant parameters: 1. the formation of different amount of nuclei (B) with dependence on charge and concentration of GAG (A); 2. their different mechanisms of lateral or longitudinal growth into spindle-like cofibrils (C) driven by electrostatic PSC-heparin interaction and steric hindrance. The 3 images in (B) and (C) represent 3 different concentrations of heparin – from top to bottom – low (e.g. 0.01 mg/ml), intermediate (e.g. 0.4 mg/ml) and high (e.g. 4.0 mg/ml).

and its steric hindrance in transport. Finally, thick spindle-like cofibrils are assembled due to the enhancement of lateral accretion of nuclei against longitudinal growth by the presence of heparin, and are furthermore stabilized by the intercalated GAG.

4.2. Structural polymorphism of collagen type I fibrils

The appearance of various types of structures, such as cofibrils, smaller nanofibrils and nuclei, raised the question about their involvement in the fibril assembly process (see section 4.1). The property of collagen systems to exhibit varying structural characteristics, else known as structural polymorphism, is a very intricate interplay between various parameters (discussed in 4.2) which define the arrangement of the collagen monomers into hierarchical suprastructures. Therefore, the formation of various polymorphic forms and structural levels was studied in detail by means of SFM and high resolution TEM.

4.2.1. Structural levels and banding periodicities

The previous analysis of the PSC – heparin system exhibited a non-linear correlation between the concentration of the GAG and the morphology of the reconstituted cofibrils with the most pronounced width-to-length ratio and average diameter at PSC and heparin concentrations of 1.2 and 0.4 mg/ml respectively. Thereby, this intermediate concentration was chosen as constant in all experiments during this study. Also, since no differences with respect to the M_W were observed, the highly sulfated GAG from now on will be only addressed as heparin. As previously discussed the reconstitution of the PSC-

heparin cofibrils is a process which involves: 1) a nucleation phase at 0 °C during which the atelocollagen molecules interact electrostatically with heparin, and 2) cofibrillogenesis taking place at 37 °C during which the already formed nucleic material participates into the formation of the big cofibrils. In order to get information about the fibrillar structures existing in the system, suspensions from already reconstituted cofibrils were subjected to analysis (Fig.4.15).

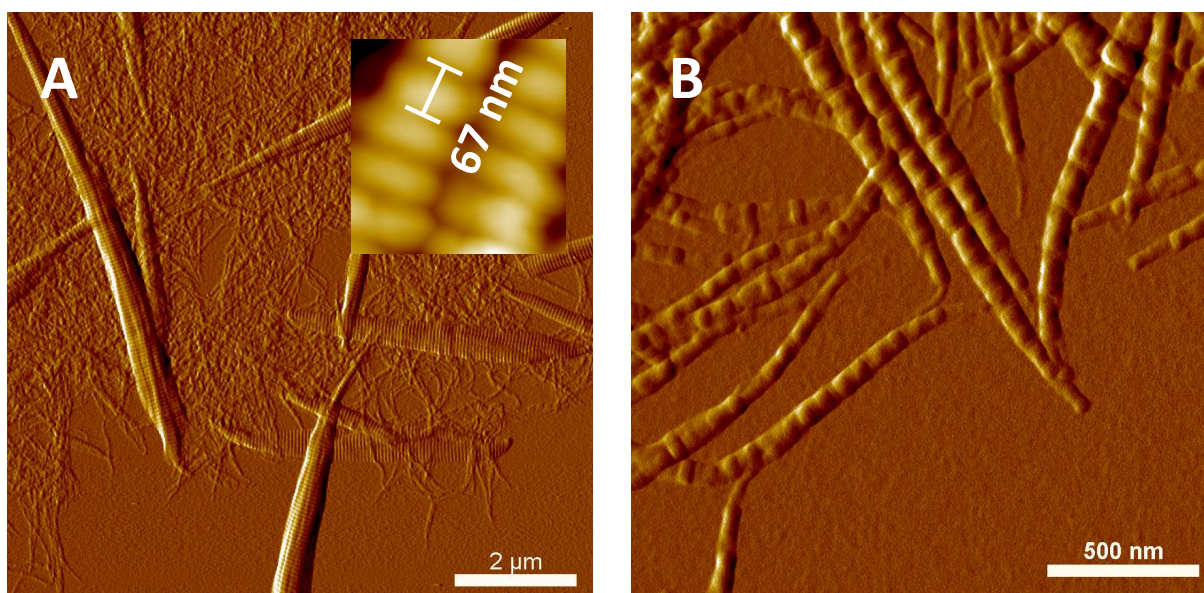


Figure 4.15.: *SFM images of the two existing structural levels in the system with reconstituted PSC – heparin fibrils: (A) ‘cofibrils’ and (B) ‘nanofibrils’ (after 24 h cofibrillogenesis at 37 °C). Inset in (A) shows the typical 67 D-banding periodicity of the cofibrils.*

The morphological analysis of the samples at the end of the 24 h cofibrillogenesis exhibited the previously observed straight and thick fibrils (diameters reaching 1 μm) which differ significantly from the twisted and thinner pure PSC fibrils (Fig.4.15 A). These big fibrillar structures coassembled from collagen I and heparin we herein refer to as ‘cofibrils’. While the cofibrils were substantially different than the PSC fibrils they shares the same D-banding periodicity of 67 nm. As already mentioned in 4.1.1.4, typical for all heparin containing samples was also the presence of a halo of smaller fibrils lying in vicinity to the big cofibrils (Fig.4.15 B). With a diameter of 80 – 100 nm they appear to be almost an order of magnitude smaller than the average cofibrils, and had a striking regularly repeating banding periodicity of 160–170 nm. Therefore, we refer to them in the following as ‘nanofibrils’. The fact that cofibrils and nanofibrils differ not only in structure and size, but also banding periodicity comes as a clear sign that they represent distinct structural levels in the system. In order to better understand the origin of the polymorphic forms and the reason for their coexistence we looked in more detail on the symmetry of their banding patterns. This analysis should help to explain the effect of heparin in the fibrillar self-assembly of PSC.

4.2.2. Cofibrils with asymmetric D-banding

The rather unusual intercalation of heparin into the cofibrils with remaining D-banding periodicity of 67 nm, discussed in 4.1.4, raised the question about the symmetry of the atelocollagen arrangement within the cofibrils. To clarify this issue, an in-depth TEM study with 3 different stainings and overall of 2 different preparation techniques was carried out (Fig.4.16).

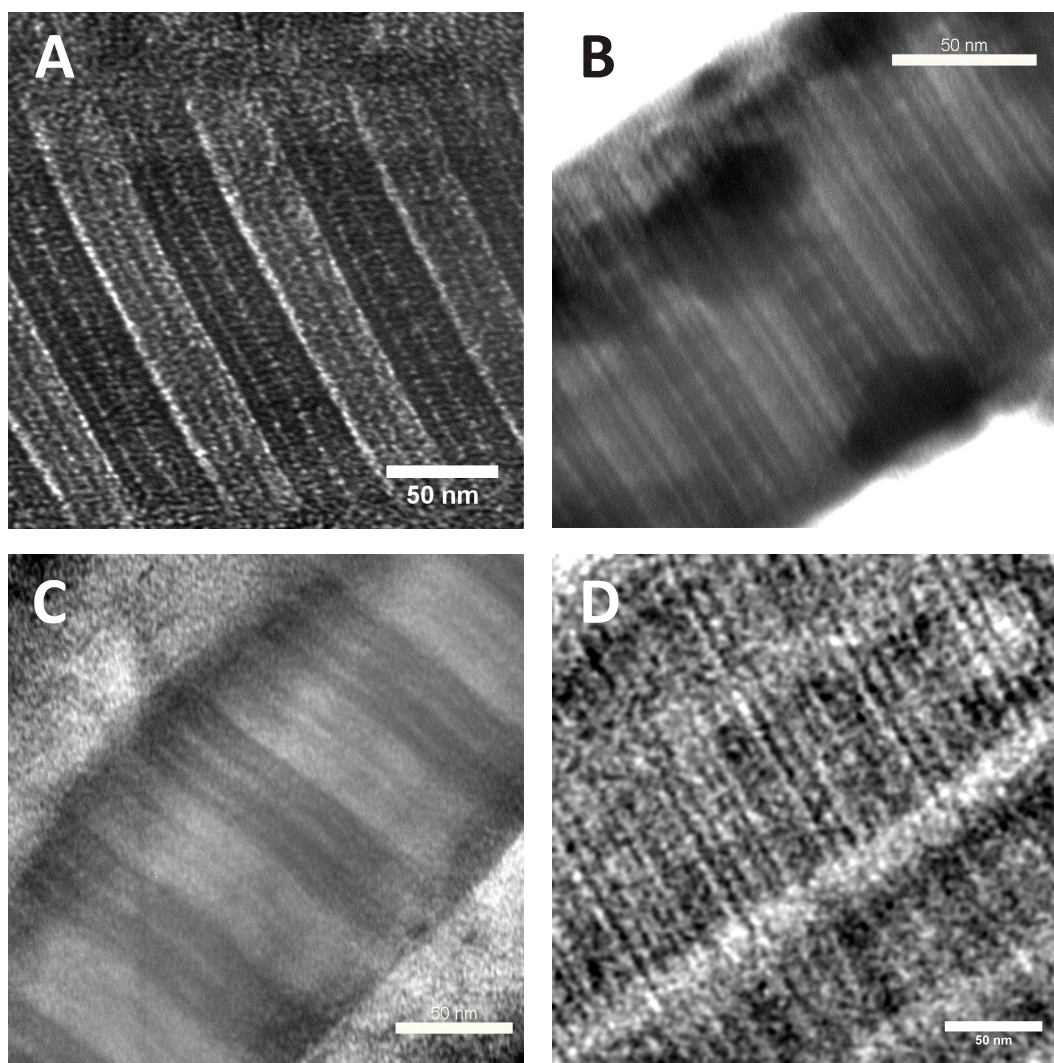


Figure 4.16.: High-resolution TEM images of PSC – heparin cofibrils. Preparations included: (A) Negative staining with 2% aq.sol. uranyl acetate (UA) (pH 4.2); (B) Staining with 1% phosphotungstic acid (pH 3.5), counterstaining with 5% filtered tannic acid and negative staining with 2% UA (pH 4.2); (C) Positive staining with 2% UA (pH 4.2); (D) 300 nm sections of UA-stained cofibrils embedded in epoxy resin.

All staining techniques revealed the formation of a D-banding pattern of 67 nm with the typical recursion of 2 major zones of unequal density. This was especially characteristic for negative staining protocols (Fig.4.16 A,B and Fig.4.17 B,C). The negatively stained samples exhibited more contrasted and preserved striations in comparison to the hardly recognizable bands in the positively stained specimen. The structures appear to

be clearly asymmetric. Although not typical for pepsin-treated tropocollagen this observation falls into a very good agreement with previous studies using enzyme-purified collagen type I and highly sulfated synthetic GAGs as pentosan-polysulfoester (SP54) and mucopolysaccharide polysulfoester (Arteparon) (129, 242). The in-depth comparison of the TEM density profiles with reported density profiles of native collagen type I (87) as a reference resulted in a very close match of both densitometric linescans (Fig.4.17).

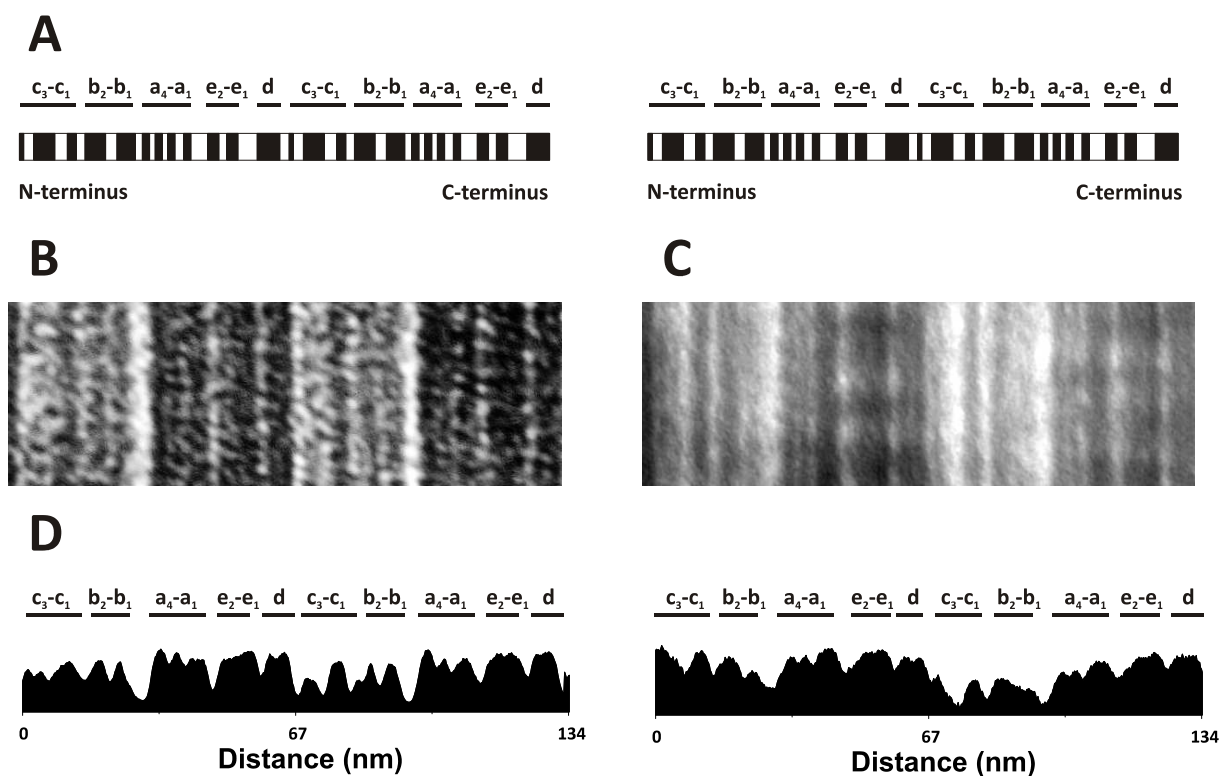


Figure 4.17.: *Asymmetric density profiles of PSC – heparin cofibrils. Samples in (B) were negatively stained with 2% UA, while specimen in (C) was stained with 1% PTA, counterstained with 5% filtered tannic acid, and negatively stained with 2% UA. Computer-generated diagrammatic representation of native collagen banding (A) (according to (87)) as opposed to 25-pixel averaged densitometric linescans (corresponding to (B) and (C) respectively) signifying the recorded density of stain uptake along 2x D-patterns (134 nm). The typical (A) and putative (D) notation of collagen bands is given above the intensity maxima. The profile in image (C) was normalized to 2 D-periods due to the small deviation (10–15%) which is expected to arise from different preparation protocols (shrinking upon beam exposure, thickness of the layer, conventional drying, etc.).*

The axial polarity of the cofibrils can be directly recognized from the images. However, since some of the subperiods are not clearly discernible a straightforward correlation is hard to make and the band assignment in the cofibril case should be taken as more informative. Nevertheless, a close comparison between them reveals characteristic features for the asymmetric collagen type I systems (93) like the 2 diffuse and tending to merge e_1 and e_2 bands, a very pronounced d band, broad and intense b_1 and b_2 bands, close and somehow indiscernible $c_1 - c_3$ bands. It's worth noting that the typical $a_1 - a_4$ quartet

looks slightly different than its typical appearance in native collagen type I systems which could be attributed to more or less significant changes in the telopeptides contributing to the density in this region.

Similar spindle-shaped fibrillar assemblies as the herein described cofibrils have been previously reported for different conditions, ranging from systems with various terminal collagen type I enzymatic modification (156, 244, 245) to environments reconstituted in the presence of natural/synthetic GAGs (24, 183). There has also been the notion that systems utilizing pepsin-modified collagen type I and GAGs are prone to forming symmetric spindle-like fibrils. It has been shown that the selective removal of the telopeptides generally affects the collagen fibrillogenesis as well as the native asymmetric banding of 67 nm. Pepsin treatment is considered responsible for the complete removal of N-telopeptide and partial truncation of the C-telopeptide (120, 161). In that case, removal of the main electrostatic regions from both termini is expected to prevent a normal electrostatic interaction of the tropocollagen moiety, leaving the hydrophobic clusters as the remaining driving force in the self-assembly. However, an interesting alternative could be the presence of high negatively charged heparin. Its small size and increased conformational flexibility (246) could ensure its serving as a potential intra- and intermolecular bridge between the atelocollagen helices. This is supported by the previously reported two specific binding sites of heparin along the monomeric tropocollagen chains, located in close proximity to the C-terminus (234) and the N-terminus (235) and the preservation of the large hydrophobic C-terminal cluster ensuring further hydrophobic interactions that are known to be critical in native collagen type I assembly. Combined with the earlier findings of heparin to be intercalated into the cofibrils (see section 4.1.4), it is plausible that D-periodic asymmetric cofibrils can be produced from PSC in the presence of heparin, as endorsed in previous studies (129, 242). Axial arrangement (parallel vs. antiparallel) has also been shown to depend on the partial or incomplete enzymatic removal of telopeptide regions (121), which combined with observations presented above, points towards the conclusion that the formation of asymmetric cofibrils is most likely a sophisticated interplay between the extent of telopeptide removal, electrostatic interaction with high negatively charged molecules (especially in the initial phase), and hydrophobic interactions being typically important in collagen type I systems. Nevertheless, exact binding of the heparin along the atelocollagen chains at this point is rather speculative. Possibilities range from heparin occupying the spaces left vacant by the missing telopeptides, positioning along some other gap regions, or binding at its specific binding sites along the atelocollagen molecule. The previous biochemical analysis showing a molecular ratio of both molecules of about 1:1 pointed towards a specific interplay between atelocollagen and heparin which could be the case of positioning along one or both of the specific binding sites reported previously. These possibilities are further investigated and discussed in section 4.3.

4.2.3. FLS IV nanofibrils with symmetric periodicity

The second structural level which was found in the system involved the so-called 'nanofibrils'. Tracking the SFM height of such molecule along its length revealed regularly repeating blocks of 165 nm with recursive appearance of major and minor grooves which seemed to be symmetric along this repeating unit (Fig.4.18).

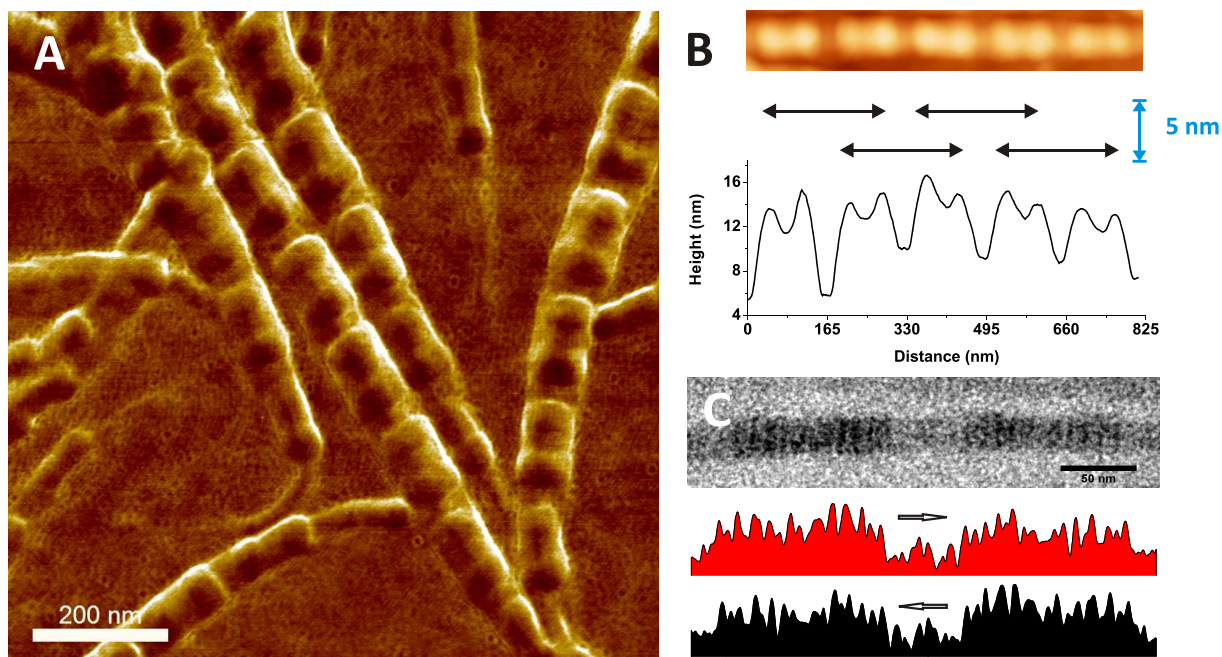


Figure 4.18.: (A) SFM phase image of symmetric nanofibrils. Cross-section along the surface of one of the nanofibrils (B) revealed a regular banding periodicity of 165 nm. (C) Juxtaposing front and reversed densitometric profiles from a TEM image of a single nanofibril accounts for a symmetric stain uptake and banding periodicity. Specimen in (C) is a 100 nm section of UA-stained nanofibrils embedded in epoxy resin.

The stepwise congruent height differences between the major and minor grooves of 5 nm (Fig.4.18 B) most probably represent a discrete step in the growth mechanism of the molecule pointing the specific building blocks. In order to draw definitive conclusion about the symmetry of the nanofibrils, analysis of 100 nm sections of UA-stained PSC-heparin gels embedded in epoxy resin after glutaraldehyde fixation, was carried out via TEM. A densitometric scan along a nanofibril length of 2 characteristic bandings of 165 nm showed similar profile to the one which was observed previously with SFM. To check the dihedral symmetry of the molecule, the front and reversed profiles of the stain uptake were transposed (Fig.4.18 C). The result is an almost impeccable match between both linescans which is another proof for the symmetry of the molecule as already implied from the SFM images. In contrast to the cofibrils, the relatively smaller nanofibrils in the system exhibited a non-D-periodic symmetric pattern, reported previously for CS-containing collagen type I systems (117, 150). The average periodicity of such a dihedral symmetry was shown to be ca. 165–170 nm and is typically referred to as FLS IV (138).

The discrete height differences of 5 nm, at the end of the FLS IV nanofibril tips in addition to the transition from a longspacing nucleic fibril to an FLS IV banding (Fig.4.18 B) is a clear sign for the mechanism of their formation by addition of small segments (see section 4.2.4), as suggested previously (138).

4.2.4. Nucleic origin of polymorphic forms

Obviously, in the system symmetric FLS IV nanofibrils coexist with asymmetric cofibrils. It has to be noted that this coexistence was not accompanied by a transition between both polymorphic forms as such a behavior was never observed in our numerous SFM and TEM investigations. This finding poses the question about the mechanisms and the building blocks leading to the concomitant formation of both structures. The importance of the nucleation phase in the fibril assembly process (as already stated in 4.1.3), as well as emphasized in previous biochemical and ultrastructural studies of collagen-GAG systems (129,166), prompted the further interest in analyzing the structure of the nuclei material formed prior to the start of the cofibrillogenesis. Previously, a direct correlation between amount of the nucleic material and the thickness of the cofibrils. Further morphological analysis of the nuclei indicated their diameter to be around 20–40 nm (Fig.4.19 A).

From the SFM images in Fig.4.19 A, no particular banding was observed for the nuclei, although their very high density and intertwined morphology would most likely obscure any of these. However, high-resolution TEM analysis revealed a banding pattern of 250–260 nm, which probably comes as a result of the multiple 4D staggering of atelocollagen molecules, and is usually assigned to either asymmetric or symmetric longspacing fibrils (Fig.4.19 B). An additional extensive SFM investigation of assembled PSC-heparin cofibrils after 24 h revealed other small building blocks similar to the nuclei. At first, a number of short longspacing segments with length of approximately 300 nm and no apparent banding was observed (Fig.4.19 C,D). A closer look at the segments revealed a number of smaller filamentous structures aggregated laterally with pronounced nodule thickenings at the beginning and the end. Similar segments are known to arise directly from either parallel or antiparallel staggering of tropocollagen molecules giving them either a symmetric (116, 117, 141) or asymmetric SLS (141) banding. Another recurring feature was the presence of thinner but longer longspacing fibrils with less pronounced nodule thickenings at every 250–260 nm (Fig.4.19 C,E). Together with the observations of the nuclei (Fig.4.19 A,B), this finding suggested that the longspacing fibrils were probably residual nuclei fibrils with the same banding pattern of 250 nm. Their significantly lower density in comparison to the one at the end of the nucleation phase implied their potential involvement as building blocks in either FLS IV nanofibrils or asymmetric cofibrils, or both at the same time. Unfortunately, neither TEM nor SFM studies of longspacing

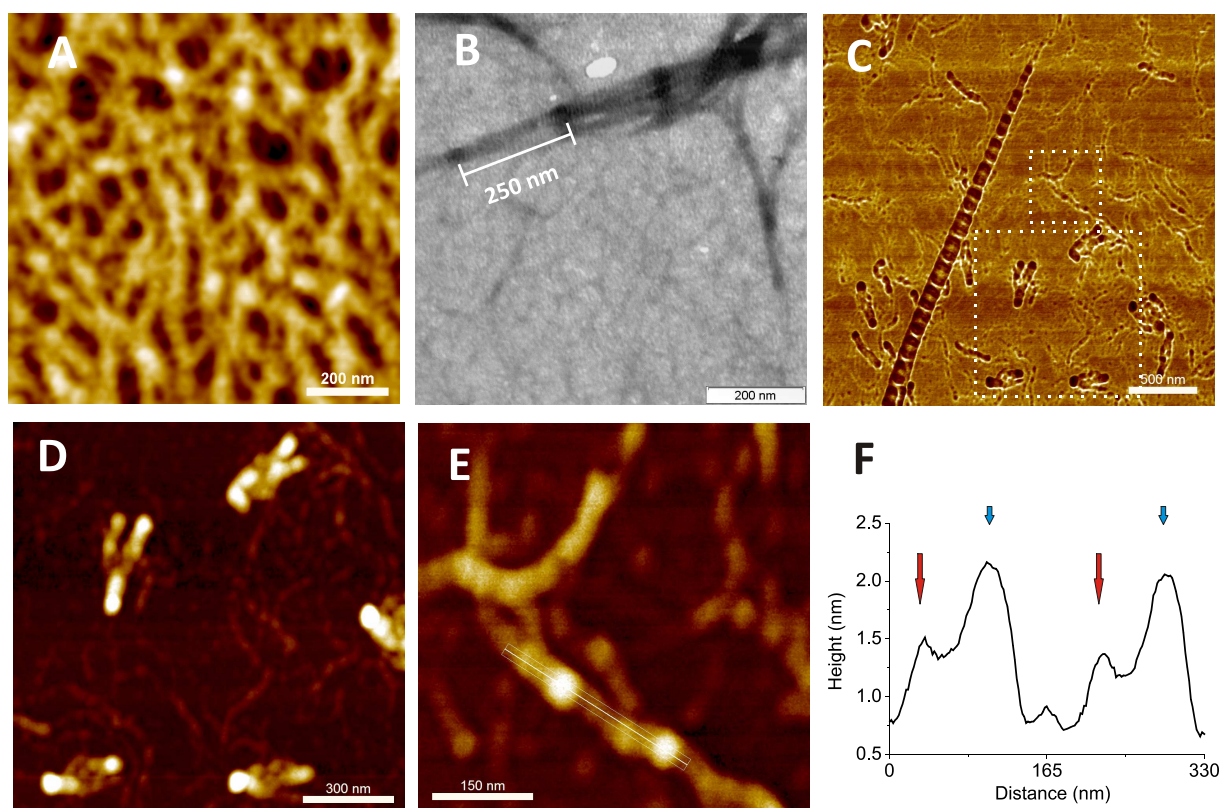


Figure 4.19.: (A) SFM and (B) TEM images of nuclei fibrils formed at 0 °C, prior to the beginning of the cofibrillogenesis. (C) SFM phase image of the structural elements, present in reconstituted collagen type I – heparin gels. Marked by a dashed line are magnified scans presented in (D) and (E) respectively. (D) Reveals the possible origin of a FLS IV nanofibril banding from a long longspacing nuclei fibril with a periodicity of 260 nm by addition of a 300 nm short longspacing segment. (E) The existence of 300 nm longspacing segments. (F) Cross-section along the fibril in (D) indicating the stepwise transition from 250–260 nm longspacing periodicity to a ‘FLS IV-like’ banding. The long red arrows represent the peaks from the longspacing fibril, while the short blue ones show the increase in height (ca. 1 nm) after the addition of a short longspacing segment with a length of 300 nm.

fibrils failed to produce conclusive patterns and clarify their either symmetric or asymmetric arrangement. Nevertheless, tracking the length of the longspacing fibrils led to another interesting conclusion about the polymorphic structures in the system (Fig.4.19 E). The profile of a longspacing fibril reveals heights of respectively 1.5 and 2.5 nm which could be the origin of a FLS IV nanofibril (Fig.4.19 F). The peaks marked with long red arrows account for the regular 250 nm banding coming from the longspacing nuclei fibrils. The second pair of peaks (marked with short blue arrows) appears with the same spacing of 250 nm. The displacement pitch of 45–50 nm resembles strikingly the pattern of the FLS IV nanofibrils in the system. At the same time, the smaller height difference and random appearance of a second pair of peaks in comparison to the fully reconstituted FLS IV nanofibrils suggest that it is most probably a product of the addition of a single short longspacing segment, rather than just lateral aggregation of more than one longspacing

nucleic fibril. A clear indication for this distinct difference to the full FLS IV nanofibrils is their more pronounced and stepwise transition between the repeating units of around 5 nm at the end of the FLS IV nanofibrils (Fig.4.18 A). This interpretation was further supported in another experiment where the contribution of the nucleation phase to the polymorphism in the PSC-heparin system was analyzed.

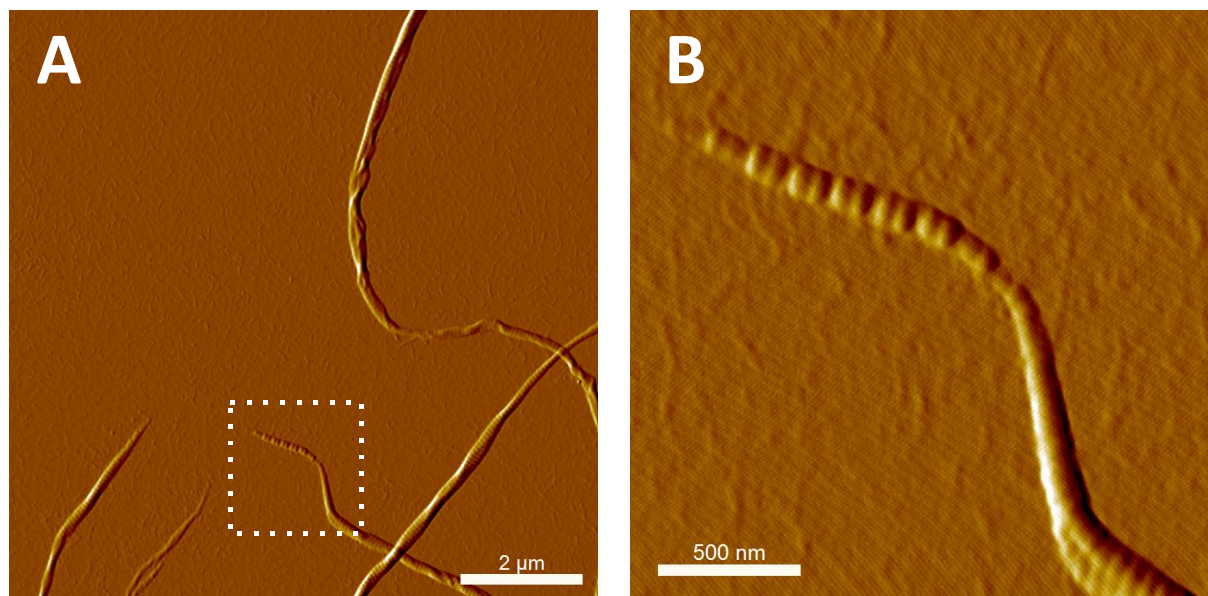


Figure 4.20.: *SFM images of PSC fibrils formed after the addition of heparin during the exponential growth phase (A). The twisted curved fibril morphology is essentially the same as the one of the pure PSC fibrils which emphasizes the importance of the nucleation phase for the formation of PSC-heparin cofibrils. The detail marked by the dashed line in (A) is presented in (B) which shows an unusual transition from a D-periodic banding (67 nm) to a FLS IV nanofibril periodicity of 165 nm.*

Earlier studies already showed that the addition of heparin at the end of the nucleation phase does not initiate the formation of cofibrils in the system (data not shown). Furthermore, a study of the influence of heparin addition at the exponential half-time point was carried out. The morphological analysis showed the presence of the typical twisted D-banded PSC fibrils (Fig.4.20 A) as the ones observed in previous studies without added heparin. The only exception was the tip of a single fibril which showed a surprising transition from an asymmetric D-banding of 67 nm to a symmetric FLS IV pattern of 165 nm (Fig.4.20 B). This observation leads to a couple of hints about the formation of the polymorphic structures discussed above. At first the presence of heparin during the formation of nuclei seems to be a prerequisite for the formation of cofibrils. Secondly, the appearance of the symmetric FLS IV banding at the very end of an asymmetric PSC fibril implies the most probable involvement of an asymmetric PSC scaffold/nucleus in the formation of FLS IV nanofibrils. On the other side, the transition from an expectedly asymmetric PSC to a symmetric FLS IV fibril suggests the existence of symmetric building blocks. This situation resembles very closely the above discussed transition from a longspacing

nuclei fibril to a FLS IV banding by the addition of short longspacing 300 nm segments.

4.2.5. Discussion - Transition and coexistence of the different structures

The coexistence of both asymmetric cofibrils and symmetric FLS IV nanofibrils in the system raises the question for the common or different principles governing the simultaneous formation of 2 essentially different polymorphic forms at the same time. The answer to that obviously lies in the electrostatic nuclei complexes formed prior to the start of the cofibrillogenesis. There are evidences that the nuclei are involved in the formation of both FLS IV nanofibrils and cofibrils. First of all, the fact that neither FLS IV fibrils nor cofibrils are present during the nucleation phase. Second of all, the substantially decreased number of nucleic fibrils during cofibrillogenesis would imply their participation as a frame for the buildup of asymmetric cofibrils and/or symmetric FLS IV nanofibrils. This is also supported by the earlier turbidimetric studies (see sections 4.1.2 and 4.1.3) indicating the size of the cofibrils in direct correlation with the amount of nucleic material prior to the start of the cofibrillogenesis. Re-analysis of the previously gathered data sets interestingly indicated the same correlation for the number of FLS IV nanofibrils. At the same time, the FLS IV nanofibril formation is suggested to depend on the occurrence of an additional building block (short segments) after the nucleation phase. Due to the lack of high resolution banding data for both the longspacing fibrils and short segments we have to consider the following 4 possibilities in axial monomeric arrangement of the building blocks to form the two different fibrillar symmetries:

1. ***Symmetric longspacing fibrils (FLS I) and symmetric short segments (symmetric SLS)*** The existence of both symmetric longspacing forms in the system would corroborate the formation of symmetric FLS IV nanofibrils (117) but not the asymmetric cofibrils observed in the system and in a similar report with pepsin-digested collagen type I (242).
2. ***Symmetric longspacing fibrils (FLS I) and asymmetric short segments (SLS)*** Formation of asymmetric cofibrils would depend solely on the asymmetric SLS segments which were however never found in the TEM investigations of nuclei samples at 0 °C. It would also contradict with the straight correlation between amount and size of the cofibrils and the nuclei in the system.
3. ***Asymmetric longspacing fibrils (SLS fibrils) and asymmetric short segments (SLS)*** The parallel 4D-staggering of asymmetric SLS fibrils appears to be the best alternative for the formation of asymmetric cofibrils, discussed in earlier reports (129, 247). However, if both asymmetric molecules are responsible for the formation of symmetric FLS IV nanofibrils, theoretically, they are expected to be

present already in the nucleation phase, but none of the investigations account for that.

4. *Asymmetric longspacing fibrils (SLS fibrils) and symmetric short segments (symmetric SLS)* Asymmetric SLS fibrils can serve as a framework for both the formation of the asymmetric cofibrils and the symmetric FLS IV fibrils. This would be in a good agreement with the relation between size/amount of nuclei and the size/amount of cofibrils and nanofibrils at the end of the cofibrillogenesis. It is also supported by the observed transition between a native 67 nm banding to a symmetric FLS IV banding by the addition of heparin in the middle of the exponential phase.

By reviewing the 4 possible arrangements for the observed longspacing nuclei fibrils and short segments, we would like to adopt the only one (asymmetric longspacing nuclei fibrils and symmetric short segments) which is in no contradiction with any of the earlier observations and suggest the following mechanism for the building principles governing the assembly of the asymmetric cofibrils and symmetric nanofibrils (Fig.4.21). In the first phase (nucleation) the atelocollagen interacts specifically with the highly negatively charged heparin thus leading eventually to the formation of asymmetric SLS fibrils with a banding of 250–260 nm, the binding site for which would be further discussed in section 4.3. The growth to asymmetric D-periodic cofibrils is initiated after a temperature switch to 37 °C and involves a quarter staggering of the asymmetric SLS fibrils, a process expectedly driven by both electrostatic and hydrophobic interactions. On the other side the transition from asymmetric longspacing fibrils to symmetric FLS IV nanofibrils is provided by the stepwise addition of probably symmetric segments of 280–300 nm, which are formed only after the nucleation phase. They use as a frame the tips of the already existing asymmetric SLS fibrils and continue to grow in a stepwise manner producing FLS IV banding.

Understanding the origin of the observed polymorphism in the system requires a closer look at the amino acid sequence of the tropocollagen molecule (138). It has been suggested that the distribution of charged and large hydrophobic residues in the triple helical region is responsible for favorable interactions at 0D, 1D, 2D, 3D and 4D-staggers, where D is about 234 residues and that a 4D-staggered longspacing fibril would most likely be a product of either parallel or antiparallel electrostatic tropocollagen interactions (248). This was shown for both symmetric FLS I fibrils with CS (116,117), and asymmetric SLS aggregates with highly negatively charged molecules including synthetic polysulfates and ATP (116,141,242). It appears that principles governing both the FLS I and SLS fibril formation are similar. The proposed mechanism (Fig.4.21) focuses on the duality of the heparin falling concomitantly in the group of the small high negatively charged molecules and naturally present sulfated GAGs. In one of the cases the combination of low tem-

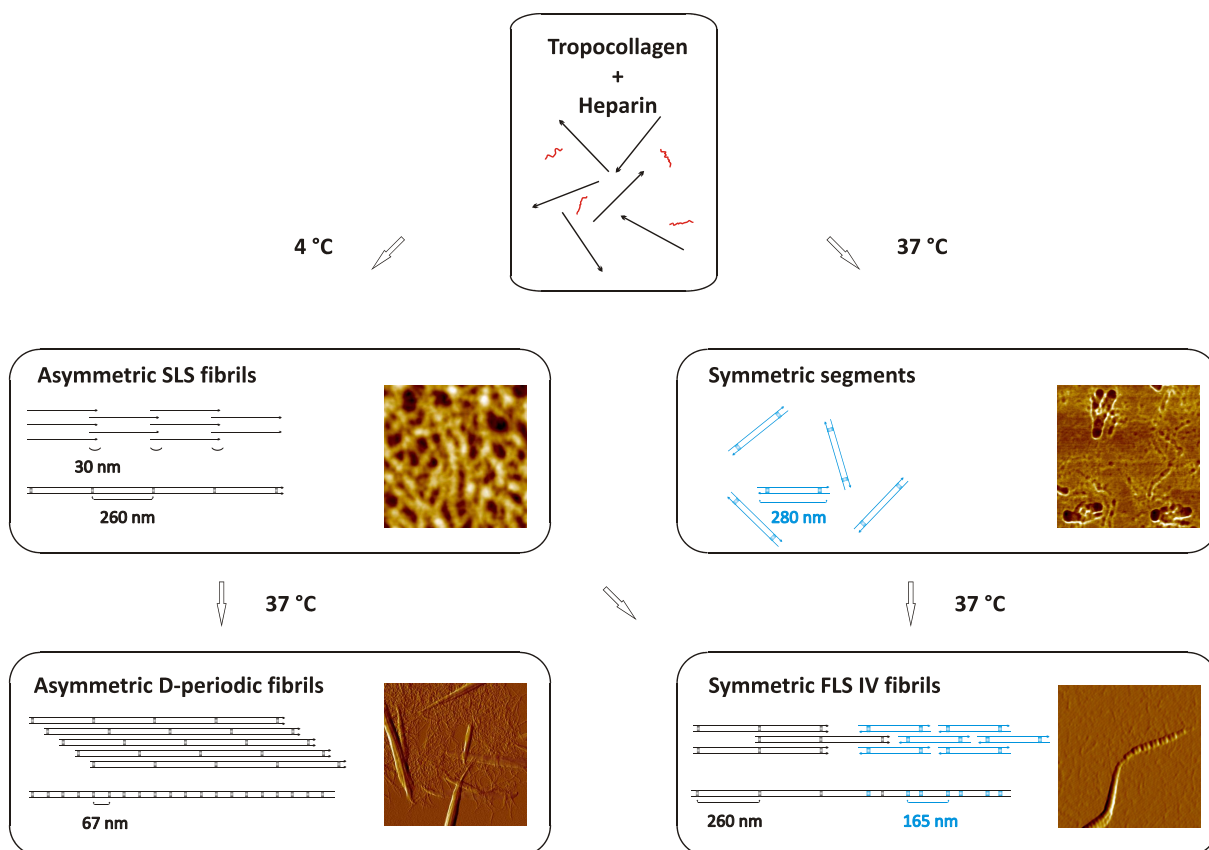


Figure 4.21.: Proposed mechanism for the hierarchical self-assembly of asymmetric D-periodic cofibrils and symmetric FLS IV nanofibrils from pepsin-treated bovine collagen type I and highly sulfated heparin.

perature and high negative charge obviously favors a polar electrostatic interaction, while physiological temperature favors the assembly of symmetric segments. This interpretation would be in agreement with a previous speculation (138) that polar SLS arrangements are normally associated with very precise positioning and overlapping of the positive charges along the tropocollagen molecule in difference to the symmetric FLS interactions. In that case, a system with lower temperature and essentially decreased particle motion would favor a more precise alignment of the heparin and its specific binding sites along the atelocollagen molecule. From this point of view temperature would seem like an important factor for the symmetric or asymmetric arrangement in the system. In terms of biological significance, it has to be noted that collagens and PGs (GAGs bound to a protein core) are typically associated on an interfibrillar level (151, 152). Due to the possible steric hindrance from the protein side, however, the question whether the pure GAGs can be intrafibrillar remains open, as it can be seen from a number of reports *in vivo* (165, 173). In that aspect the current study offers an interesting model for the formation of some structurally heterogeneous polymorphic forms which can be found in nature (114, 115).

In summary, the study of the different polymorphic fibrillar forms in the system of reconstituted PSC and heparin fibrils offers enough conclusive data for the existence of 4

different structures which are generally referred to as: 1) SLS fibrils; 2) symmetric segments; 3) FLS IV nanofibrils; 4) D-periodic cofibrils. The fact that each of them differs not only in average diameter but also in banding periodicity defines them as distinct structural levels and emphasizes the structural hierarchy in the system. The coexistence of asymmetric D-periodic cofibrils and FLS IV symmetric nanofibrils was furthermore shown in the system. Meanwhile, it provides a reasonable explanation for the simultaneous formation of symmetric and asymmetric supramolecular fibrils in the system and suggests a model for the underlying building principles pointing towards the importance of heparin as an intercalated crosslinker in the system.

4.3. Impact of heparin intercalation on intrafibrillar packing and mechanics of collagen I fibrils

The earlier study of the structural polymorphism in the PSC-heparin system suggested the formation of the asymmetric cofibrils from segment long spacing (SLS) fibrils, the latter being formed directly at 0 °C by electrostatic interaction between atelocollagen and heparin (see section 4.2). In order to answer the question about the specific loci of heparin binding along the atelocollagen chain in the case when the GAG is intercalated within the fibrils, further morphological, structural and mechanical comparison of collagen type I with (ASC) and without intact telopeptides (PSC) and PSC-heparin fibrils was carried out.

4.3.1. Impact of heparin and telopeptides on collagen type I fibrillar ultrastructure (WAXS)

The reconstitution of both ASC and PSC, in the presence of heparin at physiological temperature and *pH* for 24 h, led to the formation of fibrillar structures (Fig.4.22).

SFM analysis of the pure PSC system showed the formation of the typical thinner D-periodic (67 nm) fibrils with the characteristic ‘rope-like’ twist observed previously for native collagen I (249) (Fig.4.22 A). The PSC-heparin system exhibited the typical thicker tactoidal cofibrils with a D-periodic asymmetric banding periodicity, accompanied by the presence of previously described symmetric FLS IV fibrils with an average periodicity of 165 nm (138, 250). The presence of heparin in the case of ASC failed to reproduce any D-periodic structures even after 96 h of fibrillogenesis. On the other hand, the system abounded with FLS IV fibrils from the very beginning (after 24 h). Previous studies have shown that D-periodic fibrils can be reconstituted in ASC-heparin systems at fairly low heparin concentrations, while the increase of heparin concentrations led to partial or

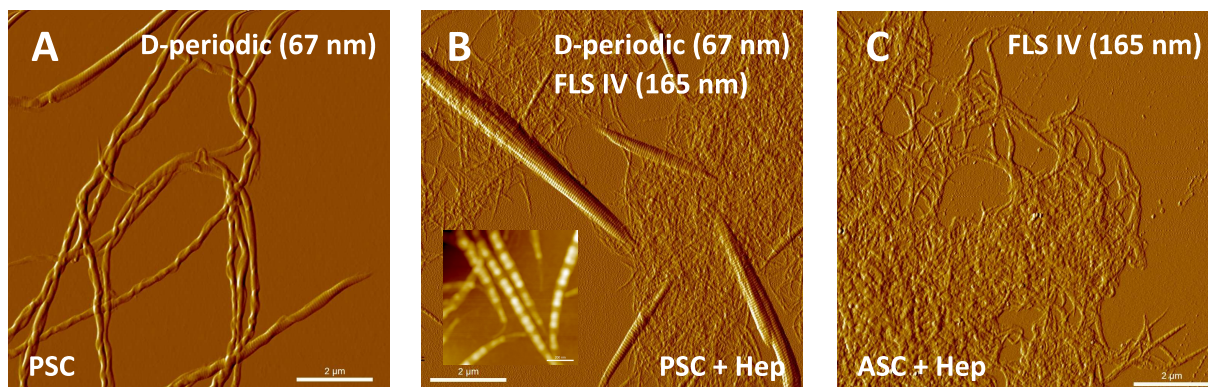


Figure 4.22.: *Impact of heparin and telopeptides on the structural polymorphism of collagen type I fibrils. Morphological analysis via SFM (amplitude images) of fibrillar suspensions reconstituted from (A) PSC (atelocollagen), (B) PSC and heparin, (C) ASC (tropocollagen). Inset in (B) shows the symmetric 165 nm average periodicity of the FLS IV fibrils.*

complete inhibition of the fibril formation (166, 229). Therefore, it is not surprising that in this case a heparin concentration of 0.4 mg/ml resulted in complete abolishment of the D-periodic fibril formation. The preservation of the FLS IV reconstitution even in the presence of telopeptides (ASC) has 2 major implications on the collagen reconstitution in the presence of heparin. The presence of both telopeptides and heparin fails to reproduce the asymmetric D-periodic pattern and it doesn't seem to affect the formation of symmetric FLS IV fibrils. It also comes to show that the PSC-heparin interaction is rather specific as previously suggested (235) and also shown in this work (see section 4.1.4), while simultaneously endorsing the idea about heparin and the telopeptides as 'competitors' for the reconstitution of the D-stagger. It would also suggest that the heparin binding site in the case of FLS IV fibrils is different than the one in the case of the PSC-heparin cofibrils since the presence of telopeptides does not affect the FLS IV formation.

As previously noted, heparin is intercalated within the PSC-heparin cofibrils seemingly without affecting their asymmetric periodicity (sections 4.1.4 and 4.2.2). Nevertheless, the potential intercalation of the GAG molecule is expected to affect the lateral packing of the atelocollagen helices in the hierarchical collagen assembly. To further explore the structure of PSC-heparin cofibrils, the dried samples of the different assemblies were subjected to wide-angle X-ray scattering (WAXS) studies (Fig.4.23).

The linear intensity profiles of the X-ray diffraction patterns from both pure PSC and ASC reconstituted fibrils show a very distinct correlation peak for ASC at $q = 6.3 \text{ nm}^{-1}$ and a less pronounced one for PSC at $q = 5.4 \text{ nm}^{-1}$, corresponding to a spacing of $d = 2\pi/q = 1.0$ and 1.2 nm, respectively (Fig.4.23 A). The differences in lateral packing suggest that the presence of telopeptides in the ASC sample is responsible for the more compact collagen structure. In contrast, the absence of telopeptides (in the PSC sample) favors a looser packing of atelocollagen helices. Nevertheless, fibrillar assembly is still possible

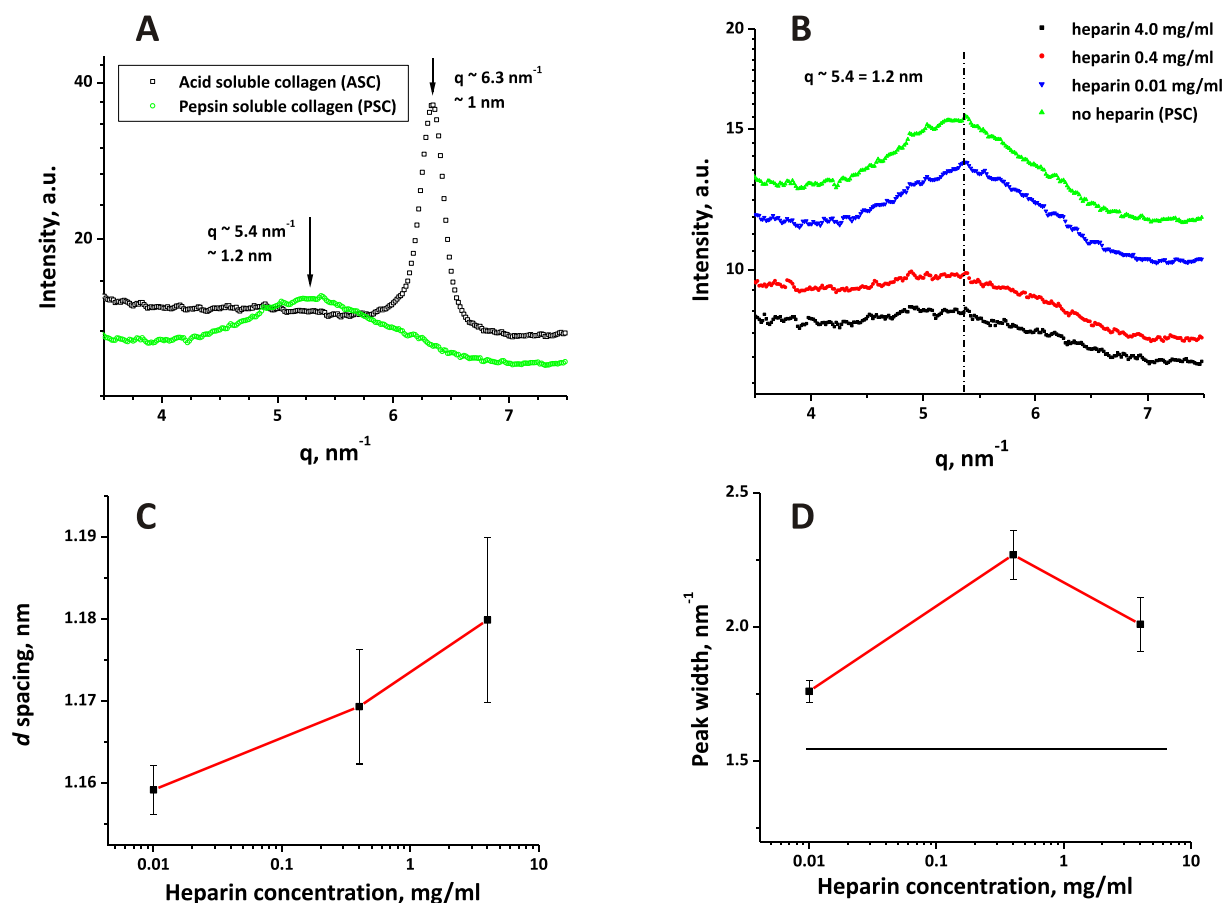


Figure 4.23.: Impact of the presence of heparin and telopeptides on the interhelical packing of collagen I. WAXS data of fibrils reconstituted from atelocollagen (PSC) and tropocollagen (ASC) (A) as compared to atelocollagen with different concentrations of heparin, data are shifted in y-direction for clarity (B). (C) and (D) implicate the dependence of parameters 'd' spacing and peak width on heparin concentration, attained after all peaks from (B) were fit to a Lorentzian function (data for pure PSC in (D) is given as horizontal line).

in this case, due to the typical mechanisms found for pure collagen (i.e. electrostatic and hydrophobic interactions). Additionally, the effect of heparin concentration on the d spacings of PSC-heparin cofibrils was studied. The data analysis revealed a slight shift of the correlation peak towards lower q values with increasing heparin concentration (corresponding to higher d from 1.16 to 1.18 nm) (Fig.4.23 B,C). It was accompanied by a substantial broadening of the peak with a correspondingly increasing heparin concentration (Fig.4.23 B,D). The latter observation might be related to an increase in the planar disorder in the system. On the other hand, a local increase of the interhelical fibril spacings along the atelocollagen molecules is also a potential explanation for the broadened features (251). The increase in d spacing with added heparin could possibly support this interhelical distance increase coming only from a small number of regions (like previously reported specific binding sites along the tropocollagen termini). Nevertheless, this conclusion should be regarded with caution, due to the presence of other structures (e.g. FLS IV) in the system which have a different axial arrangement and could potentially influence

overall 'shape' of the final scattering pattern.

4.3.2. Covalent immobilization of freestanding fibrils

With respect to the earlier suggestion about the role of heparin as intrafibrillar cross-linker and the straight and thick morphologies of the PSC-heparin cofibrils, further analysis was undertaken, regarding the evaluation of their mechanical properties as compared to pure ASC and PSC fibrils. The application of the EULER-BERNOULLI beam theory for micromechanical bending of a double-clamped rod requires a suitable platform for suspending and immobilization of the protein fibrils. The double-clamped beam model is usually assumed in literature, since measurements are almost always done in dry state and the adhesion forces between the measured fibers and the substrate are considered sufficient to ensure the fixation of both ends (see section 2.4.3). Nevertheless, in order to measure the mechanical properties of such objects in their 'native' state, i.e. physiological buffer with similar pH and ionic strength, measurements have to be done in liquid which means that the assumption for the 'sufficient' adhesion forces is not valid any longer. Hence, a decision to modify the surface chemistry, in order to ensure the covalent immobilization of the suspended cofibril and apply the double clamped beam model directly, was taken. In order to choose the best immobilization strategy the effect of both physical (hydrophobic vs. hydrophilic) and chemical immobilization (aldehyde- and NHS-derivatized surfaces) on the rate of cofibril suspension over PDMS and silicon gratings was studied (Fig.4.24).

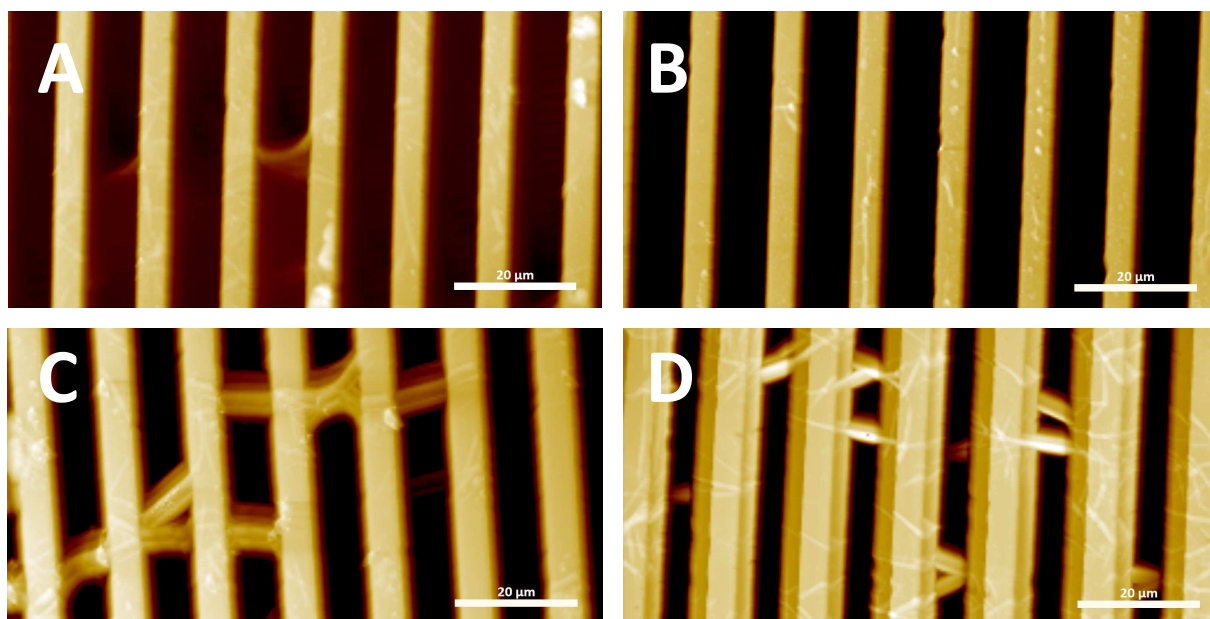


Figure 4.24.: *Immobilization tests of PSC-heparin cofibrils on different types of functionalized substrates ranging from hydrophilic (A) and hydrophobic (B) to aldehyde- (C) and NHS-derivatized surfaces (D).*

The SFM analysis of PSC-heparin cofibrils deposited onto hydrophilized and hydropho-

bized silicon gratings did not provide optimal conditions for successful suspending and stretching (Fig.4.24 A,B). Analysis of at least 10 different imaging fields per sample showed that only a small number of filaments were suspended but none of them was actually stretched over the channel. An evidence of that is the presence of two fibrils in Fig.4.24 A, taking the topography of the channel over which they are deposited. In contrast, both chemical immobilization protocols appear to be sufficient for the suspending and stretching of individual cofibrils (Fig.4.24 C,D). The binding in both cases is non-specific and random but at a density which would allow further mechanical probing of the fibrils. The aldehyde-derivatized chemistry makes use of the interaction between the side-chain NH_2 -groups of the proteins and the quite reactive (towards amino groups) aldehyde groups from the substrate (252). The formation of labile SCHIFF's base (imine group) can be further stabilized by reductive amination but the reversibility rate is usually rather low which does not make it necessary. In the case of NHS-functionalization, the dissociated COOH -groups are activated by the presence of carbodiimide to a reactive *o*-acylisourea ester. In excess of *N*-hydroxysuccinimide, the latter is forming a semi-stable amine-reactive NHS-ester which in the presence of proteins is forming stable amide bonds (253).

4.3.3. Micromechanical bending

To examine the E_B of the fibrils, the linear behavior of deflections during force spectroscopy is analyzed (for details see 3.2.3.2). Micromechanical bending tests were performed by bending the elastic fibrils at single point in the middle of suspended filaments, or via a multiple point bending test along the length of the fibrils. The collected deflection vs. piezo displacement curves, were obtained directly from the micromechanical bending tests and converted to force-separation curves. The average diameters of the freestanding fibrils in hydrated state are usually between 200–400 nm. In that sense using pyramidal silicon nitride V-shaped cantilevers with a diameter of 100 nm is a rather good compromise between 'speculative' indentation and resolution which is required to determine the radius of the suspended fibrils later on. The calculations showed that the PDMS deformation in liquid is lower than 3% for the range of applied bending forces of around 20 nN, thereby considered negligible. This is however becoming a problem in dry state, where initial bending experiments with the fibrils showed higher E_B . Therefore, in that case a switch to silicon substrates was necessary.

Fig.4.25 shows an example of the fibril deformation over the channel. The typical force deformation curves at points (1) and (2) both in liquid state show almost no indentation. These force curves are essentially the characteristics of the substrate and the fibril lying on the substrate indicating a negligible indentation. Force curves of points (3) and (4) are taken on the suspended fibrils close to the channel edge and in the center, respectively.

As expected from the applied linear elastic model, the slopes are decreasing when the tip is moved from the edge of the grooves toward the center of the suspended cofibril.

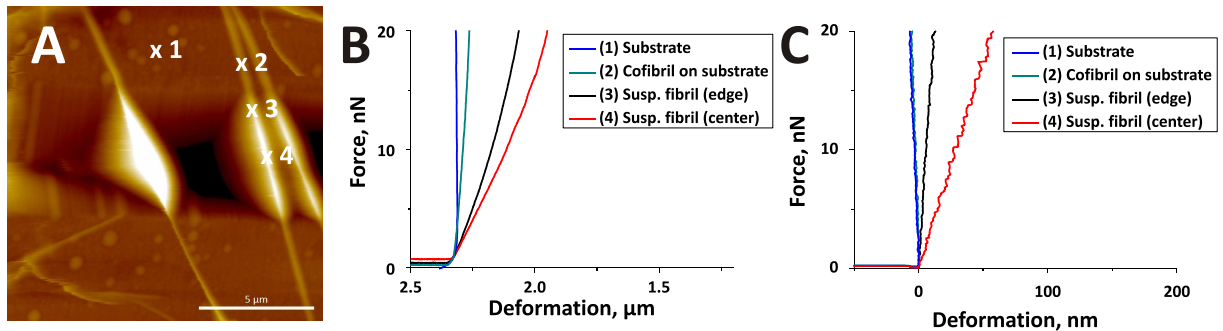


Figure 4.25.: *Change of the linear regime of force-separation curves with respect to position of the bending points along the surfaces of a single cofibril. (A) Contact mode SFM height image of suspended PSC-heparin cofibrils. Force-separation curves at positions from 1 to 4 collected in hydrated and dry mode are shown in (B) and (C) respectively.*

As seen from Eq.2.3 of the double-clamped beam model (see section 2.4.3) the radius appears to be a major contributor to the calculation of E_B . Hence, its determination is critical and a major source of error in the measurements. Further complications arise from the fact that the cofibril diameter can only be measured across the fibril part which is lying on the substrate but not the suspended one. As a deformation of the cofibrils due to the adhesion to the substrate was observed both in dry (height:diameter \approx 5:1) and hydrated state (h:d \approx 4:1) the common practice of taking directly the fibril diameters from the adherent part of the fibril is not correct. To overcome this issue, the cofibrils are considered as incompressible elements from which an equality of cross-sectional area of suspended and adherent fibril parts can be expected. By fitting the cross-sectional profiles of the adherent part of the cofibrils (measured in intermittent contact mode) to a modified inverse polynomial function, the diameters of the cofibrils in their suspended parts can be calculated with over 99% precision (see Appendix, section A.4). Due to the tactoidal morphology of the molecules a certain change of diameter across the length of the cofibrils might occur. Nevertheless, with respect to the small channel width over which the cofibrils are suspended in comparison the fibril length, these changes are considered negligible in the experiments.

In order to prove the successful chemical immobilization of the cofibrils across the channels, a test whether the linear deformation across the channel is consistent with a double-clamped (fixed ends) or simple supported (slipping) beam deflection model, was carried out. Despite the reproducibility of the surface chemistry, the concomitant binding and suspending of the cofibrils are a stochastic and impossible to control process, therefore not all of the cofibrils imaged in liquid were successfully immobilized. Additionally, due to thermal instabilities in the system (limiting the number of bending points to 10–15), as well as frequently occurring asymmetric bending (sliding of the pyramidal tip

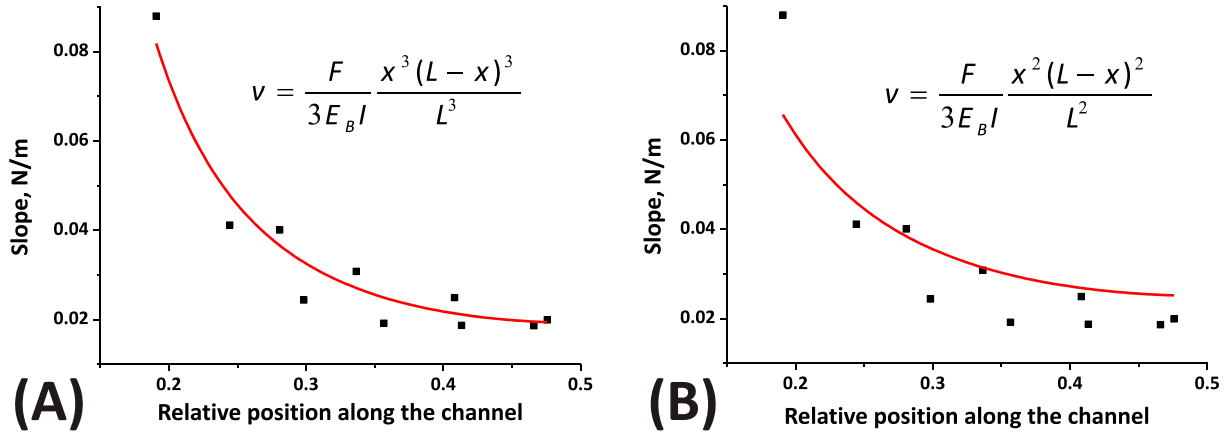


Figure 4.26.: Experimental validation of 'double-clamped' (A) vs. 'simple supported' model (B) by utilizing a multiple point bending test along single suspended cofibril.

sideways to the cofibril) the double-clamped model couldn't be applied efficiently all the time. Nevertheless, in the cases when cofibrils were firmly attached and suspended over the gratings, the bending behavior can be 'fit' successfully with a double-clamped beam model ($R^2 \approx 0.94$) in contrast to the simple supported one ($R^2 \approx 0.77$), as illustrated in Fig.4.26, by plotting the slope of the deflection curves vs. the relative position along the fibril suspended over the channel via a multiple point bending test. Additional proof that the cofibrils are fixed during the bending was an indistinguishable rescan of the fibril in contact mode SFM after the end of bending test.

4.3.4. Bending and shear moduli of collagen fibrils

As described earlier, the cofibrils were initially suspended and covalently immobilized over aldehyde-derivatized PDMS gratings containing microchannels. As the double-clamped model was proven for the experimental setup (section 4.3.3) a single point micromechanical bending test was used to analyze the mechanical properties of the fibrils (for setup refer to Fig.3.3). E_B of fully hydrated D-periodic fibrils (150 mM PBS buffer, pH 7.4) is determined by using the slope of the force-displacement curves recorded in liquid state in the low force range (8 to 20 nN) via Eq.2.3. Experiments in this force range were provoked by earlier collagen studies showing that the stretch below 8–12% deformation is rather entropic and linear elastic (254–257). Working in the higher force regime as described in the forementioned work by BUEHLER results in stress-strain non-linearities. Data from the bending test showed an almost 2-fold decrease in E_B from the pure ASC fibrils, with a modulus of 379 ± 241 MPa, to the pure PSC fibrils, with a modulus of 221 ± 78 MPa (Fig.4.27).

As mentioned in section 2.4.3, the shear modulus (G) of the cofibrils, sometimes defined as the ratio between shear stress and shear strain, can be neglected. Nevertheless, the values can be calculated according to Eq.2.8. In the case of cylindrical rods (as the cofibrils

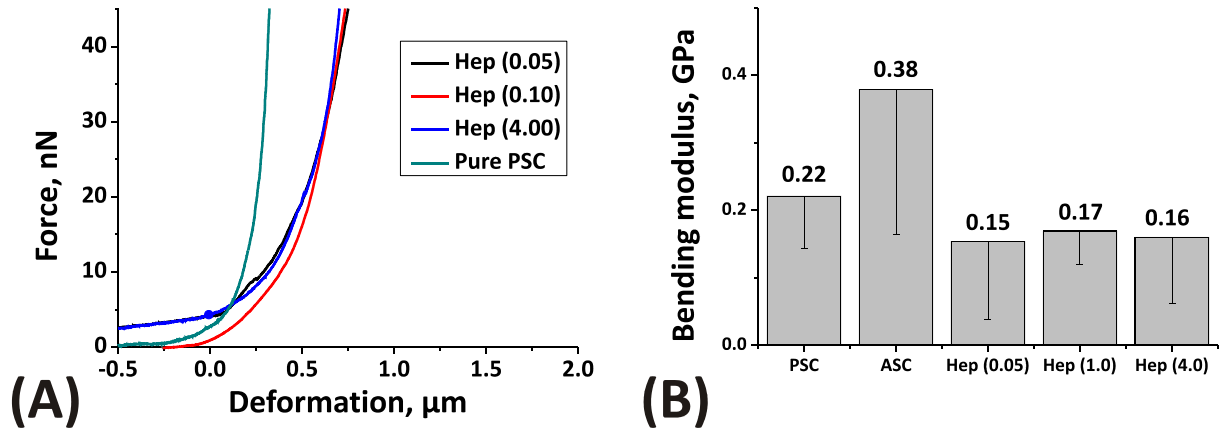


Figure 4.27.: Impact of telopeptides and heparin concentration on the slope (A) and E_B (B) calculated from force-separation curves after a single point bending test of ASC, PSC and PSC-heparin cofibrils. Curves in (A) are an average of at least 10 measurements (error bars in (B) representing standard deviation).

are), G can be determined from the slope of the linear relation between $1/E_B$ and R^2/L^2 (Fig.4.28). Fitting with 2 variables (G , E) in this case returns the highest G values for pure PSC fibrils (1.6 MPa) as compared to ones reconstituted in the presence of heparin with concentrations 0.05 and 4 mg/ml - 0.07 and 0.16 MPa respectively. All values turn out to be very small and hence negligible for the bending measurements, as it was assumed in the beginning.

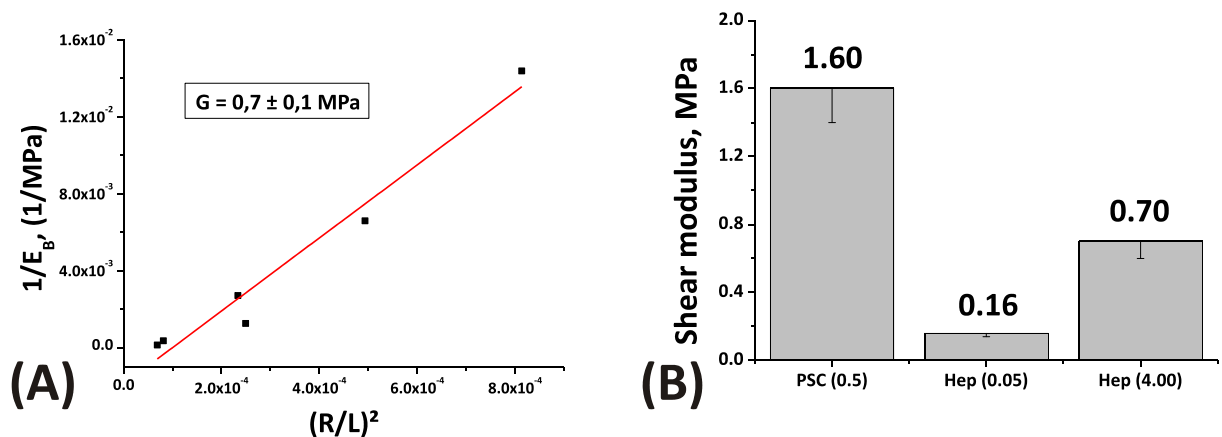


Figure 4.28.: Impact of heparin on the shear modulus of PSC fibrils. (A) is a linear fit of $1/E_B$ vs. R^2/L^2 used for the calculation of G shown in (B) (error bars show standard deviation).

The values of E_B from the single point bending tests are in a good agreement with those from other groups measuring hydrated native ASC fibrils, and glutaraldehyde fixed ones (221). The differences between PSC and ASC once again emphasize the importance of the telopeptides, considered to be responsible for providing the basis for restraining cross-links in native collagen, which then impact the mechanical properties of the fibrillar assemblies. The cross-linking profile varies with tissues, but in skin collagen (where telopeptide Lys is barely hydroxylated) the predominant immature cross-links are formed between Lys

aldehyde and triple-helical hLys, forming a divalent aldimine cross-link that is further stabilized by His residues (258)). This is a potential explanation for the significantly higher E_B measured for ASC, since these immature cross-links are simply unable to form in PSC. The fact that the E_B and G of PSC fibrils with added heparin is even lower can be explained by the likely localized separation of stacked atelocollagen helices in the presence of intercalated GAG chains. The low impact of heparin concentration on E_B comes to emphasize the specific interaction which was suggested earlier. The nature of the different cross-links, being ionic in the case of heparin and covalent in the case of the telopeptide cross-links, is consistent with this interpretation of the measurements. Moreover, the impairment of the mechanical properties of the PSC-heparin cofibrils again supports the heparin to be intercalated within them.

4.3.5. Discussion - Competitive binding site of telopeptides and heparin in collagen fibril assembly

The idea for specific heparin binding to collagen was heavily endorsed in a number of earlier studies with both monomeric (234, 235) and fibrillar molecules (235). It was also hypothesized that heparin might be acting as a cross-linker of tropocollagen molecules in the process of fibrillar assembly (182). Nevertheless, there are no reports which provide sufficient conclusive evidence for the *in vitro* intercalation of heparin within collagen type I fibrils. The morphological, structural, and mechanical differences between ASC and PSC-heparin fibrils presented here contribute to the existing body of knowledge in this area. Based on that I favor a model where heparin acts as an intrafibrillar cross-linker, which competes for a binding site at places along the atelocollagen helix that are occupied by telopeptides in fibrillar ASC.

The native staggering of collagen type I requires an unidirectional head-to-tail asymmetric alignment of 300 nm tropocollagen helices with a regular stagger of about 233 amino acid residues, thus resulting in the D-periodic banding of 67 nm (88, 93). Following the completion of the assembly process, the fibrils undergo cross-linking to an extent that varies with different tissue types. In skin collagen, where the telopeptide Lys residues are barely hydroxylated, the predominant cross-link is a divalent aldimine formed between Lys aldehyde and hLys, resulting in dehydro-hydroxylysinonorleucine (deH-HLNL) which is usually stable under physiological conditions (258). An earlier study about the partial hydrolysis of native collagen showed the reversible disassembly of collagen I fibrils into SLS fibril fragments with 270 nm banding periodicity and approximately 30 nm (about 90 amino acids) overlap (147). This would suggest a potential cross-linking site between the tropocollagen short non-helical Lys-containing telopeptides and a hLys-rich locus displaced by about 90 amino acids on the other side of the neighboring tropocollagen

helix (Fig.4.29).

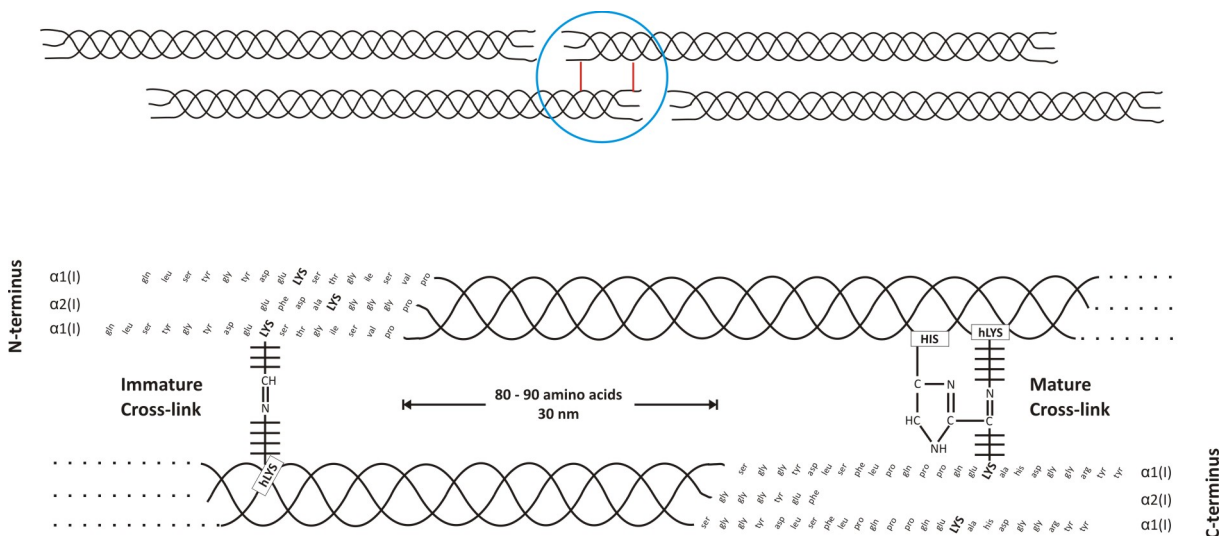


Figure 4.29.: Molecular origins for the native tropocollagen cross-linking in collagen I fibril assembly. The classical staggering of native collagen fibrils involves a later stabilization via an immature aldimine cross-link between Lys-aldehyde from the telopeptides and triple-helical hLys. The bond is stable at physiological conditions although it can further 'mature' by involving a triple-helical His in order to form a histidinohydroxylysinonorleucine. The bond is more characteristic for the C-terminus but can be found at N-terminal region as well.

The inspection of the bovine collagen type I sequence (UniProtKB/Swiss-Prot, P02453 (CO1A1_BOVIN), P02465 (CO1A2_BOVIN)) shows that such a site exists. This type of cross-link is also suggested *in situ*, probably taking place between Lys-17 from the partially folded C-telopeptide and triple helical hLys-87 (259), while at the same time it coincides with the previously reported N- and C-terminal binding sites for heparin. The N-terminal locus, reported previously by SAN ANTONIO et al. (235), involves a highly basic sequence of nine positive amino acids, six of which are contributed by the $\alpha 1(I)$ chains, and three by the $\alpha 2(I)$ chain (Fig.4.30).

Three of the basic amino acids within this segment are hLys residues, which are usually involved in cross-links (see above), and are reported to additionally function as disaccharide acceptor sites (261). The hypothesized C-terminal binding site (234, 235) also represents a highly basic domain involving 8 positive amino acids (including a few hLys) with a slightly different composition and arrangement, but also reported as a binding site for disaccharides. The rather high *pI* of these clusters, of 11.00 and 10.39 respectively, indicates that at physiological *pH* they are positively charged and therefore plausible binding sites for the highly negatively charged heparin. Therefore, it is plausible that such longspacing structures can reconstitute a D-periodic fibrillar arrangement in the presence of small negative molecules as heparin (see section 4.2), as well as ATP (116), synthetic polysulfonates (242).

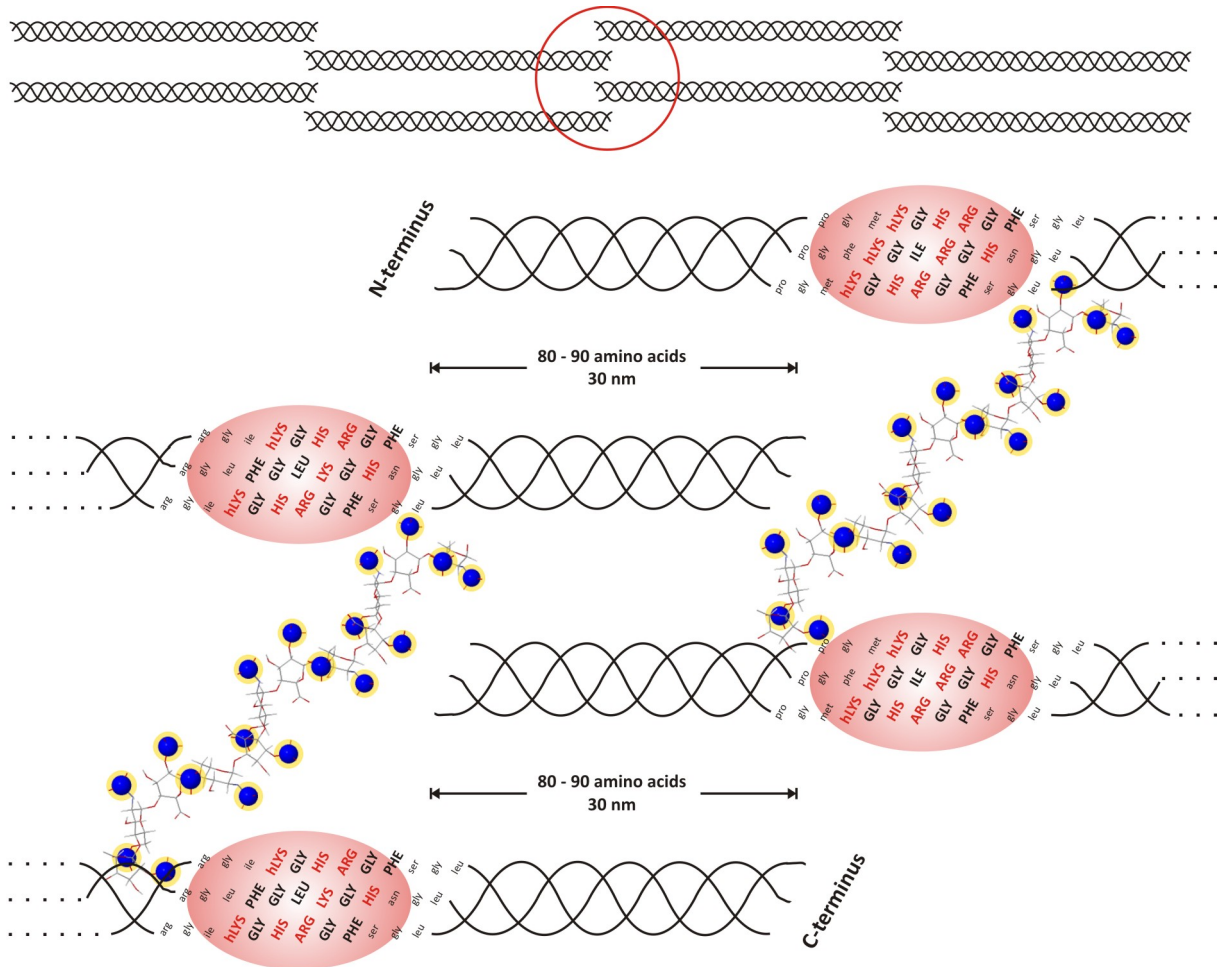


Figure 4.30.: A schematic representation of the already suggested heparin binding clusters which appear to be almost symmetrically allocated at both C- and N-termini. The absence of telopeptide creates a highly basic binding pocket, which could be a favorable site for binding of the highly negative heparin molecule. The skeletal model of heparin is from a previously reported NMR coordinates (260), emphasizing on VAN DER WAALS surface representation of the negatively charged sulfate groups.

Now it comes into play that at this position telopeptides may form cross-links in ASC. However, an access of heparin binding at this position prior to fibril assembly could probably inhibit this interaction. Additionally, not only the blocking of the binding site but further steric hindrance of bound heparin and telopeptides would inhibit fibril formation (compare Fig.4.29 and Fig.4.30). On the other side without telopeptides in PSC heparin can fill in the space of depleted non-helical termini and may bind as an intermolecular cross-linking agent in PSC-heparin cofibrils. The rather high specificity of heparin binding to the suggested region along the collagen triple helix is supported by the facts that symmetric FLS IV fibrils form in the presence of heparin independently of the presence of telopeptides probably making use of the heparin binding clusters allocated almost symmetrically at both C- and N-termini.

Section 4.2 already showed that SLS fibrils can be formed from PSC and heparin at 0 °C, which furthermore can reconstitute a D-periodic asymmetric pattern. The morphological

analysis in this section suggested that telopeptides obstruct the formation of cofibrils and most likely SLS fibrils as well. The latter comes as an aftermath of the possible loading of the atelocollagen molecules with heparin and their inability to form initial 4D-periodic segments which eventually should start aligning and forming the 1D-periodic pattern (152) as previously shown for tropocollagen *in vitro*. In contrast, the formation of PSC-heparin SLS fibrils and their further assembly into cofibrils is ensured by the fact that heparin most likely occupies the position of the missing telopeptides, thus preserving the asymmetric banding periodicity as shown previously for atelocollagen-GAG systems (129). This fact is also supported by the nearly identical interhelical distances between pure PSC and PSC-heparin fibrils as observed from the WAXS measurements. This idea is in agreement with the results from section 4.1.4 on heparin intercalation pointing to this specific GAG binding in PSC-heparin fibrils, as concluded by the 1:1 molar ratio of heparin and collagen helices. Apart from the possibility for heparin to find its way inside the PSC-heparin cofibrils due to highly positively charged specific binding sites, its stable intercalation in the fibrils might be realized by its substantial conformational flexibility. The presence of L-iduronic acid in the structure of most naturally present heparins gives them the potential to move from one conformation to another (1C_4 to 2S_0), essentially through a rotation around the C_2 - C_3 bond, and by that to introduce an extra degree of freedom in the polysaccharide chain (246). This makes heparin the molecule with the highest affinity to polyvalent proteins among all naturally occurring GAGs.

The different mechanical properties (analyzed here as the E_B) in the case of ASC, PSC and PSC-heparin fibrils reveal that although heparin supports the asymmetric periodicity in a telopeptide depleted system, it cannot compensate for the intermolecular cross-linking functions of the telopeptides. As a matter of fact, heparin further impairs the mechanical properties as seen from the decreased E_B between PSC and PSC-heparin, which implies that the nature of the cross-linker (ionic in the case of heparin, or covalent in the case of the telopeptides) is essential for the preservation of the native mechanical properties in collagen systems. Interestingly, the decreased mechanical resistance is reflected by the increased interhelical spacing, which directly points to the effect of the modulation of the cross-linking type. This finding is also very significant in light of the use of less immunogenic PSC and various GAGs in contemporary advanced cell culture systems as those systems would not allow the reconstitution with the same mechanical characteristics as *in vivo* matrices, which in turn would affect cell growth and tissue development therein.

In summary, the morphological, structural and mechanical analysis of both ASC and PSC-heparin cofibrils has three major implications on the fibril formation of any PSC system in the presence of heparin or other highly sulfated natural/synthetic GAGs. The heparin cannot substitute the mechanical properties of the impaired telopeptide-free collagen fibrils while its molecular localization in the *in vitro* case is most likely intrafibrillar in

difference to most of the non-pathogenic native systems. PSC is predestined to intercalate highly negatively charged molecules, judging from the small structural differences between PSC and PSC-heparin and the structurally favorable conditions, created by its positive binding sites in SLS fibrils. The preservation of the asymmetric periodicity is ensured by the unaffected molecular packing which is possible due to the absent telopeptides. These findings are particularly important with respect to previous studies emphasizing the importance of preservation of native collagen periodicity with respect to cellular response in advanced cell culture studies (262). Furthermore, with the finding of a competitive binding site of telopeptides and heparin at tropocollagen triple helices an intriguing argument is provided for the *in vivo* dogma in which GAGs are not intercalated into naturally occurring collagen fibrils.

5. Conclusion

Synthetic biomaterials are constantly being developed and play central roles in contemporary strategies in regenerative medicine and tissue engineering as artificial extracellular microenvironments. Such scaffolds provide 2D- and 3D-support for interaction with cells and thus convey spatial and temporal control over their function and multicellular processes, such as differentiation and morphogenesis. A model fibrillar system with tunable viscoelastic properties, comprised of 2 native ECM components like collagen type I and the GAG heparin, is presented here. Although the individual components comply with the adhesive, mechanical and bioinductive requirements for artificial reconstituted ECMs, their interaction and structural characterization remains an intriguing conundrum.

As discussed in 4.1 and 4.3, the interaction between the pepsin-solubilized form of collagen type I and the high negatively charged polysaccharide heparin is a process which results in the formation of straight tactoidal cofibrils with significantly different morphological characteristics than the pure collagen systems. The morphogenic effect exerted by the GAG onto the final cofibrillar assemblies was shown to be strongly affected by concentration, surface charge (pH value) and degree of sulfation. As further portrayed in 4.2 the system exhibits characteristic for collagen systems structural polymorphism which strongly depends on a number of factors. Within these are the binding specificity between the collagen monomers and GAG in terms of binding sites, axial arrangement in the polymorphic forms, as well as presence of telopeptides (structural feature of the collagen monomers). In that sense, the interplay of all these conditions determines the build-up, symmetry and banding periodicity of the various polymorphic forms in the system (Fig.5.1).

The 'cornerstone' which determines the fate of the fibrillogenesis appears to be the binding specificity which is affected by the binding loci, as well as the presence of telopeptides. The two distinct structural levels, described earlier as asymmetric D-periodic cofibrils (average periodicity (AP) of 67 nm) and symmetric FLS IV nanofibrils (AP = 165 nm) are strictly an aftermath of the specific or non-specific interaction between collagen monomers and heparin. Both hierarchical suprastructures depend on the existence of two other polymorphic forms, previously described as asymmetric SLS fibrils (nuclei with AP = 260 nm) and short symmetric segments (AP = 280 nm). The axial arrangement of the latter is responsible for the arrangement of the top 2 structural levels. The specific interaction between the atelocollagen monomers and the heparin in the D-periodic cofibrils was

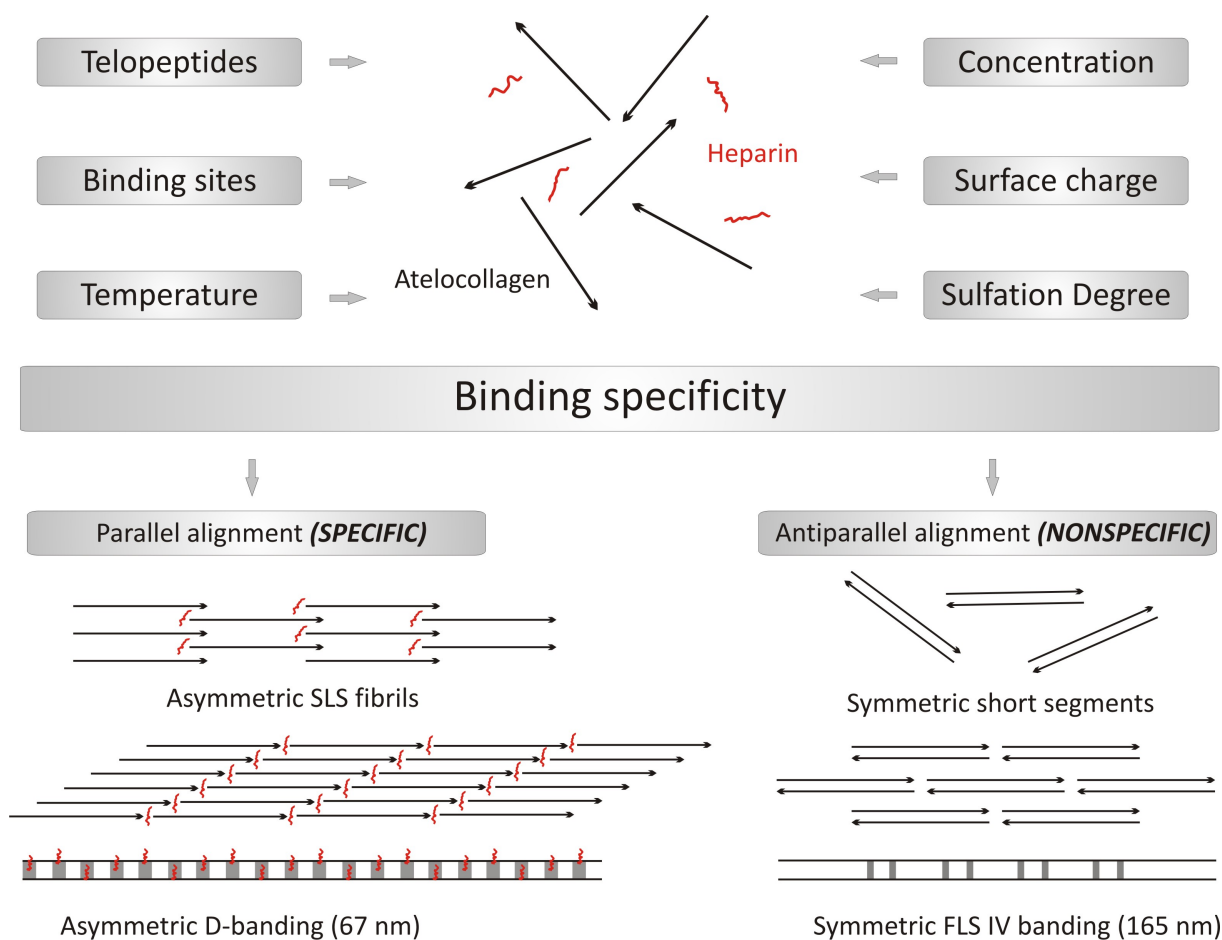


Figure 5.1.: Influence of structural and physico-chemical characteristics on the binding specificity and assembly of collagen type I - heparin cofibrils.

already suggested by both the intercalation of the polysaccharide and the almost equal molar ratio between both components (4.1.4). Furthermore, AP of 260 nm in the SLS fibrils pointed towards a terminal binding site along the collagen triple helix. The existence of such a site have already been suggested for both monomeric and fibrillar forms of collagen (234, 235), while at the same time being involved in the organization of intermolecular cross-links. Such cross-links usually take place between high positively charged clusters located in the non-helical terminal parts of tropocollagen, such as telopeptides. The inability of telopeptide-intact tropocollagen to reconstitute the D-periodic form of collagen in the presence of heparin, unlike atelocollagen, was a further proof that heparin acts as a competitive intermolecular bridge and is binding at the places left vacant by the telopeptides (4.3.5). Additionally, as shown by the micromechanical bending tests, the type of cross-link influences the mechanical properties of the fibrillar structures, being significantly impaired (2-fold) upon substitution of the telopeptides with heparin (4.3.4). At the same time, formation of FLS IV nanofibrils does not appear to be affected by the presence of telopeptides, therefore suggesting that the heparin binding site in that case is different than the one in the case of the D-periodic PSC-heparin cofibrils. In addition, the

multiple reports of FLS IV fibrils formed in systems with collagen I and variously sulfated GAGs, as well the multiple possibilities for binding of the polysaccharides along the symmetrically and equidistantly allocated possible binding sites along the collagen monomers, point towards a non-specific binding locus. Nevertheless, in both cases the binding principles that govern the formation of the initial symmetric and asymmetric polymorphic forms appear to be electrostatic, as significant variation of the surface charge was shown to change, or even abolish the fibrillogenesis.

The proposed building principle, focuses on the duality of the heparin falling concomitantly in the group of the small high negatively charged molecules and naturally present sulfated GAGs. In case of the D-periodic cofibrils, the combination of low temperature and high negative charge obviously favors a polar electrostatic interaction, while physiological temperature favors the assembly of symmetric molecules (as the 300 nm short segments and FLS IV molecules) (4.2.5). This interpretation would be in agreement with a previous speculation (138) that polar SLS arrangements are normally associated with very precise positioning and overlapping of the positive charges along the tropocollagen molecule in difference to the symmetric FLS interactions. In that case, a system with lower temperature and essentially decreased particle motion would favor a more precise alignment of the heparin and its specific binding sites along the atelocollagen molecule. From this point of view temperature would seem like an important factor for the symmetric or asymmetric arrangement in the system. The further association of the symmetric segments or SLS fibrils to their corresponding suprastructures (Fig.5.1) involves the typical staggering characteristic for either D-periodic cofibrils or FLS IV fibrils, a process which is expectedly driven by both hydrophobic and electrostatic interactions.

In terms of biological significance, it has to be noted that collagens and PGs (GAGs bound to a protein core) are typically associated on an interfibrillar level (151,152), most likely due to the sterical hindrance from the protein side. Nevertheless, the question whether the pure GAGs can be intrafibrillar remains open, as it can be seen from a number of reports *in vivo* (165,173). The current work is the first of its kind, offering the first enough experimentally and theoretically supported hypothesis explaining the intercalation of GAGs *in vitro*, while reaching out for a discussion and revisiting the dogma according to which GAGs cannot be intercalated in collagens *in vivo*. In that aspect the current study also offers an interesting model for the formation of some structurally heterogeneous polymorphic forms which can be found in nature (114,115). It also emphasizes the correlation between the types of intrafibrillar cross-links and the mechanics of the fibrils.

6. Summary

The aim of the work was to analyze and structurally characterize a xenogeneic *in vitro* cell culture scaffold reconstituted from two native ECM components, collagen type I and the highly negatively charged glycosaminoglycan heparin. Utilizing a broad spectrum of structural analysis it could be shown that pepsin-solubilized collagen type I fibrils, reconstituted *in vitro* in the presence of heparin, exhibit an unusually thick and straight shape, with a non-linear dependence in size distribution, width-to-length ratio, and morphology over a wide range of GAG concentrations. The experiments imply a pronounced impact of the nucleation phase on the cofibril morphology as a result of the strong electrostatic interaction of heparin with atelocollagen. Heparin is assumed to stabilize the collagen-GAG complexes and to enhance their parallel accretion during cofibrillogenesis, furthermore corroborated by the heparin quantitation data showing the GAG to be intercalated as a linker molecule with a specific binding site inside the cofibrils. In addition, the exerted morphogenic effect of the GAG, appears to be influenced by factors as degree of sulfation, charge, and concentration.

Further detailed structural analysis of the PSC-heparin gels using TEM and SFM showed a hierarchy involving 3 different structural levels and banding patterns in the system: asymmetric segment longspacing (SLS) fibrils and symmetric segments with an AP of 250–260 nm, symmetric fibrous longspacing (FLS IV) nanofibrils with AP of 165 nm, and cofibrils exhibiting an asymmetric D-periodicity of 67 nm with a striking resemblance to the native collagen type I banding pattern. The intercalation of the high negatively charged heparin in the cofibrils was suggested as the main trigger for the hierarchical formation of the polymorphic structures. We also proposed a model explaining the unexpected presence of a symmetric and asymmetric form in the system and the principles governing the symmetric or asymmetric fate of the molecules.

The last section of the experiments showed that the presence of telopeptides and heparin both had significant effects on the structural and mechanical characteristics of *in vitro* reconstituted fibrillar collagen type I. The implemented structural analysis showed that the presence of telopeptides in acid soluble collagen (ASC) impeded the reconstitution of D-periodic collagen fibrils in the presence of heparin, leaving behind only a symmetric polymorphic form with a repeating unit of 165 nm (FLS IV). Further x-ray diffraction analysis of both telopeptide-free and telopeptide-intact collagen fibrils showed that the

absence of the flanking non-helical termini in pepsin-solubilized collagen (PSC) resulted in a less compact packing of triple helices of atelocollagen with an increase of interhelical distance from 1.0 to 1.2 nm in dried samples. The looser packing of the triple helices was accompanied by a decrease in bending stiffness of the collagen fibrils, which demonstrated that the intercalated heparin cannot compensate for the depletion of telopeptides. Based on morphological, structural and mechanical differences between ASC and PSC-heparin fibrils reported here, we endorsed the idea that heparin acts as an intrafibrillar cross-linker which competed for binding sites at places along the atelocollagen helix that are occupied *in vivo* by telopeptides in the fibrillar collagen type I.

The performed studies are of particular interest for understanding and gaining control over a rather versatile and already exploited xenogeneic cell culture system (24–27). The reconstituted cofibrils with their unusual morphology and GAG intercalation – a phenomenon not reported *in vivo* – are expected to exhibit interesting biochemical behavior as a biomaterial for ECM scaffolds. Varying the experimental conditions, extent of telopeptide removal, and heparin concentration provides powerful means to control the kinetics, structure, dimensions, as well as mechanical properties of the system which is particularly important for predicting a certain cell behavior towards the newly developed matrix. The GAG intercalation could be interesting for studies with required long-term 'release upon demand' of the GAG, as well as native binding and stabilization of growth factors, cytokines, chemokines, thus providing a secondary tool to control cell signaling and fate, and later on tissue morphogenesis.

There are a few challenging aspects which remain to be addressed in the system. At one side, although the stable heparin binding was shown, the structural accessibility and specific binding of growth factors as bFGF, VEGF, SDF1 to the GAG remains to be elucidated. Furthermore, despite of the gel-like structure of the heparin-collagen assemblies, the interconnectivity between fibrils and cofibrils is still an issue. Transition from 2D- to 3D- structure could make use of some other collagen types as III, V or VI, as well as PGs which inclusion to the system remains to be clarified concerning timepoints and concentrations. Another interesting point could be the extent of telopeptide removal and the correlated control of mechanical properties and resulting cell behavior.

Bibliography

- [1] Farach-Carson MC, Wagner RC, Kiick KL (2007) *Extracellular Matrix: Structure, Function, and Applications to Tissue Engineering: in Tissue Engineering* eds Fisher JP, Mikos AG, Bronzino JD (CRC Press, Taylor & Francis Group).
- [2] Badylak SF (2007) The extracellular matrix as a biologic scaffold material. *Biomaterials* 28:3587–3593.
- [3] Lutolf MP, Hubbell JA (2005) Synthetic biomaterials as instructive extracellular microenvironments for morphogenesis in tissue engineering. *Nat Biotechnol* 23:47–55.
- [4] Davison PF, Levine L, Drake MP, Rubin A, Bump S (1967) The serologic specificity of tropocollagen telopeptides. *J Exp Med* 126:331–346.
- [5] Takaoka K, Koezuka M, Nakahara H (1991) Telopeptide-depleted bovine skin collagen as a carrier for bone morphogenetic protein. *J Orthop Res* 9:902–907.
- [6] Hubbell JA (2003) Materials as morphogenetic guides in tissue engineering. *Curr Opin Biotechnol* 14:551–558.
- [7] Lullo GAD, Sweeney SM, Korkko J, Ala-Kokko L, Antonio JDS (2002) Mapping the ligand-binding sites and disease-associated mutations on the most abundant protein in the human, type I collagen. *J Biol Chem* 277:4223–4231.
- [8] Galbraith CG, Sheetz MP (1998) Forces on adhesive contacts affect cell function. *Curr Opin Cell Biol* 10:566–571.
- [9] Geiger B, Bershadsky A, Pankov R, Yamada KM (2001) Transmembrane crosstalk between the extracellular matrix–cytoskeleton crosstalk. *Nat Rev Mol Cell Biol* 2:793–805.
- [10] Kresse H, Schönherr E (2001) Proteoglycans of the extracellular matrix and growth control. *J Cell Physiol* 189:266–274.
- [11] Gallagher J (2007) Messages in the matrix: proteoglycans go the distance. *Dev Cell* 13:166–167.
- [12] Bülow HE, Hobert O (2006) The molecular diversity of glycosaminoglycans shapes animal development. *Annu Rev Cell Dev Biol* 22:375–407.
- [13] Bishop JR, Schuksz M, Esko JD (2007) Heparan sulphate proteoglycans fine-tune mammalian physiology. *Nature* 446:1030–1037.
- [14] Boonthekul T, Mooney DJ (2003) Protein-based signaling systems in tissue engineering. *Curr Opin Biotechnol* 14:559–565.

- [15] Chen RR, Mooney DJ (2003) Polymeric growth factor delivery strategies for tissue engineering. *Pharm Res* 20:1103–1112.
- [16] Zisch AH, et al. (2003) Cell-demanded release of VEGF from synthetic, biointeractive cell ingrowth matrices for vascularized tissue growth. *FASEB J* 17:2260–2262.
- [17] Richardson TP, Peters MC, Ennett AB, Mooney DJ (2001) Polymeric system for dual growth factor delivery. *Nat Biotechnol* 19:1029–1034.
- [18] Zisch AH, Lutolf MP, Hubbell JA (2003) Biopolymeric delivery matrices for angiogenic growth factors. *Cardiovasc Pathol* 12:295–310.
- [19] Zisch AH, Schenk U, Schense JC, Sakiyama-Elbert SE, Hubbell JA (2001) Covalently conjugated VEGF–fibrin matrices for endothelialization. *J Control Release* 72:101–113.
- [20] Sakiyama-Elbert SE, Panitch A, Hubbell JA (2001) Development of growth factor fusion proteins for cell-triggered drug delivery. *FASEB J* 15:1300–1302.
- [21] Peattie RA, et al. (2006) Dual growth factor-induced angiogenesis in vivo using hyaluronan hydrogel implants. *Biomaterials* 27:1868–1875.
- [22] Stamov D, Grimmer M, Salchert K, Pompe T, Werner C (2008) Heparin intercalation into reconstituted collagen I fibrils: Impact on growth kinetics and morphology. *Biomaterials* 29:1–14.
- [23] Stamov D, Salchert K, Springer A, Werner C, Pompe T (2009) Structural polymorphism of collagen type I-heparin cofibrils. *Soft Matter* 5:3461–3468.
- [24] Wollenweber M, et al. (2006) Mimicked bioartificial matrix containing chondroitin sulphate on a textile scaffold of poly(3-hydroxybutyrate) alters the differentiation of adult human mesenchymal stem cells. *Tissue Eng* 12:345–359.
- [25] Franke K, Pompe T, Bornhäuser M, Werner C (2007) Engineered matrix coatings to modulate the adhesion of CD133+ human hematopoietic progenitor cells. *Biomaterials* 28:836–843.
- [26] Douglas T, et al. (2007) Interactions of collagen types I and II with chondroitin sulfates A-C and their effect on osteoblast adhesion. *Biomacromolecules* 8:1085–1092.
- [27] Lanfer B, et al. (2009) The growth and differentiation of mesenchymal stem and progenitor cells cultured on aligned collagen matrices. *Biomaterials* 30:5950–5958.
- [28] Kreis T (1999) *Guidebook to the Extracellular Matrix, Anchor and Adhesion Proteins* eds Kreis T, Vale R (A Sambrook and Tooze Publication, Oxford University Press), 2nd edition.
- [29] Reece JB, Campbell NA (2004) *Biology* (Benjamin Cummings), 7th edition.
- [30] Badylak SF (2004) Xenogeneic extracellular matrix as a scaffold for tissue reconstruction. *Transpl Immunol* 12:367–377.
- [31] Heino J (2007) The collagen family members as cell adhesion proteins. *Bioessays* 29:1001–1010.

- [32] Myllyharju J, Kivirikko KI (2004) Collagens, modifying enzymes and their mutations in humans, flies and worms. *Trends Genet* 20:33–43.
- [33] Hulmes DJS (2008) *Collagen Diversity, Synthesis and Assembly: in Collagen: Structure and Mechanics* ed Fratzl P (Springer Science + Business Media, LLC), 1st edition, pp 15 – 47.
- [34] Franzke CW, Bruckner P, Bruckner-Tuderman L (2005) Collagenous transmembrane proteins: recent insights into biology and pathology. *J Biol Chem* 280:4005–4008.
- [35] Heino J, Huhtala M, Käpylä J, Johnson MS (2009) Evolution of collagen-based adhesion systems. *Int J Biochem Cell Biol* 41:341–348.
- [36] Velling T, Risteli J, Wennerberg K, Mosher DF, Johansson S (2002) Polymerization of type I and III collagens is dependent on fibronectin and enhanced by integrins alpha 11beta 1 and alpha 2beta 1. *J Biol Chem* 277:37377–37381.
- [37] Mihai C, Iscru DF, Druhan LJ, Elton TS, Agarwal G (2006) Discoidin domain receptor 2 inhibits fibrillogenesis of collagen type 1. *J Mol Biol* 361:864–876.
- [38] Daley WP, Peters SB, Larsen M (2008) Extracellular matrix dynamics in development and regenerative medicine. *J Cell Sci* 121:255–264.
- [39] Gesslbauer B, Rek A, Falsone F, Rajkovic E, Kungl AJ (2007) Proteoglycanomics: tools to unravel the biological function of glycosaminoglycans. *Proteomics* 7:2870–2880.
- [40] Lindahl U, Lidholt K, Spillmann D, Kjellén L (1994) More to "heparin" than anticoagulation. *Thromb Res* 75:1–32.
- [41] Jackson RL, Busch SJ, Cardin AD (1991) Glycosaminoglycans: molecular properties, protein interactions, and role in physiological processes. *Physiol Rev* 71:481–539.
- [42] Powell AK, Yates EA, Fernig DG, Turnbull JE (2004) Interactions of heparin/heparan sulfate with proteins: appraisal of structural factors and experimental approaches. *Glycobiology* 14:17R–30R.
- [43] Sugahara K, et al. (2003) Recent advances in the structural biology of chondroitin sulfate and dermatan sulfate. *Curr Opin Struct Biol* 13:612–620.
- [44] Sugahara K, Mikami T (2007) Chondroitin/dermatan sulfate in the central nervous system. *Curr Opin Struct Biol* 17:536–545.
- [45] Honke K, Taniguchi N (2002) Sulfotransferases and sulfated oligosaccharides. *Med Res Rev* 22:637–654.
- [46] Carulli D, Laabs T, Geller HM, Fawcett JW (2005) Chondroitin sulfate proteoglycans in neural development and regeneration. *Curr Opin Neurobiol* 15:116–120.
- [47] Handel TM, Johnson Z, Crown SE, Lau EK, Proudfoot AE (2005) Regulation of protein function by glycosaminoglycans—as exemplified by chemokines. *Annu Rev Biochem* 74:385–410.

- [48] Capila I, Linhardt RJ (2002) Heparin-protein interactions. *Angew Chem Int Ed Engl* 41:391–412.
- [49] Lopes CC, Dietrich CP, Nader HB (2006) Specific structural features of syndecans and heparan sulfate chains are needed for cell signaling. *Braz J Med Biol Res* 39:157–167.
- [50] Johnson Z, Proudfoot AE, Handel TM (2005) Interaction of chemokines and glycosaminoglycans: a new twist in the regulation of chemokine function with opportunities for therapeutic intervention. *Cytokine Growth Factor Rev* 16:625–636.
- [51] Sanderson RD, et al. (2005) Enzymatic remodeling of heparan sulfate proteoglycans within the tumor microenvironment: growth regulation and the prospect of new cancer therapies. *J Cell Biochem* 96:897–905.
- [52] Harmer NJ (2006) Insights into the role of heparan sulphate in fibroblast growth factor signalling. *Biochem Soc Trans* 34:442–445.
- [53] Kjellén L, Lindahl U (1991) Proteoglycans: structures and interactions. *Annu Rev Biochem* 60:443–475.
- [54] Laurent TC, Fraser JR (1992) Hyaluronan. *FASEB J* 6:2397–2404.
- [55] Iozzo RV (1998) Matrix proteoglycans: from molecular design to cellular function. *Annu Rev Biochem* 67:609–652.
- [56] Hardingham TE, Fosang AJ (1992) Proteoglycans: many forms and many functions. *FASEB J* 6:861–870.
- [57] Haylock DN, Nilsson SK (2006) The role of hyaluronic acid in hemopoietic stem cell biology. *Regen Med* 1:437–445.
- [58] Badylak SF, et al. (1995) The use of xenogeneic small intestinal submucosa as a biomaterial for Achilles tendon repair in a dog model. *J Biomed Mater Res* 29:977–985.
- [59] Badylak S, Meurling S, Chen M, Spievack A, Simmons-Byrd A (2000) Resorbable bioscaffold for esophageal repair in a dog model. *J Pediatr Surg* 35:1097–1103.
- [60] Lindberg K, Badylak SF (2001) Porcine small intestinal submucosa (SIS): a bioscaffold supporting in vitro primary human epidermal cell differentiation and synthesis of basement membrane proteins. *Burns* 27:254–266.
- [61] McPherson TB, Liang H, Record RD, Badylak SF (2000) Gal-alpha(1,3)-Gal epitope in porcine small intestinal submucosa. *Tissue Eng* 6:233–239.
- [62] Galili U (2005) The alpha-gal epitope and the anti-Gal antibody in xenotransplantation and in cancer immunotherapy. *Immunol Cell Biol* 83:674–686.
- [63] Mantovani A, Sica A, Locati M (2005) Macrophage polarization comes of age. *Immunity* 23:344–346.
- [64] Stock UA, Schenke-Layland K (2006) Performance of decellularized xenogeneic tissue in heart valve replacement. *Biomaterials* 27:1–2.

- [65] Abbas AK, Murphy KM, Sher A (1996) Functional diversity of helper T lymphocytes. *Nature* 383:787–793.
- [66] Beck K, Brodsky B (1998) Supercoiled protein motifs: the collagen triple-helix and the alpha-helical coiled coil. *J Struct Biol* 122:17–29.
- [67] Bella J, Eaton M, Brodsky B, Berman HM (1994) Crystal and molecular structure of a collagen-like peptide at 1.9 Å resolution. *Science* 266:75–81.
- [68] McBride DJ, Choe V, Shapiro JR, Brodsky B (1997) Altered collagen structure in mouse tail tendon lacking the alpha 2(I) chain. *J Mol Biol* 270:275–284.
- [69] Cowan PM, McGavin S, North AC (1955) The polypeptide chain configuration of collagen. *Nature* 176:1062–1064.
- [70] Okuyama K (2008) Revisiting the molecular structure of collagen. *Connect Tissue Res* 49:299–310.
- [71] Emsley J, Knight CG, Farndale RW, Barnes MJ, Liddington RC (2000) Structural basis of collagen recognition by integrin alpha2beta1. *Cell* 101:47–56.
- [72] Sweeney SM, Guy CA, Fields GB, Antonio JDS (1998) Defining the domains of type I collagen involved in heparin- binding and endothelial tube formation. *Proc Natl Acad Sci U S A* 95:7275–7280.
- [73] Sweeney SM, et al. (2008) Candidate cell and matrix interaction domains on the collagen fibril, the predominant protein of vertebrates. *J Biol Chem* 283:21187–21197.
- [74] Shoulders MD, Raines RT (2009) Collagen structure and stability. *Annu Rev Biochem* 78:929–958.
- [75] Brodsky B, Ramshaw JA (1997) The collagen triple-helix structure. *Matrix Biol* 15:545–554.
- [76] Chan VC, Ramshaw JA, Kirkpatrick A, Beck K, Brodsky B (1997) Positional preferences of ionizable residues in Gly-X-Y triplets of the collagen triple-helix. *J Biol Chem* 272:31441–31446.
- [77] Beck K, et al. (2000) Destabilization of osteogenesis imperfecta collagen-like model peptides correlates with the identity of the residue replacing glycine. *Proc Natl Acad Sci U S A* 97:4273–4278.
- [78] Cram DJ (1988) The design of molecular hosts, guests, and their complexes. *Science* 240:760–767.
- [79] Berg RA, Prockop DJ (1973) The thermal transition of a non-hydroxylated form of collagen. Evidence for a role for hydroxyproline in stabilizing the triple-helix of collagen. *Biochem Biophys Res Commun* 52:115–120.
- [80] Sakakibara S, et al. (1973) Synthesis of (Pro-Hyp-Gly)_n of defined molecular weights. Evidence for the stabilization of collagen triple helix by hydroxyproline. *Biochim Biophys Acta* 303:198–202.

- [81] Suzuki E, Fraser RDB, MacRae TP (1980) Role Of Hydroxyproline In The Stabilization Of The Collagen Molecule Via Water-Molecules. *International Journal Of Biological Macromolecules* 2:54–56.
- [82] Holmgren SK, Taylor KM, Bretscher LE, Raines RT (1998) Code for collagen's stability deciphered. *Nature* 392:666–667.
- [83] Holmgren SK, Bretscher LE, Taylor KM, Raines RT (1999) A hyperstable collagen mimic. *Chem Biol* 6:63–70.
- [84] Kadler KE, Holmes DF, Trotter JA, Chapman JA (1996) Collagen fibril formation. *Biochem J* 316 (Pt 1):1–11.
- [85] Kadler KE, Hojima Y, Prockop DJ (1987) Assembly of collagen fibrils de novo by cleavage of the type I pC-collagen with procollagen C-proteinase. Assay of critical concentration demonstrates that collagen self-assembly is a classical example of an entropy-driven process. *J Biol Chem* 262:15696–15701.
- [86] Wess TJ (2008) *Collagen Fibrillar Structure and Hierarchies: in Collagen: Structure and Mechanics* ed Fratzl P (Springer Science + Business Media, LLC), 1st edition, pp 49 – 80.
- [87] Chapman JA, Tzaphlidou M, Meek KM, Kadler KE (1990) The collagen fibril—a model system for studying the staining and fixation of a protein. *Electron Microsc Rev* 3:143–182.
- [88] Hulmes DJ, Miller A, Parry DA, Piez KA, Woodhead-Galloway J (1973) Analysis of the primary structure of collagen for the origins of molecular packing. *J Mol Biol* 79:137–148.
- [89] Ortolani F, Giordano M, Marchini M (2000) A model for type II collagen fibrils: distinctive D-band patterns in native and reconstituted fibrils compared with sequence data for helix and telopeptide domains. *Biopolymers* 54:448–463.
- [90] Cameron GJ, Cairns DE, Wess TJ (2007) The variability in type I collagen helical pitch is reflected in the D periodic fibrillar structure. *J Mol Biol* 372:1097–1107.
- [91] Bailey NCAAJ (2008) *Restraining Cross-Links Responsible for the Mechanical Properties of Collagen Fibers: Natural and Artificial: in Collagen: Structure and Mechanics* ed Fratzl P (Springer Science + Business Media, LLC), 1st edition, pp 81 – 110.
- [92] Chapman JA, Hardcastle RA (1974) The staining pattern of collagen fibrils. II. A comparison with patterns computer-generated from the amino acid sequence. *Connect Tissue Res* 2:151–159.
- [93] Chapman JA (1974) The staining pattern of collagen fibrils. I. An analysis of electron micrographs. *Connect Tissue Res* 2:137–150.
- [94] Smith JW (1968) Molecular pattern in native collagen. *Nature* 219:157–158.
- [95] Holmes DF, et al. (2001) Corneal collagen fibril structure in three dimensions: Struc-

- tural insights into fibril assembly, mechanical properties, and tissue organization. *Proc Natl Acad Sci U S A* 98:7307–7312.
- [96] Fraser RD, MacRae TP, Miller A, Suzuki E (1983) Molecular conformation and packing in collagen fibrils. *J Mol Biol* 167:497–521.
- [97] Wess TJ, Hammersley A, Wess L, Miller A (1995) Type I collagen packing, conformation of the triclinic unit cell. *J Mol Biol* 248:487–493.
- [98] Piez KA, Trus BL (1981) A new model for packing of type-I collagen molecules in the native fibril. *Biosci Rep* 1:801–810.
- [99] Orgel JPRO, Irving TC, Miller A, Wess TJ (2006) Microfibrillar structure of type I collagen in situ. *Proc Natl Acad Sci U S A* 103:9001–9005.
- [100] Köster S, Leach JB, Struth B, Pfohl T, Wong JY (2007) Visualization of flow-aligned type I collagen self-assembly in tunable pH gradients. *Langmuir* 23:357–359.
- [101] Cisneros DA, Hung C, Franz CM, Muller DJ (2006) Observing growth steps of collagen self-assembly by time-lapse high-resolution atomic force microscopy. *J Struct Biol* 154:232–245.
- [102] Fraser RD, MacRae TP, Miller A (1987) Molecular packing in type I collagen fibrils. *J Mol Biol* 193:115–125.
- [103] Wess TJ, Hammersley AP, Wess L, Miller A (1998) A consensus model for molecular packing of type I collagen. *J Struct Biol* 122:92–100.
- [104] Fratzl P, Fratzl-Zelman N, Klaushofer K (1993) Collagen packing and mineralization. An x-ray scattering investigation of turkey leg tendon. *Biophys J* 64:260–266.
- [105] Prockop DJ, Fertala A (1998) The collagen fibril: the almost crystalline structure. *J Struct Biol* 122:111–118.
- [106] Gutschmann T, et al. (2003) Evidence that collagen fibrils in tendons are inhomogeneously structured in a tubelike manner. *Biophys J* 84:2593–2598.
- [107] Wen CK, Goh MC (2004) AFM nanodissection reveals internal structural details of single collagen fibrils. *Nano Letters* 4:129–132.
- [108] Hulmes DJ, Wess TJ, Prockop DJ, Fratzl P (1995) Radial packing, order, and disorder in collagen fibrils. *Biophys J* 68:1661–1670.
- [109] Hulmes DJ, Holmes DF, Cummings C (1985) Crystalline regions in collagen fibrils. *J Mol Biol* 184:473–477.
- [110] Parry DAD, Craig AS (1979) Electron-Microscope Evidence For An 80-A Unit In Collagen Fibrils. *Nature* 282:213–215.
- [111] Perumal S, Antipova O, Orgel JPRO (2008) Collagen fibril architecture, domain organization, and triple-helical conformation govern its proteolysis. *Proc Natl Acad Sci U S A* 105:2824–2829.
- [112] Bruns RR (1976) Supramolecular structure of polymorphic collagen fibrils. *J Cell Biol* 68:521–538.

- [113] Wen CK, Goh MC (2006) Fibrous long spacing type collagen fibrils have a hierarchical internal structure. *Proteins* 64:227–233.
- [114] Dingemans KP, Teeling P (1994) Long-spacing collagen and proteoglycans in pathologic tissues. *Ultrastruct Pathol* 18:539–547.
- [115] Mallinger R, Kulnig W, Böck P (1992) Symmetrically banded collagen fibrils: observations on a new cross striation pattern in vivo. *Anat Rec* 232:45–51.
- [116] Olsen BR (1963) Electron microscope studies on collagen. II. Mechanism of linear polymerization of tropocollagen molecules. *Z Zellforsch Mikrosk Anat* 59:199–213.
- [117] Chapman JA, Armitage PM (1972) An analysis of fibrous long spacing forms of collagen. *Conn Tiss Res* 1:31–37.
- [118] Birk DE, Fitch JM, Babiarz JP, Doane KJ, Linsenmayer TF (1990) Collagen fibrillogenesis in vitro: interaction of types I and V collagen regulates fibril diameter. *J Cell Sci* 95 (Pt 4):649–657.
- [119] Romanic AM, Adachi E, Kadler KE, Hojima Y, Prockop DJ (1991) Copolymerization of pNcollagen III and collagen I. pNcollagen III decreases the rate of incorporation of collagen I into fibrils, the amount of collagen I incorporated, and the diameter of the fibrils formed. *J Biol Chem* 266:12703–12709.
- [120] Capaldi MJ, Chapman JA (1982) The C-terminal extrahelical peptide of type I collagen and its role in fibrillogenesis in vitro. *Biopolymers* 21:2291–2313.
- [121] Leibovich SJ, Weiss JB (1970) Electron microscope studies of the effects of endo- and exopeptidase digestion on tropocollagen. A novel concept of the role of terminal regions in fibrillogenesis. *Biochim Biophys Acta* 214:445–454.
- [122] Lian JB, Morris S, Faris B, Albright J, Franzblau C (1973) The effects of acetic acid and pepsin on the crosslinkages and ultrastructure of corneal collagen. *Biochim Biophys Acta* 328:193–204.
- [123] Kadler KE, Hojima Y, Prockop DJ (1988) Assembly of type I collagen fibrils de novo. Between 37 and 41 degrees C the process is limited by micro-unfolding of monomers. *J Biol Chem* 263:10517–10523.
- [124] Christiansen DL, Huang EK, Silver FH (2000) Assembly of type I collagen: fusion of fibril subunits and the influence of fibril diameter on mechanical properties. *Matrix Biol* 19:409–420.
- [125] Harris JR, Reiber A (2007) Influence of saline and pH on collagen type I fibrillogenesis in vitro: fibril polymorphism and colloidal gold labelling. *Micron* 38:513–521.
- [126] Highberger JH, Gross J, Schmitt FO (1951) The Interaction Of Mucoprotein With Soluble Collagen - An Electron Microscope Study. *Proceedings Of The National Academy Of Sciences Of The United States Of America* 37:286–291.
- [127] Paige MF, Rainey JK, Goh MC (2001) A study of fibrous long spacing collagen ultrastructure and assembly by atomic force microscopy. *Micron* 32:341–353.
- [128] Hodge AJ, Schmitt FO (1960) The charge profile of the tropocollagen macromolecule

- and the packing arrangement in native-type collagen fibrils. *Proc Natl Acad Sci U S A* 46:186–197.
- [129] Lilja S, Barrach HJ (1983) Normally sulphated and highly sulphated glycosaminoglycans (GAG) affecting fibrillogenesis of type I and type II collagen in vitro. *Exp Pathol* 23:173–181.
- [130] Ghosh SK, Mitra HP (1975) Oblique banding pattern in collagen fibrils reconstituted in vitro after trypsin treatment. *Biochim Biophys Acta* 405:340–346.
- [131] Olsen BR (1963) Electron microscope studies on collagen. I. Native collagen fibrils. *Z Zellforsch Mikrosk Anat* 59:184–198.
- [132] Bard JB, Chapman JA (1968) Polymorphism in collagen fibrils precipitated at low pH. *Nature* 219:1279–1280.
- [133] Meek KM, Chapman JA, Hardcastle RA (1979) The staining pattern of collagen fibrils. Improved correlation with sequence data. *J Biol Chem* 254:10710–10714.
- [134] Kühn K, Schupple G, Kühn J (1964) Kollagenfibrillen Mit Anormalem Querstreifungsmuster. *Naturwissenschaften* 51:337–&.
- [135] Williams BR, Gelman RA, Poppke DC, Piez KA (1978) Collagen fibril formation. Optimal in vitro conditions and preliminary kinetic results. *J Biol Chem* 253:6578–6585.
- [136] Porter KR, Pappas GD (1959) Collagen formation by fibroblasts of the chick embryo dermis. *J Biophys Biochem Cytol* 5:153–166.
- [137] Kajikawa K (1961) Structure Of Collagen Fibrils As Revealed By Electron Microscopy. *Journal Of Electron Microscopy* 10:1–6.
- [138] Doyle BB, Hukins DW, Hulmes DJ, Miller A, Woodhead-Galloway J (1975) Collagen polymorphism: its origins in the amino acid sequence. *J Mol Biol* 91:79–99.
- [139] Doyle BB, et al. (1974) Axially projected collagen structures. *Proc R Soc Lond B Biol Sci* 187:37–46.
- [140] Bruns RR, Trelstad RL, Gross J (1973) Cartilage collagen: a staggered substructure in reconstituted fibrils. *Science* 181:269–271.
- [141] Schmitt FO, Gross J, Highberger JH (1953) A New Particle Type in Certain Connective Tissue Extracts. *Proc Natl Acad Sci U S A* 39:459–470.
- [142] Hodge AJ, Schmitt FO (1958) Interaction properties of sonically fragmented collagen macromolecules. *Proc Natl Acad Sci U S A* 44:418–424.
- [143] Hulmes DJ, Bruns RR, Gross J (1983) On the state of aggregation of newly secreted procollagen. *Proc Natl Acad Sci U S A* 80:388–392.
- [144] Paige MF, Goh MC (2001) Ultrastructure and assembly of segmental long spacing collagen studied by atomic force microscopy. *Micron* 32:355–361.
- [145] Hormann H, von Wilm M (1964) Kollagensegmente Mit Symmetrischer Querstreifung. *Naturwissenschaften* 51:464–&.

- [146] Swann DA, Caulfield JB, Broadhurst JB (1976) The altered fibrous form of vitreous collagen following solubilization with pepsin. *Biochim Biophys Acta* 427:365–370.
- [147] Silver FH, Trelstad RL (1980) Type I collagen in solution. Structure and properties of fibril fragments. *J Biol Chem* 255:9427–9433.
- [148] Highberger JH, Gross J, Schmitt FO (1950) Electron Microscope Observations Of Certain Fibrous Structures Obtained From Connective Tissue Extracts. *Journal Of The American Chemical Society* 72:3321–3322.
- [149] Kühn K, Zimmer E (1961) Über Eine Neue Form Der Long-Spacing-Fibrillen Des Kollagens. *Naturwissenschaften* 48:220–&.
- [150] Mallinger R, Schmut O (1985) In vitro fibrillogenesis of interstitial collagens: electron microscopical studies of long-spacing forms induced by chondroitin sulfate. *J Submicrosc Cytol* 17:177–182.
- [151] Wood GC, Keech MK (1960) The formation of fibrils from collagen solutions. 1. The effect of experimental conditions: kinetic and electron-microscope studies. *Biochem J* 75:588–598.
- [152] Silver FH, Trelstad RL (1979) Linear aggregation and the turbidimetric lag phase: type I collagen fibrillogenesis in vitro. *J Theor Biol* 81:515–526.
- [153] Wood GC (1960) The formation of fibrils from collagen solutions. 2. A mechanism of collagen-fibril formation. *Biochem J* 75:598–605.
- [154] Comper WD, Veis A (1977) The mechanism of nucleation for in vitro collagen fibril formation. *Biopolymers* 16:2113–2131.
- [155] Gelman RA, Poppke DC, Piez KA (1979) Collagen fibril formation in vitro. The role of the nonhelical terminal regions. *J Biol Chem* 254:11741–11745.
- [156] Kadler KE, Hojima Y, Prockop DJ (1990) Collagen fibrils in vitro grow from pointed tips in the C- to N-terminal direction. *Biochem J* 268:339–343.
- [157] Bakerman S, Hartman BK (1966) Titration of human skin collagen extracted with acid. *Biochemistry* 5:3488–3493.
- [158] Brennan M, Davison PF (1981) Influence of the telopeptides on type I collagen fibrillogenesis. *Biopolymers* 20:2195–2202.
- [159] Helseth DL, Veis A (1981) Collagen self-assembly in vitro. Differentiating specific telopeptide-dependent interactions using selective enzyme modification and the addition of free amino telopeptide. *J Biol Chem* 256:7118–7128.
- [160] Prockop DJ, Fertala A (1998) Inhibition of the self-assembly of collagen I into fibrils with synthetic peptides. Demonstration that assembly is driven by specific binding sites on the monomers. *J Biol Chem* 273:15598–15604.
- [161] Capaldi MJ, Chapman JA (1984) The C-terminal extrahelical peptide of type I collagen and its role in fibrillogenesis in vitro: effects of ethylurea. *Biopolymers* 23:313–323.

- [162] Silver FH, Langley KH, Trelstad RL (1979) Type I collagen fibrillogenesis: initiation via reversible linear and lateral growth steps. *Biopolymers* 18:2523–2535.
- [163] Gobeaux F, et al. (2008) Fibrillogenesis in dense collagen solutions: a physicochemical study. *J Mol Biol* 376:1509–1522.
- [164] Scott JE (1980) Collagen–proteoglycan interactions. Localization of proteoglycans in tendon by electron microscopy. *Biochem J* 187:887–891.
- [165] Scott JE, Orford CR, Hughes EW (1981) Proteoglycan-Collagen Arrangements In Developing Rat Tail Tendon - An Electron-Microscopical And Biochemical Investigation. *Biochemical Journal* 195:573–81.
- [166] Obrink B (1973) The influence of glycosaminoglycans on the formation of fibers from monomeric tropocollagen in vitro. *Eur J Biochem* 34:129–137.
- [167] Wood GC (1960) The formation of fibrils from collagen solutions. 3. Effect of chondroitin sulphate and some other naturally occurring polyanions on the rate of formation. *Biochem J* 75:605–612.
- [168] Obrink B (1973) A study of the interactions between monomeric tropocollagen and glycosaminoglycans. *Eur J Biochem* 33:387–400.
- [169] Lowther DA, Natarajan M (1972) The influence of glycoprotein on collagen fibril formation in the presence of chondroitin sulphate proteoglycan. *Biochem J* 127:607–608.
- [170] Iozzo RV (1999) The biology of the small leucine-rich proteoglycans. Functional network of interactive proteins. *J Biol Chem* 274:18843–18846.
- [171] McEwan PA, Scott PG, Bishop PN, Bella J (2006) Structural correlations in the family of small leucine-rich repeat proteins and proteoglycans. *J Struct Biol* 155:294–305.
- [172] Graham HK, Holmes DF, Watson RB, Kadler KE (2000) Identification of collagen fibril fusion during vertebrate tendon morphogenesis. The process relies on unipolar fibrils and is regulated by collagen-proteoglycan interaction. *J Mol Biol* 295:891–902.
- [173] Scott JE (2003) Elasticity in extracellular matrix 'shape modules' of tendon, cartilage, etc. A sliding proteoglycan-filament model. *J Physiol* 553:335–343.
- [174] Sigma-Aldrich (2009) Decorin (MSDS)., (Sigma-Aldrich), Technical report.
- [175] Scott PG, et al. (2004) Crystal structure of the dimeric protein core of decorin, the archetypal small leucine-rich repeat proteoglycan. *Proc Natl Acad Sci U S A* 101:15633–15638.
- [176] Neame PJ, Kay CJ, McQuillan DJ, Beales MP, Hassell JR (2000) Independent modulation of collagen fibrillogenesis by decorin and lumican. *Cell Mol Life Sci* 57:859–863.
- [177] MacBeath JR, Shackleton DR, Hulmes DJ (1993) Tyrosine-rich acidic matrix pro-

- tein (TRAMP) accelerates collagen fibril formation in vitro. *J Biol Chem* 268:19826–19832.
- [178] Minamitani T, et al. (2004) Modulation of collagen fibrillogenesis by tenascin-X and type VI collagen. *Exp Cell Res* 298:305–315.
- [179] Kvist AJ, et al. (2006) Chondroitin sulfate perlecan enhances collagen fibril formation. Implications for perlecan chondrodysplasias. *J Biol Chem* 281:33127–33139.
- [180] Sullivan MM, et al. (2006) Matricellular hevin regulates decorin production and collagen assembly. *J Biol Chem* 281:27621–27632.
- [181] Halász K, Kassner A, Mörgelin M, Heinegård D (2007) COMP acts as a catalyst in collagen fibrillogenesis. *J Biol Chem* 282:31166–31173.
- [182] McPherson JM, Sawamura SJ, Condell RA, Rhee W, Wallace DG (1988) The effects of heparin on the physicochemical properties of reconstituted collagen. *Coll Relat Res* 8:65–82.
- [183] Tsai SW, Liu RL, Hsu FY, Chen CC (2006) A study of the influence of polysaccharides on collagen self-assembly: nanostructure and kinetics. *Biopolymers* 83:381–388.
- [184] Birk DE, Bruckner P (2005) Collagen suprastructures. *Collagen* 247:185–205.
- [185] Wenstrup RJ, et al. (2004) Type V collagen controls the initiation of collagen fibril assembly. *J Biol Chem* 279:53331–53337.
- [186] Hörber JKH (2002) *Local Probe Techniques in: Atomic Force Microscopy in Cell Biology*, Methods in Cell Biology eds Jena BP, Hörber JKH (Academic Press, Elsevier Science) Vol. 68.
- [187] Binnig, Quate, Gerber (1986) Atomic force microscope. *Phys Rev Lett* 56:930–933.
- [188] Braga PC, Ricci D (2003) *Imaging Methods in Atomic Force Microscopy*, Methods in Molecular Biology eds Braga PC, Ricci D (Humana Press) Vol. 242.
- [189] Albrecht TR, Akamine S, Carver TE, Quate CF (1990) Microfabrication Of Cantilever Styli For The Atomic Force Microscope. *Journal Of Vacuum Science & Technology A - Vacuum Surfaces And Films* 8:3386–3396.
- [190] Tortonese M (1997) Cantilevers and tips for atomic force microscopy. *IEEE Eng Med Biol Mag* 16:28–33.
- [191] Agilent (year?) AFM Elements on www.pacificnanotech.com.
- [192] Israelachvili JN (1992) *Intermolecular & Surface Forces* ed Israelachvili JN (Academic Press, Harcour Brace & Company), 2nd edition.
- [193] Thornton J (1998) *Training Book v3 (Digital Instruments)* (Digital Instruments Veeco Metrology Group, 112 Robin Hill blvd.), 3 edition.
- [194] Gould S, et al. (1988) Molecular Resolution Images Of Amino-Acid Crystals With The Atomic Force Microscope. *Nature* 332:332–334.
- [195] Drake B, et al. (1989) Imaging crystals, polymers, and processes in water with the atomic force microscope. *Science* 243:1586–1589.

- [196] Weisenhorn AL, et al. (1990) Immobilized proteins in buffer imaged at molecular resolution by atomic force microscopy. *Biophys J* 58:1251–1258.
- [197] Hansma HG, Hoh JH (1994) Biomolecular imaging with the atomic force microscope. *Annu Rev Biophys Biomol Struct* 23:115–139.
- [198] Butt HJ, Downing KH, Hansma PK (1990) Imaging the membrane protein bacteriorhodopsin with the atomic force microscope. *Biophys J* 58:1473–1480.
- [199] Hoh JH, Lal R, John SA, Revel JP, Arnsdorf MF (1991) Atomic force microscopy and dissection of gap junctions. *Science* 253:1405–1408.
- [200] Hansma HG (2001) Surface biology of DNA by atomic force microscopy. *Annu Rev Phys Chem* 52:71–92.
- [201] Schabert FA, Henn C, Engel A (1995) Native Escherichia coli OmpF porin surfaces probed by atomic force microscopy. *Science* 268:92–94.
- [202] Müller DJ, Büldt G, Engel A (1995) Force-induced conformational change of bacteriorhodopsin. *J Mol Biol* 249:239–243.
- [203] Müller DJ, Schabert FA, Büldt G, Engel A (1995) Imaging purple membranes in aqueous solutions at sub-nanometer resolution by atomic force microscopy. *Biophys J* 68:1681–1686.
- [204] Radmacher M, Tillamnn RW, Fritz M, Gaub HE (1992) From molecules to cells: imaging soft samples with the atomic force microscope. *Science* 257:1900–1905.
- [205] Touhami A, Jericho MH, Beveridge TJ (2004) Atomic force microscopy of cell growth and division in Staphylococcus aureus. *J Bacteriol* 186:3286–3295.
- [206] Pelling AE, Li Y, Shi W, Gimzewski JK (2005) Nanoscale visualization and characterization of Myxococcus xanthus cells with atomic force microscopy. *Proc Natl Acad Sci U S A* 102:6484–6489.
- [207] Humphris ADL, Miles MJ, Hobbs JK (2005) A mechanical microscope: High-speed atomic force microscopy. *Applied Physics Letters* 86:034106.
- [208] Ando T, et al. (2007) High-speed atomic force microscopy for observing dynamic biomolecular processes. *J Mol Recognit* 20:448–458.
- [209] Picco LM, et al. (2007) Breaking the speed limit with atomic force microscopy. *Nanotechnology* 18:044030.
- [210] Ando T, Uchihashi T, Fukuma T (2008) High-speed atomic force microscopy for nano-visualization of dynamic biomolecular processes. *Progress In Surface Science* 83:337–437.
- [211] Hinterdorfer P (2004) *Molecular Recognition Force Spectroscopy in: Springer Handbook of Nanotechnology* ed Bhushan B (Springer-Verlag, Berlin).
- [212] Riener CK, et al. (2003) Heterobifunctional crosslinkers for tethering single ligand molecules to scanning probes. *Analytica Chimica Acta* 497:101–114.
- [213] Hinterdorfer P, Baumgartner W, Gruber HJ, Schilcher K, Schindler H (1996) De-

- tection and localization of individual antibody-antigen recognition events by atomic force microscopy. *Proc Natl Acad Sci U S A* 93:3477–3481.
- [214] Engler AJ, Sen S, Sweeney HL, Discher DE (2006) Matrix elasticity directs stem cell lineage specification. *Cell* 126:677–689.
- [215] Wells RG (2008) The role of matrix stiffness in regulating cell behavior. *Hepatology* 47:1394–1400.
- [216] Heim AJ, Koob TJ, Matthews WG (2007) Low strain nanomechanics of collagen fibrils. *Biomacromolecules* 8:3298–3301.
- [217] Wenger MPE, Bozec L, Horton MA, Mesquida P (2007) Mechanical properties of collagen fibrils. *Biophys J* 93:1255–1263.
- [218] Graham JS, Vomund AN, Phillips CL, Grandbois M (2004) Structural changes in human type I collagen fibrils investigated by force spectroscopy. *Exp Cell Res* 299:335–342.
- [219] van der Rijt JAJ, van der Werf KO, Bennink ML, Dijkstra PJ, Feijen J (2006) Micromechanical testing of individual collagen fibrils. *Macromol Biosci* 6:697–702.
- [220] Smith JF, Knowles TPJ, Dobson CM, Macphee CE, Welland ME (2006) Characterization of the nanoscale properties of individual amyloid fibrils. *Proc Natl Acad Sci U S A* 103:15806–15811.
- [221] Yang L, et al. (2008) Mechanical properties of native and cross-linked type I collagen fibrils. *Biophys J* 94:2204–2211.
- [222] Kis A, et al. (2002) Nanomechanics of microtubules. *Phys Rev Lett* 89:248101.
- [223] Ugural AC (2008) *Mechanics of Materials* (John Wiley & Sons, Inc.).
- [224] Niu LJ, Chen XY, Allen S, Tendler SJB (2007) Using the bending beam model to estimate the elasticity of diphenylalanine nanotubes. *Langmuir* 23:7443–7446.
- [225] Salchert K, Pompe T, Sperling C, Werner C (2003) Quantitative analysis of immobilized proteins and protein mixtures by amino acid analysis. *J Chromatogr A* 1005:113–122.
- [226] Bhushan B (2004) *Mechanical Properties of Nanostructures in: Springer Handbook of Nanotechnology* ed Bhushan B (Springer-Verlag, Berlin).
- [227] Spurr AR (1969) A low-viscosity epoxy resin embedding medium for electron microscopy. *J Ultrastruct Res* 26:31–43.
- [228] Salchert K, et al. (2004) In vitro reconstitution of fibrillar collagen type I assemblies at reactive polymer surfaces. *Biomacromolecules* 5:1340–1350.
- [229] Mathews MB, Decker L (1968) The effect of acid mucopolysaccharides and acid mucopolysaccharide-proteins on fibril formation from collagen solutions. *Biochem J* 109:517–526.
- [230] Guidry C, Grinnell F (1987) Heparin modulates the organization of hydrated collagen gels and inhibits gel contraction by fibroblasts. *J Cell Biol* 104:1097–1103.

- [231] Gupta P, et al. (1998) Structurally specific heparan sulfates support primitive human hematopoiesis by formation of a multimolecular stem cell niche. *Blood* 92:4641–4651.
- [232] Madihally SV, Flake AW, Matthew HW (1999) Maintenance of CD34 expression during proliferation of CD34+ cord blood cells on glycosaminoglycan surfaces. *Stem Cells* 17:295–305.
- [233] Gama CI, et al. (2006) Sulfation patterns of glycosaminoglycans encode molecular recognition and activity. *Nat Chem Biol* 2:467–473.
- [234] Keller KM, Keller JM, Kuhn K (1986) The C-terminus of type I collagen is a major binding site for heparin. *Biochimica Et Biophysica Acta* 882:1–5.
- [235] Antonio JDS, Lander AD, Karnovsky MJ, Slayter HS (1994) Mapping the heparin-binding sites on type I collagen monomers and fibrils. *J Cell Biol* 125:1179–1188.
- [236] Boeckmann B, et al. (2003) The SWISS-PROT protein knowledgebase and its supplement TrEMBL in 2003. *Nucleic Acids Res* 31:365–370.
- [237] Trus BL, Piez KA (1976) Molecular packing of collagen: three-dimensional analysis of electrostatic interactions. *J Mol Biol* 108:705–732.
- [238] Young RD (1985) The ultrastructural organization of proteoglycans and collagen in human and rabbit scleral matrix. *J Cell Sci* 74:95–104.
- [239] Scott JE (1988) Proteoglycan-fibrillar collagen interactions. *Biochem J* 252:313–323.
- [240] Hirsch M, Prenant G, Renard G (2001) Three-dimensional supramolecular organization of the extracellular matrix in human and rabbit corneal stroma, as revealed by ultrarapid-freezing and deep-etching methods. *Exp Eye Res* 72:123–135.
- [241] Brightman AO, et al. (2000) Time-lapse confocal reflection microscopy of collagen fibrillogenesis and extracellular matrix assembly in vitro. *Biopolymers* 54:222–234.
- [242] Lilja S, Barrach HJ (1981) An electron microscopical study of the influence of different glycosaminoglycans on the fibrillogenesis of collagen type I and II in vitro. *Virchows Arch A Pathol Anat Histol* 390:325–338.
- [243] Scott JE, Orford CR (1981) Dermatan Sulfate-Rich Proteoglycan Associates With Rat Tail Tendon Collagen At The D-Band In The Gap Region. *Biochemical Journal* 197:213–216.
- [244] Holmes DF, Lowe MP, Chapman JA (1994) Vertebrate (chick) collagen fibrils formed in vivo can exhibit a reversal in molecular polarity. *J Mol Biol* 235:80–83.
- [245] Thurmond FA, Trotter JA (1994) Native collagen fibrils from echinoderms are molecularly bipolar. *J Mol Biol* 235:73–79.
- [246] Casu B, Lindahl U (2001) Structure and biological interactions of heparin and heparan sulfate. *Adv Carbohydr Chem Biochem* 57:159–206.

- [247] Gross J, Highberger JH, Schmitt FO (1954) Collagen structures considered as states of aggregation of a kinetic unit. The tropocollagen particle. *Proc Natl Acad Sci U S A* 40:679–688.
- [248] Doyle BB, et al. (1974) Origins and implications of D-stagger in collagen. *Biochemical And Biophysical Research Communications* 60:858–864.
- [249] Bozec L, van der Heijden G, Horton M (2007) Collagen fibrils: nanoscale ropes. *Biophys J* 92:70–75.
- [250] Armitage PM, Chapman JA (1971) New fibrous long spacing form of collagen. *Nat New Biol* 229:151–152.
- [251] Guinier A (1963) *Displacement Disorder in Crystals: in X-Ray Diffraction in Crystals, Imperfect Crystals, and Amorphous Bodies* eds Foley HM, Ruderman MA (W. H. Freeman and Company, San Francisco), pp 185 – 251.
- [252] Rusmini F, Zhong Z, Feijen J (2007) Protein immobilization strategies for protein biochips. *Biomacromolecules* 8:1775–1789.
- [253] Hermanson GT (2008) *The Chemistry of Reactive Groups: in Bioconjugate Techniques* ed Hermanson GT (Academic Press, London, UK), 2nd edition, pp 171 – 172.
- [254] Buehler MJ (2006) Nature designs tough collagen: explaining the nanostructure of collagen fibrils. *Proc Natl Acad Sci U S A* 103:12285–12290.
- [255] Buehler MJ (2006) Atomistic and continuum modeling of mechanical properties of collagen: Elasticity, fracture, and self-assembly. *Journal Of Materials Research* 21:1947–1961.
- [256] Harley BA, Leung JH, Silva ECCM, Gibson LJ (2007) Mechanical characterization of collagen-glycosaminoglycan scaffolds. *Acta Biomater* 3:463–474.
- [257] Buehler MJ, Wong SY (2007) Entropic elasticity controls nanomechanics of single tropocollagen molecules. *Biophys J* 93:37–43.
- [258] Bailey AJ, Peach CM (1968) Isolation and structural identification of a labile intermolecular crosslink in collagen. *Biochem Biophys Res Commun* 33:812–819.
- [259] Orgel JP, Wess TJ, Miller A (2000) The in situ conformation and axial location of the intermolecular cross-linked non-helical telopeptides of type I collagen. *Structure* 8:137–142.
- [260] Mulloy B, Forster MJ, Jones C, Davies DB (1993) N.m.r. and molecular-modelling studies of the solution conformation of heparin. *Biochem J* 293 (Pt 3):849–858.
- [261] Butler WT, Cunningham LW (1966) Evidence for the linkage of a disaccharide to hydroxylysine in tropocollagen. *J Biol Chem* 241:3882–3888.
- [262] Geiger B, Spatz JP, Bershadsky AD (2009) Environmental sensing through focal adhesions. *Nat Rev Mol Cell Biol* 10:21–33.

List of Figures

2.1. Schematic structural organization vs. native complexity of the ECM.	5
2.2. Representative structures of GAGs.	9
2.3. Triple-helical organization of collagen type I.	12
2.4. N- and C-terminal enzymatic processing of procollagen type I.	14
2.5. Axial structure of D-periodic collagen fibrils.	15
2.6. Microfibrillar structure of collagen type I.	16
2.7. Cylindrical packing models of collagen type I.	17
2.8. Schematic linear and lateral growth models for type I collagen fibrillogenesis.	20
2.9. 'Horseshoe' model for interfibrillar localization of decorin.	24
2.10. Heterotypic assembly of collagen type I and V.	25
2.11. Scanning probe tip structures shown at different scales.	27
2.12. Principle and setup of SFM.	28
2.13. Tip modification and subsequent single molecule recognition event detected by SFM.	31
2.14. Models for the deflection of a concentric beam upon application of concen- trated load.	33
3.1. Aldehyde-derivatization strategy applied for covalent immobilization of col- lagen fibrils.	47
3.2. NHS-derivatization strategy applied for covalent immobilization of collagen fibrils.	48
3.3. Experimental setup of the micromechanical bending.	50
4.1. Morphological analysis of pure PSC fibrils.	54
4.2. Reconstitution of PSC fibrils in the presence of hyaluronic acid.	55
4.3. Impact of HS on the morphology of PSC fibrils.	55
4.4. Morphogenic effect of LMWH on PSC fibrils.	56
4.5. Impact of LMWH concentration on size distribution and width-to-length ratio of PSC-LMWH cofibrils.	57
4.6. Effect of GAG concentration on the kinetics of PSC-LMWH cofibrillogenesis.	58

4.7. Influence of LMWH concentration on t_{EXP} and $\frac{dOD}{dt}(t_{1/2})$ of PSC-LMWH fibrillogenesis.	59
4.8. Influence of GAG concentration on the molar ratio between LMWH and atelocollagen after stability tests.	60
4.9. cLSM image of a single PSC-FITC labeled heparin cofibril of varying diameter.	61
4.10. Linear regression of the maximum fluorescence intensity of cofibril cross-section vs. FWHM ²	62
4.11. Absence of linear extrapolation of maximum fluorescence intensity vs. FWHM.	62
4.12. Impact of HMWH concentration on size distribution and width-to-length ratio of PSC-HMWH cofibrils.	63
4.13. Impact of pH value and degree of sulfation on the morphology of PSC-LMWH and PSC-HS cofibrils.	64
4.14. Proposed scheme of the important steps in PSC-heparin cofibrillogenesis.	68
4.15. SFM amplitude images of the two existing structural levels in the system with reconstituted PSC-heparin cofibrils.	69
4.16. High-resolution TEM images of PSC - heparin cofibrils.	70
4.17. Asymmetric density profiles of PSC-heparin cofibrils.	71
4.18. SFM and TEM analysis of symmetric FLS IV nanofibrils with 165 nm periodicity.	73
4.19. Analysis of nuclei longspacing fibrils and 300 nm-short segments as other polymorphic forms found in the system.	75
4.20. SFM images of PSC fibrils formed after the addition of heparin during the exponential growth phase.	76
4.21. Proposed mechanism for the hierarchical self-assembly of asymmetric D-periodic cofibrils and symmetric FLS IV nanofibrils from pepsin-treated bovine collagen type I and highly sulfated heparin.	79
4.22. Impact of heparin and telopeptides on the structural polymorphism of collagen type I fibrils.	81
4.23. Impact of the presence of heparin and telopeptides on the interhelical packing of collagen I.	82
4.24. Comparison of physical vs. chemical immobilization strategies used for PSC-heparin cofibrils suspended over silicon gratings.	83
4.25. Change of the linear regime of force-separation curves with respect to position of the bending points along the surfaces of a single cofibril.	85
4.26. Experimental validation of the 'double-clamped' vs. 'simple supported' model.	86

4.27. Impact of telopeptides and heparin concentration on the mechanical properties of collagen type I.	87
4.28. Impact of heparin on the shear modulus of PSC fibrils.	87
4.29. Molecular origins for the native tropocollagen cross-linking in collagen I fibril assembly.	89
4.30. Molecular origins for the <i>in vitro</i> atelocollagen-heparin fibrillar assembly. .	90
5.1. Influence of structural and physico-chemical characteristics on the binding specificity and assembly of collagen type I - heparin cofibrils.	94
A.1. Turbidimetric analysis of the effect of PSC concentration on the kinetics of fibril formation	A-1
A.2. Turbidimetric analysis of the effect of solution <i>pH</i> value on the kinetics of fibril formation	A-2
A.3. Impact of HS concentration on the size distribution of PSC-HS cofibrils. . .	A-3

List of Tables

2.1. Classification of collagen types in vertebrates.	6
2.2. Observed polymorphic forms of collagen type I.	18
2.3. Comparison of the most basic SFM modi.	29
3.1. Protocol for preparing collagen-GAG gels.	44
3.2. Modified SPURR kit components and resin infiltration protocol.	48
3.3. Programme for polymerization of epoxy resin embedded with biological samples.	49

Nomenclature

AC alternating current

AFM atomic force microscope(y)

AP average periodicity

APTES 3-aminopropyltriethoxysilane

ASC acid soluble collagen

ATP adenosin triphosphate

CRP collagen-related peptide

CS chondroitin sulfate

DC direct current

DDR discoidin domain receptor

DDR2 discoidin domain receptor 2

DPS D-periodic symmetric

DS dermatan sulfate

ECM extracellular matrix

EDC ethylcarbodiimide

FACIT fibrill associated collagens with interrupted triple helices

FGF fibroblast growth factor

FGF1 fibroblast growth factor 1

FGF2 fibroblast growth factor 2

FITC fluorescein isothiocyanate

FLS fibrous long spacing

fps frames per second

FWHM	full width at half maximum
GAG	glycosaminoglycan
HA	hyaluronic acid
HBEGF	heparin-binding epidermal growth factor
HGF	hepatocyte growth factor
HMWH	high molecular weight heparin
HPLC	high pressure liquid chromatography
HS	heparan sulfate
HUVEC	human umbilical cord endothelial cells
IFN	interferon
IL2	interleukin 2
IL7	interleukin 7
KS	keratan sulfate
LMWH	low molecular weight heparin
MES	2-[morpholino]ethanesulfonic acid
MMP	matrix metalloproteinase
NHS	N-hydroxysuccinimide
NMR	nuclear magnetic resonance
OD	optical density
ON	overnight
PBS	phosphate buffered saline
PDB	protein database
PDGF	platelet derived growth factor
PDMS	polydimethylsiloxane
PEMA	poly-(ethylene alt maleic anhydride)
PF4	platelet factor 4
PG	proteoglycan

POMA	poly-(octadecene alt maleic anhydride)
PSC	pepsin-solubilized collagen
PTFE	polytetrafluoroethylene
RGD	arginine glycine asparagine
RHAMM	receptor for hyaluronan-mediated motility
RIE	reactive ion etched
ROC	radius of tip curvature
rpm	revolutions per minute
RT	room temperature
SDF1	stromal cell-derived factor 1
SLRP	small leucine-rich proteoglycans
SLS	segment long spacing
TEM	transmission electron microscopy
THF	tetrahydrofuran
TIMP	tissue inhibitors of matrix metalloproteinases
TNF	tumor necrosis factor
UA	uranyl acetate
VEGF	vascular endothelial growth factors
WAXS	wide-angle x-ray scattering

A. Appendices

A.1. Impact of PSC concentration on the kinetics of fibril formation

Turbidimetric analysis of the pure PSC fibrillogenesis at different collagen concentrations showed that it had an accelerating effect on length of the exponential phase, as well as the time of exponential offset (Fig.A.1). The minimum PSC concentration for fibrillogenesis within the studied 4 h time period appears to be 0.5 mg/ml. At concentrations above 1 mg/ml of PSC, all samples reached the plateau of their fibrillogenesis within 90 min after transfer to 37 °C. Therefore, for kinetic and most of the structural studies the collagen concentrations was always kept at 1.2 mg/ml.

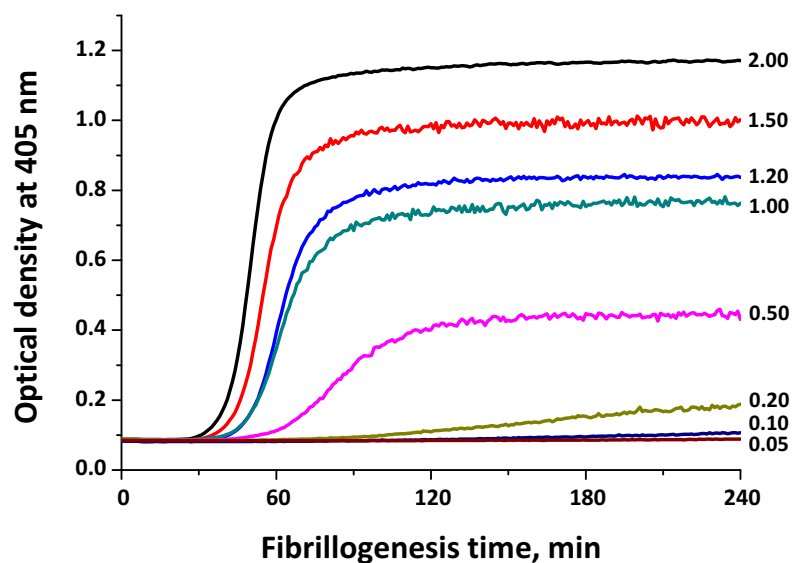


Figure A.1.: Turbidimetric analysis of the effect of PSC concentration on the kinetics of fibril formation (Concentrations in mg/ml are given on the right).

A.2. Impact of pH on the kinetics of PSC fibrillogenesis

The shift of pH values to a more alkaline environment led to an expected shortening of both nucleation and exponential phases (Fig.A.2). The exponential half timepoints for 3 representative pH values (6.4, 7.4 and 8.4) showed a gradual decrease of 71, 56 and 49 min. The concentration in all experiments was kept at 1.2 mg/ml.

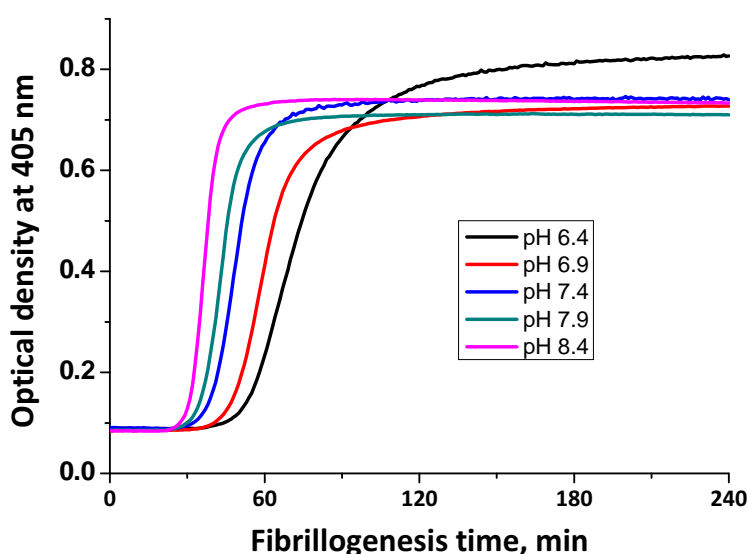


Figure A.2.: Turbidimetric analysis of the effect of solution pH value on the kinetics of fibril formation (PSC concentration 1.2 mg/ml).

A.3. Impact of HS concentration on the size distribution of PSC - HS fibrils

The cofibrillogenesis in the presence of HS resulted in the formation of cofibrils with a much smaller dependence on HS concentration in comparison to the PSC-heparin cofibrils (4.5). A small, but significant increase in the cofibril size ($n = 100$, $p < 0.001$, one-way ANOVA, Bonferroni Test) was only observed for the 1.0 and 0.4 mg/ml HS resulting in mean thicknesses of 300 and 252 nm, respectively, in comparison to 230–240 nm for pure PSC (Fig.A.3). A further increase of the HS concentration (4 mg/ml) resulted in a complete inhibition of the cofibril formation over the time range of 24 h.

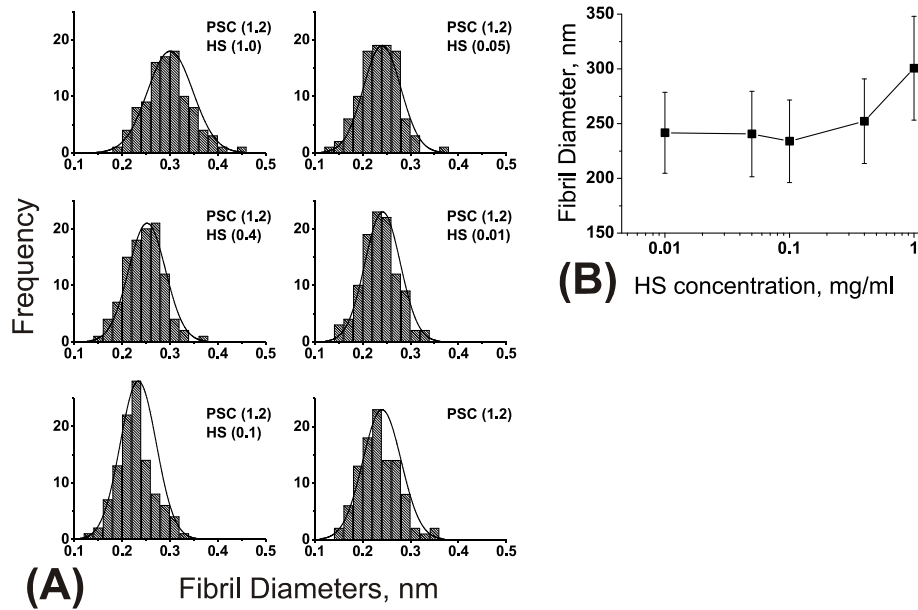


Figure A.3.: Size distributions of the PSC-HS cofibrils (A) at various deployed HS concentrations with a graphical representation of the diameter vs. concentration (B) (error bars represent standard deviation). Concentrations of 4 mg/ml HS inhibited the cofibril formation after 24 h.

A.4. Routine for fitting of adherent fibril cross-sections via modified inverse polynomial function

In order to determine the correct fibril diameters, fibrils were imaged in tapping mode. Furthermore the tips were characterized and deconvolution of the images was carried out in order to subtract the finite contribution of the SFM tip geometry. All deconvoluted fibrillar cross-sections were fit via a modified inverse polynomial function (Eq.A.1)

$$y = y_0 + \frac{A}{1 + A_1 \left(2 \frac{x-x_c}{w}\right)^2 + A_2 \left(2 \frac{x-x_c}{w}\right)^{12}} \quad (\text{A.1})$$

Furthermore we calculated the width at 10% maximum in order to eliminate the background noise contribution for the calculation of the diameters.

The routine for routine for the modified inverse polynomial function is:

[GENERAL INFORMATION]

Function Name=InvsPolyMod

Brief Description=Inverse polynomial peak function with center (Modified)

Function Source=fgroup.InvsPolyMod

Function Type=Built-in

Function Form=Expression

Number Of Parameters=6

Number Of Independent Variables=1

A.4 Routine for fitting of adherent fibril cross-sections via modified inverse polynomial function

```
Number Of Dependent Variables=1
Analytical Derivatives for User-Defined=Off
[FITTING PARAMETERS]
Naming Method=User-Defined
Names=y0,xc,w,A,A1,A2
Meanings=offset,center,width,amplitude,coefficient,coefficient
Initial Values=
Lower Bounds=--,--,0.0(X,ON),--,0.0(I,ON),0.0(I,ON)
Upper Bounds=---,---,---,---,---,---
Number Of Significant Digits=
[FORMULA]  $y_0 + A / (1 + A_1 * (2 * (x - x_c) / w)^2 + A_2 * (2 * (x - x_c) / w)^{12})$ 
[CONSTRAINTS]
[CONSTANTS]
[Parameters Initialization]
sort(x_y_curve);
smooth(x_y_curve);
y0 = yatxmin( x_y_curve );
w = fwhm( x_y_curve, y0 );
A = area( x_y_curve, y0 );
if ( A > 0 )
{
xc = xatymax( x_y_curve );
A = max( y_data ) - y0;
}
else
{
xc = xatymmin( x_y_curve );
A = min( y_data ) - y0;
}
A1 = 1.0;
A2 = 1.0;
[INITIALIZATIONS]
[AFTER FITTING]
[ON PARAM CHANGE]
[INDEPENDENT VARIABLES]
x=
[DEPENDENT VARIABLES]
y=
[CONTROLS]
General Linear Constraints=Off
Initialization Scripts=Off
Scripts After Fitting=Off
Number Of Duplicates=0
Duplicate Offset=2
Duplicate Unit=6
Generate Curves After Fitting=Yes
Curve Point Spacing=Uniform on X-Axis Scale
Generate Peaks After Fitting=Yes
```

Generate Peaks During Fitting=Yes
Generate Peaks with Baseline=Yes
Paste Parameters to Plot After Fitting=Yes
Paste Parameters to Notes Window After Fitting=Yes
Generate Residuals After Fitting=No
Keep Parameters=No
Enable Parameters Initialization=N/A
Compile On Param Change Script=1
[COMPILE FUNCTION]
Compile=0
Compile Parameters Initialization=1
On Param Change Scripts Enabled=N/A
[ORIGIN C FUNCTION HEADER]
[ORIGIN C PARAMETER INITIALIZATION HEADER]

B. Others

B.1. Statements

1. Pepsin-solubilized collagen (PSC) type I fibrils reconstituted in the presence of the highly sulfated low molecular weight heparin (LMWH) (4–6 kDa) have spindle-like morphology in contrast to pure PSC fibrils. In comparison, hyaluronic acid has almost no effect on the cofibril structure, influencing only their diameters probably due to sterical size exclusion and concentrating the PSC monomers.
2. LMWH concentration has a non-linear effect on size distribution and width-to-length ratio of PSC-LMWH cofibrils. Intermediate concentrations led to formation of thickest and shortest cofibrils with blunt ends, while lower and higher concentrations exhibited thinner cofibrils with tapered ends.
3. LMWH concentration also influences the kinetics of PSC fibrillogenesis. Increase of LMWH led to shortening of the nucleation phase (portrayed as time for exponential offset t_{EXP}), as well as decreasing the exponential half-time ($\frac{dOD}{dt} (t_{1/2})$). The optical density (OD) of the PSC-LMWH electrostatic complexes formed prior to the cofibrillogenesis shows a non-linear trend with respect to the deployed concentration, similarly to the cofibrils diameters.
4. The LMWH is intercalated in the cofibrils, as concluded from its molecular ratio to atelocollagen (calculated after stability tests), as well as structural analysis with cLSM and FITC-labeled heparin.
5. Substituting LMWH with heparan sulfate (HS) (changing degree of sulfation) has pronounced effect on the cofibril morphology, exhibiting only a small tendency to form linear structures at very high concentrations. Changing the molecular weight of heparin to 17–19 kDa (high molecular weight heparin, HMWH) shows no impact on cofibril morphology or kinetics (as portrayed for LMWH in points 1 - 4).
6. Variation of pH had a much more pronounced effect on PSC-heparin rather than PSC-HS, mainly in decreasing cofibril diameters with increase of pH, whereas in the case of PSC-HS it led to a loss of linearity in the cofibril morphology.
7. Further structural analysis of the PSC-heparin gels showed the existence of 2 polymorphic forms, differing in both size and average periodicity (AP), therefore classi-

- fying them as separate structural levels in the system - big tactoidal cofibrils with D-periodic banding of 67 nm, as well as small nanofibrils with AP of 165 nm.
8. Both positive and negative transmission electron microscopy (TEM) staining techniques helped to identify the banding pattern of the cofibrils as asymmetric.
 9. In contrast to the cofibrils, the nanofibrils show a dihedral 165 nm recurring symmetry which classifies them as previously reported in other systems FLS IV (fibrous long spacing) polymorphic forms.
 10. Further TEM studies of the 20–40 nm thick fibrillar electrostatic complexes of atelocollagen and heparin (referred to as 'nuclei') prior to cofibrillogenesis shows that they exhibit different average periodicity (250 nm) as compared to the cofibrils and the FLS IV nanofibrils. Additional SFM studies confirmed the presence of another polymorphic form, such as 300 nm short segments.
 11. Introducing heparin in the middle of the exponential phase of PSC fibrillogenesis led to the formation of 'hybrids' of mainly D-periodic PSC fibrils with FLS IV termini thus accounting for a startling polymorphic transition. Symmetric FLS IV nanofibrils require an asymmetric scaffold for their formation.
 12. A model for the origin of the polymorphic forms is suggested. Atelocollagen and heparin interact electrostatically to form longspacing nuclei (AP, 250 nm), which furthermore form asymmetric D-periodic cofibrils (AP, 67 nm) by parallel quarter-staggering. The 300 nm short segments together with the longspacing nuclei are involved in the formation of symmetric FLS IV nanofibrils.
 13. Heparin impairs the D-periodic banding in full-length collagen (ASC, containing telopeptides), whereas the reconstitution of FLS IV nanofibrils is not affected.
 14. Inability of ASC collagen to reconstitute D-periodic banding in the presence of heparin is hypothesized to result from competitive binding of telopeptides and heparin along the tropocollagen chain.
 15. Depletion of telopeptides (ASC) led to increase in interhelical collagen spacing, while heparin intercalation had much less pronounced effect in the case of PSC fibrils.
 16. A strategy for covalent immobilization and suspending of fibrils over microstructured silicon gratings in physiological state utilizes either aldehyde- or N-hydroxysuccinimide derivatization of surfaces with increased sensitivity towards amino groups from the proteins.
 17. A micromechanical test via SFM for calculating the bending (E_B) and shear (G) moduli of hydrated ASC, PSC and PSC-heparin fibrils was established. It models the beam deflection from the suspended freestanding fibrils upon the application of a concentrated point load at defined points along the suspended filaments via a double clamped (fixed ends) model.

-
18. Loss of telopeptides (ASC) and heparin intercalation (PSC-heparin) weakens the mechanics of the collagen fibrils. Single point measurements showed E_B values of 379 MPa, 221 MPa and 170 MPa for hydrated ASC (0.5), PSC (0.5) and PSC (1.2) - heparin (1.0) fibrils respectively.
 19. Heparin is assumed to act as an intrafibrillar cross-linker in PSC-heparin cofibrils, which competes for binding sites at the places along the tropocollagen helix that are typically occupied by the telopeptides in ASC fibrils.

B.2. List of publications

Articles

B. Lanfer, F. P. Seib, U. Freudenberg, D. STAMOV, T. Bley, M. Bornhäuser, C. Werner; The growth and differentiation of mesenchymal stem and progenitor cells cultured on aligned collagen matrices; *Biomaterials* 30 (30), 5950-5958 (2009).

D. STAMOV, K. Salchert, A. Springer, C. Werner, T. Pompe; Structural polymorphism of collagen type I - heparin cofibrils; *Soft Matter* 5 (18), 3461-3468 (2009).

B. Lanfer, U. Freudenberg, R. Zimmermann, D. STAMOV, V. Körber, C. Werner; Aligned fibrillar collagen matrices obtained by shear flow deposition; *Biomaterials* 29 (28), 3888-3895 (2008).

D. STAMOV, M. Grimmer, K. Salchert, T. Pompe, C. Werner; Heparin intercalation into reconstituted collagen I fibrils: Impact on growth kinetics and morphology; *Biomaterials* 29 (1), 1-14 (2008).

Talks

D. STAMOV, T. A. K. Nguyen, C. Werner, T. Pompe; *Micromechanical bending of polymorphic collagen type I - heparin cofibrils*; XVII SPM Workshop "Scanning Probe Microscopies and Organic Materials", Bremen (Germany), June 2009.

D. STAMOV, K. Salchert, M. Grimmer, C. Werner, T. Pompe; *Structure, composition and growth of collagen type I - heparin cofibrils*; Max-Bergmann Symposium "Molecular Designed Biological Coating", Dresden (Germany), November 2008.

Posters

D. STAMOV, M. Grimmer, K. Salchert, C. Werner, T. Pompe; *Structural hierarchy and polymorphism of collagen type I - heparin cofibrils*; Gordon Research Conference on Collagen "The Functional Continuum of Cells and Matrix", New London (United States), July 2009.

D. STAMOV, T. A. K. Nguyen, K. Salchert, C. Werner, T. Pompe; *Collagen type I - heparin xenogeneic scaffolds: versatile platform for tissue engineering*; 3rd CRTD Summer Conference on Regenerative Medicine, Dresden (Germany), June 2009.

D. STAMOV, M. Grimmer, K. Salchert, C. Werner, T. Pompe; *Collagen type I - heparin cofibrils. Transition between 3 different polymorphic forms*; Xth Annual Agilent Workshop "Advances in Single-Molecule Research for Biology & Nanoscience, Linz (Austria), February 2008.

B.3. Acknowledgments

I'd like to thank PROF. CARSTEN WERNER and PROF. DANIEL MÜLLER for giving me the opportunity to work on that challenging and interesting for me topic, as well as learning from some of the world renown experts in the field of Biofunctional Materials and Scanning Force Microscopy. I'd particularly like to point out my direct supervisor and mentor, DR. TILO POMPE, for his flowing and inexhaustible feedback throughout the course of experiments, stoic patience and willingness to listen to and answer all my questions. I'd also like to hold in reverence PROF. KATRIN SALCHERT for her initial work on the topic, as well as, valuable assistance and advices along the way.

For the friendly and scientific atmosphere, where I found endless motivation to pursue the goals of the project contributed the whole Biofunctional Polymer Materials department at the *Leibniz Institute of Polymer Research (IPF)*, in which I was an integrant part from the very beginning. I've enjoyed every minute spent on both scientific and leisure outdoor activities, a vibrant part of which were HANS-GEORG BRAUN, JULIANE DRICHEL, KATJA FRANKE, RINGO GROMBE, RALF HELBIG, CLAUDIA HINÜBER, MARTIN KAUFMANN, BABETTE LANFER, MICHAEL LANG, MANFRED MAITZ, EIKE MÜLLER, THUY ANH KHOA NGUYEN, MARINA PREWITZ, LARS RENNER, DAVID SEBINGER, PHILIPP SEIB, LIDIA SOBKOW, MARIANA TASSO, MIKHAIL TSURKAN.

I've really appreciated the administrative and technical assistance of other IPF colleagues as LARS ANGERSTEIN, KATJA BOCHNIG, SUSANNE BOYE, MARTIN ESPIG, MARTINA FRANKE JR., UWE FREUDENBERG, MILA GRIMMER, BRITTA GRÜSSNER, STEFFI HEMPEL, MANUELA HERKLOTZ, ANDREAS JANKE, DIETER JEHNICHEN, ALBENA LEDERER, TINA LENK, YVONNE MÜLLER, MIRKO NITSCHKE, NELLY REIN, PETRA WELZEL, PIT WIEDEMANN.

I'd also like to thank external collaborators as THOMAS PFOHL and HEATHER EVANS (*Uni Göttingen*), ANDREAS FERY and STEPHAN SCHMIDT (*Uni Bayreuth*), ARMIN SPRINGER and IMAD IBRACHIM (*TU Dresden*), CHARLES FERGUSON and KEVIN MANYGOATS (*MPI-CBG Dresden*).

I owe a debt of gratitude to former supervisors and mentors as PROF. WOLFGANG POMPE, DR. JÖRG OPITZ, DR. MICHAEL MERTIG and DR. STEFAN DIEZ for always supporting me throughout the course of my scientific 'evolution'.

Last but not least, I'd like to thank my ♡ wife, SLAVA STAMOVA, all my family members, and friends, whom I dearly love and appreciate, for their neverending support in tackling the scientific and 'post-scientific' problems in my daily life.

Sincerely,

DIMITAR STAMOV

B.4. Declaration

Hiermit versichere ich, dass ich die vorliegende Arbeit ohne unzulässige Hilfe Dritter und ohne Benutzung anderer als der angegebenen Hilfsmittel angefertigt habe; die aus fremden Quellen direkt oder indirekt übernommenen Gedanken sind als solche kenntlich gemacht. Bei der Auswahl und Auswertung des Materials sowie bei der Herstellung des Manuskripts habe ich Unterstützungsleistungen von folgenden Personen erhalten:

- DR. HANS-GEORG BRAUN, DR. MANFRED MAITZ, DR. KANDICE LEVENTAL, JULIANE DRICHEL, BABETTE LANFER (*IPF Dresden*)
- PROF. KATRIN SALCHERT (*Uni Lausitz*), MILA GRIMMER, TINA LENK (*IPF Dresden*)
- DR. ARMIN SPRINGER (*TU Dresden*), ANDREAS JANKE (*IPF Dresden*), KEVIN MANYGOATS, CHARLES FERGUSON (*MPI-CBG Dresden*)
- PROF. THOMAS PFOHL, DR. HEATHER EVANS (*MPI-DS Göttingen*)
- Praktikanten – THUY ANH KHOA NGUYEN – JIAWEI ZHANG – LARS ANGERSTEIN

Weitere Personen waren an der geistigen Herstellung der vorliegenden Arbeit nicht beteiligt. Insbesondere habe ich nicht die Hilfe eines kommerziellen Promotionsberaters in Anspruch genommen. Dritte haben von mir keine geldwerten Leistungen für Arbeiten erhalten, die in Zusammenhang mit dem Inhalt der vorgelegten Dissertation stehen. Die Arbeit wurde bisher weder im Inland noch im Ausland in gleicher oder ähnlicher Form einer anderen Prüfungsbehörde vorgelegt und ist auch noch nicht veröffentlicht worden.

Die Promotionsordnung der Fakultät Maschinenwesen der Technischen Universität Dresden vom 1. Juli 2001 erkenne ich hiermit an.

Dresden, 22.03.2010.

.....

DIMITAR STAMOV